

https://dspace.org/

An attainable region approach to optimizing product size distribution for flotation purposes

Chimwani, Ngonidzashe

2014-09-05
http://hdl.handle.net/10539/15419

Downloaded from a DSpace repository. https://dspace.org/

AN ATTAINABLE REGION APPROACH TO OPTIMIZING PRODUCT SIZE DISTRIBUTION FOR FLOTATION PURPOSES

Ngonidzashe Chimwani

A thesis submitted to the Faculty of Engineering and the Built Environment, University of the Witwatersrand, Johannesburg, in fulfilment of the requirements for the degree of Doctor of Philosophy in Engineering

Johannesburg, 2014

Declaration

I declare that this thesis is my own unaided work. It is being submitted for the degree of Doctor of Philosophy in Engineering in the University of the Witwatersrand, Johannesburg. It has never been submitted either in part or in whole for a degree in this or any other University.

.....

Ngonidzashe Chimwani

.....day of.....year.....

Abstract

In this thesis, experimental and modelling techniques were used to investigate the breakage of a typical South African platinum group minerals ore in a ball mill to optimize product size distribution (PSD) for flotation purposes.

Batch milling experiments were conducted on three narrow-sized feeds using three different ball sizes to determine the milling parameters of the platinum ore. Verification of the parameters was done by doing additional tests beyond the previous experimental range. This confirmed that the parameters were good estimates for the ore. A scale-up procedure for batch grinding data was used to obtain parameters for an industrial mill on which a performance survey had been done. The survey data was used to verify the scale-up parameters. Following this, the effects of mill rotational speed, ball filling level, slurry filling and ball sizes on milling kinetics were explored and analysed using the attainable region (AR) technique.

The outcomes of the simulations showed that a finer product is achieved when small balls are used. Lower mill hold-up and fewer grinding balls were also shown to enhance finer grinding. However, factors that produced a coarser product as shown by the particle size analysis were shown to yield the greatest amount of the desired size class when analysed using AR.

Next, the AR technique was used to analyse simulation outputs of a continuous mill over a wide range of operating conditions. The analysis was limited to plug-flow and well-mixed mill transport models without exit classification. The AR analysis showed that industrial milling conditions could be tailored to the desired product by reducing residence time, mill speed while increasing ball size.

Extension of the AR framework to a more realistic transport model also produced similar results. The importance of optimally controlling the residence time of material inside a mill as well as energy was demonstrated when maximising the desired size range. The results showed that operating the ball mill at lower speeds and higher ball filling saves energy.

Finally, combining the population balance modelling technique and the AR enabled a better understanding and effective optimisation of milling for downstream processes, particularly for flotation.

Publications

The papers published by the author on the contents of this thesis are as follows:

Chimwani, N., Glasser, D., Hildebrandt, D., Metzger, M.J., Mulenga, F.K., 2013. Determination of the milling parameters of a platinum group minerals ore to optimize product size distribution for flotation purposes. Minerals Engineering, vol. 43 – 44, pp. 67 – 78

Chimwani, N., Mulenga, F.K.., Glasser, D., Hildebrandt, D., Bwalya, M., 2014. Scale-up of batch grinding data for simulation of industrial milling of platinum group minerals ore. Minerals Engineering, in press

Mulenga, F.K., **Chimwani**, N., 2013. Introduction to the use of the attainable region method in determining the optimal residence time of a ball mill. International Journal of Mineral Processing, vol. 125, pp. 39 – 50

Chimwani, N., Mulenga, F.K.., Glasser, D., Hildebrandt, D., Bwalya, M., 2014. Use of the attainable region method to simulate a full-scale ball mill with a realistic transport model, presented at the Comminution 14’ in Cape Town, Minerals Engineering International Conference

Dedications

This work is dedicated to all my
family members

Acknowledgements

Firstly, I would like to exalt the Almighty GOD, the author of my life, who allowed me to do a PhD thesis. My LORD, thank you for giving me wisdom, proper guidance and for bringing the right people to assist me in this work.

I thank Prof Diane Hildebrandt, Prof David Glasser, Dr Murray Bwalya and Dr François Mulenga for their supervision, encouragement, invaluable support and diligent guidance. This work would not have succeeded without their supervision.

Prof Michael Moys and Dr Matthew Metzger are also greatly acknowledged for their advice, contribution and unqualified encouragement. Pippa Lange is acknowledge for her contribution in improving my English writing.

My colleagues Mr Nkosikana Hlabangana, Dr Gwiranai Danha, Mr David Vetter are acknowledged for the stimulating discussions, timely advice, and critical suggestions which helped to enhance the quality of this work.

I also want to thank my family and friends for their understanding and moral support during the course of this work.

Last but not least, the funding from the National Research Fund (NRF), the Centre of Materials and Process Synthesis (COMPS) and the University of the Witwatersrand (Postgraduate Merit Award and bursary) which enabled the execution of this research work.

Table of Contents

Declaration ..... **ii**

Abstract ..... **iii**

Publications ..... **v**

Dedications ..... **vi**

Acknowledgements ..... **vii**

Table of Contents ..... **viii**

List of Figures ..... **xii**

List of Tables ..... **xvi**

Chapter 1: Introduction **1**

1.1 Background and motivation 1
1.2 Problem statement 2
1.3 Research objectives and envisaged contribution 3
1.4 Layout of the dissertation 4

Chapter 2: Literature Review **6**

2.1 Introduction 6
2.2 Theory of milling 7
2.2.1 Selection function 7
2.2.2 Breakage function 11
2.2.3 Batch grinding equation 14
2.3 Population balance model applied to a continuous mill 14
2.4 Scale-up procedure for batch grinding data 16
2.5 Factors affecting the breakage rate 19
2.5.1 Ball filling 20
2.5.2 Mill filling by powder 21
2.5.3 Critical speed 23
2.5.4 Ball diameter 24
2.6 Axial flow through a ball mill 27
2.6.1 Residence time distribution 27
2.6.2 Simplified flow through a ball mill 29
2.7 The Attainable Region technique 30
2.8 Optimal floatable particle size 34
2.9 Power draw in ball mills: The Morrell model 35
2.10 Net power draw and milling efficiency 37
2.11 Classical configuration of milling circuits 38
2.12 Summary 40

Chapter 3 Experimental programme, equipments and simulation strategies used.....41

3.1 Introduction 41
3.2 Experimental equipment and programme.....41
3.2.1 Description of the laboratory grinding mill.....41
3.2.2 Laboratory testing protocol.....43
3.3 Feed material preparation.....44
3.3.1 Feed preparation.....44
3.3.2 Preparation of grinding balls.....46
3.3.3 The batch grinding tests.....46
3.3.4 Particle size analysis.....47
3.3.5 Data collection and processing.....47
3.4 Estimation of the breakage characteristics of the ore.....48
3.5 Scale-up Methodology.....49
3.5.1 Batch test data.....49
3.5.2 The industrial mill.....49
3.5.3 The scale-up procedure.....50
3. 6 Simulation of the residence time.....51
3.7 Simulation of the power draw.....53
3.8 Summary.....53

Chapter 4 Determination of the milling parameters of a Platinum Group Minerals ore to optimize product size distribution for flotation purposes.....54

4.1 Introduction.....56
4.2 Results and discussions.....57
4.2.1 Determination of the selection function parameters……..…….57
4.2.2 Determination of the breakage function parameters……..……60
4.2.3 Particle size distributions……62
4.3 Conclusion.....65
4.4 Summarised findings.....66

Chapter 5 Scale-up of batch grinding data for simulation of industrial milling of platinum group minerals ore.....68

5.1 Introduction.....70
5.2 Results and Discussions……...71
5.2.1 Validation of the scale-up procedure…….……72
5.2.2 Using modelling to explore effects of varying operational conditions ……..73
5.2.2.1 Effects of mill speed on milling kinetics.....73
5.2.2.2 Effect of ball filling on milling.....76
5.2.2.3 Effect of ball diameter on milling.....77
5.2.2.4 Effects of slurry filling on milling.....79

5.3 Conclusion.....83

Chapter 6 Use of the attainable region method in determining the optimal residence time of a ball mill.....85

6.1 Introduction.....86
6.2 Data collection and analysis.....87
6.2.1 Effects of ball filling on mill production.....88
6.2.2 Effects of ball size on mill production.....92
6.2.3 Effects of mill speed on mill production.....95
6.3 Summarised findings.....96
6.4 Conclusion.....98
6.5 Future outlook.....99

Chapter 7 Use of the attainable region method to simulate a full-scale ball mill with a realistic transport model.....101

7.1 Introduction.....103
7.2 The mill transport model.....104
7.3 Data collection and analysis.....104
7.3.1 Effects of ball filling on mill production.....105
7.3.2 Effects of ball size on mill production.....107
7.3.3 Effects of mill speed on mill production.....109
7.4 Energy consumption of the mill.....110
7.5 Summarised findings.....114

Chapter 8 Conclusions and recommendations.....117

8.1 Introduction.....117
8.2 Characterisation of the PGM ore.....117
8.3 Extension of the AR region method to continuous milling.....118
8.4 Summary of the major findings.....118
8.5 Overall conclusion.....122
8.6 Recommendations for future work.....122

List of references.....124

Appendices.....132
A.1 Batch grinding data.....132
A.2 Determination of the milling properties of the ore.....138
A.2.1 Search engine for population balance model parameters.....138
A.2.1.1 The driver used for the parameter search based on batch grinding data available.....138
A.2.1.2 The function file for the generation of product side distribution once PBM parameters are inputted.....139

A2.1.3 The plotting facility of the product size distribution based on back-calculated parameters……..141
A.2.2 Simulator for the milling kinetics of the size class of interest……143
A.2.3 Flowchart for the parameter search algorithm.....145
A.3 Scale-up procedure for laboratory-based PBM parameters.....146
A.4 Optimisation of the residence time.....149
A.5 Matlab version of the Morrell power model.....154
A.6 Matlab code to calculate energy.....156

List of figures

Figure 2.1 Schematic illustration of first order plots (Yekeler, 2007).....9

Figure 2.2 Non-first-order grinding of a narrow-sized feed (Bilgili *et al.*, 2006).....10

Figure 2.3 Variation of the selection function with particle size (Austin *et al.*, 1984).....11

Figure 2.4 Breakage function of typical material (after Yekeler, 2007).....13

Figure 2.5 Illustration of the difference in load behaviour for different ball charge levels but same mill speed (after Fortsch *et al.* 2006).....20

Figure 2.6 Motion of charge in ball mills (Wills and Napier-Munn, 2006).....23

Figure 2.7 Ball mill flow regime as a function of increasing speed (after Boateng and Barr, 1996).....24

Figure 2.8 Variation of specific rate of breakage with ball diameter (after Napier-Munn *et al.* 1996).....26

Figure 2.9 Example of tracer response of a full-scale mill: ball filling J = 25 % and slurry at 67.3 % solids concentration (after Makokha, 2011).....29

Figure 2.10 RTD's of a plug-flow, a perfectly mixed and a real ball mill.....30

Figure 2.11 (a) Grinding profiles of all six class sizes versus time. (b) Cumulative mass fraction versus average particle size (Metzger *et al.* 2009).....32

Figure 2.12 Grinding kinetics as plotted for the three size classes m_1, m_2 and m_3 (Katubilwa *et al.*, 2011).....32

Figure 2.13 Mass fraction of size class two versus number of revolutions (Metzger *et al.*, 2009).....33

Figure 2.14 Representing particle size distributions as a single trajectory in the AR space (Khumalo *et al.*, 2007).....33

Figure 2.15 Typical flotation size/recovery curve (Rule and Anyimadu, 2007)...34

Figure 2.16 The combined closed circuit (from Austin *et al.*, 1984).....39

Figure 3.1 View of the laboratory ball mill.....42

Figure 3.2 Picture of the laboratory grinding mill used for the experiments.....42

Figure 3.3 Diagrammatic representation of the simulator used.....48

Figure 3.4 Schematic representation of the tanks in series model with dead time (after Makokha *et al.*,2011.....51

Figure 4.1 First-order plot for UG2 ore mono-size class (-600 +425 µm) ground with different media sizes (d_T): (a) 10 mm; (b) 20 mm; (c) 30 mm.....58

Figure 4.2 (a) Variation of *S* with particle size (b) Graphical procedure for the determination of the parameters (Austin *et al.* 1984).....60

Figure 4.3 Variation of breakage function values with feed size.....61

Figure 4.4 Measured and predicted particle size distributions corresponding to 10 mm ball size and feed sizes: (a) -850 +600 µm (b) -600 +425 µm and (c) -425 +300 µm.....63-64

Figure 4.5 Milling kinetics of the desired size class for 20 mm balls and feed size -850 +650 µm.....65

Figure 5.1 Comparison between experimentally measured data and the predicted PSD using the scale up method for the large scale mill: (a) J = 24.6 % and 74.5 % solids, (b) J = 32.9 % and 67.7 % solids, (c) J = 32.8 % and 65.1 % solids, (d) J = 32.9 % and 72.1 % solids.....73

Figure 5.2 Predicted PSD's for four mill speeds: J = 40%, U = 0.75, d = 40 mm and varying residence times.....74

Figure 5.3 Plot of mass fraction of m_2 versus number of revolutions for different speeds ϕ_c; J = 40 %, U = 0.75, and d = 40 mm.....75

Figure 5.4 Effect of ball filling J on PSD: ϕ_c = 75 %, U = 0.75, d = 40 mm.....76

Figure 5.5 Plot of mass fraction of m_2 versus number of revolutions for ball filling J on PSD: ϕ_c = 75 %, U = 0.75, d = 40 mm.....77

Figure 5.6 PSD for different media sizes; ϕ_c = 75 %, U = 0.75, J = 40 %.....78

Figure 5.7 Plot of mass fraction of m_2 versus number of revolutions for different ball sizes; J = 40 %, ϕ_c = 75 %, U = 0.75.....79

Figure 5.8 PSDs for three slurry fillings; ϕ_c = 75 %, J = 40 %, d = 40 mm.....80

Figure 5. 9 Plot of mass fraction of m_2 versus number of revolutions for different slurry fillings; J = 40 %, ϕ_c = 75 %, and d = 40 mm.....81

Figure 5.10 Summary of various simulations, optimised solution and industrial operating conditions……..82

Figure 6.1 Geometric parameters considered for the industrial mill at rest……...88

Figure 6.2 Throughput of the mill for the two RTD profiles. Simulation conditions: J = 30 %, U = 1.35, d = 40 mm and ϕ_c = 70 % critical……..……..…90

Figure 6.3 Prediction of ball filling effects on mill throughput for a fully mixed mill. Simulation conditions: d = 40 mm and ϕ_c = 70 % of critical…..91

Figure 6.4 Effects of ball diameter on mill throughput for the two RTD profiles. Simulation conditions: J = 30 %, U = 1.35, d = 10 mm and ϕ_c = 70 % of critical.....93

Figure 6.5 Effects of ball size on mill throughput for a well-mixed mill. Simulation conditions: J = 30 %, U = 1.35, and ϕ_c = 70 % of critical..94

Figure 6.6 Effects of mill speed on mill throughput for a fully mixed mill. Simulation conditions: J = 25 %, U = 1.92 and d = 30 mm.....95

Figure 6.7 Residence time τ_{optim} as a function of mill speed ϕ_c for J = 30 % under varying ball diameters. Solid and dashed lines in the plot area represent the well-mixed and plug-flow mill models respectively.....98

Figure 7.2 Throughput profiles of the mill for the three transport models. Simulation conditions: J = 30 %, U = 1.35, d = 40 mm and ϕ_c = 70 % of critical.....105

Figure 7.3 Prediction of ball filling effects on mill throughput for the TIS model. Simulation conditions: d = 40 mm and ϕ_c = 70 % of critical.....106

Figure 7.4 Effects of ball size on mill throughput for the TIS model. Simulation conditions: J = 25 %, U = 1.92, and ϕ_c = 70 % of critical.....108

Figure 7.5 Effects of mill speed on mill throughput for the TIS model. Simulation conditions: J = 30 %, U = 1.35 and d = 40 mm.....109

Figure 7.6 Effects of ball filling on energy.....111

Figure 7.7 Effects of mill speed on energy consumed.....112

Figure 7.8 Effects of mill speed on mill throughput on the extent of energy draw. Simulation conditions: J = 30 %, U = 1.35 and d = 40 mm.....113

Figure 7.9 Effects of media filling level on mill throughput on the extent of energy used. Simulation conditions: ϕ_c = 40 % of critical and d = 40 mm.....114

Figure 7.10 Optimum mean residence time τ_{optim} as a function of mill speed ϕ_c for J = 30 % under varying ball diameters.....115

Figure 7.11 Optimal residence time versus ball filling at different speeds.....116

Figure A.1 The Wits laboratory ball mill used for experimentation.....132

Figure A.2 Power calibration chart of the laboratory mill.....132

A.2.3 Flowchart for the parameter search algorithm…….....145

List of tables

Table 3.1 Specifications of the mill.....43

Table 3.2 Experimental design.....44

Table 3.3 Mass retained on each sieve at different times……..……45

Table 3.4 Mono-size media charges used.....46

Table 4.1 Selection functions for different feed sizes and media sizes.....59

Table 4.2 The UG2 ore selection and breakage function parameters.....62

Table 5.1 Breakage parameters as scaled-up to industrial mill.....72

Table 5.2 Individual milling parameters and corresponding optimum throughput.....82

Table 6.1 Correlation between ball filling J and slurry filling U used.....89

Table 6.2 Mean residence times τ_{optim} for d = 40 mm and ϕ_c = 70 % of critical....91

Table 6.3 Mean residence times τ_{optim} for J = 30 % and ϕ_c = 70 % of critical.....94

Table 6.4 Optimum mean residence times τ_{optim} for J = 25 % and d = 30 mm.....95

Table 7.1 Mean residence times τ_{optim} for d = 40 mm and ϕ_c = 70 % of critical..107

Table 7.2 Mean residence times τ_{optim} for J = 25 % and ϕ_c = 70 % of critical.....108

Table 7.3 Optimum mean residence times τ_{optim} for J = 30 % and d = 40 mm....109

Table 7.4 Optimal residence time, net power and energy of 40 mm ball size for varying fraction of speed and ball filling.....110-111

Table 8.1 The PGMs ore breakage characteristics.....117

Table A.1 Measured particle size distribution for ball size 10 mm, feed size (-850 +600 μm), U = 0.75, J = 20 %, ϕ_c = 75 of critical, f_c = 0.06.....133

Table A.2 Measured particle size distribution for ball size 10 mm, feed size (-600 +425 μm), U = 0.75, J = 20 %, ϕ_c = 75 of critical, f_c = 0.06.....133

Table A.3 Measured particle size distribution for ball size 10 mm, feed size (-425 +300 μm), U = 0.75, J = 20 %, ϕ_c = 75 of critical, f_c = 0.06.....134

Table A.4 Measured particle size distribution for ball size 20 mm, feed size (-850 +600 μm), U = 0.75, J = 20 %, ϕ_c = 75 of critical, f_c = 0.06.....134

Table A.5 Measured particle size distribution for ball size 20 mm, feed size (-600 +425 μm), U = 0.75, J = 20 %, ϕ_c = 75 of critical, f_c = 0.06.....135

Table A.6 Measured particle size distribution for ball size 20 mm, feed size (-425 +300 μm), U = 0.75, J = 20 %, ϕ_c = 75 of critical, f_c = 0.06.....135

Table A.7 Measured particle size distribution for ball size 30 mm, feed size (-850 +600 μm), U = 0.75, J = 20 %, ϕ_c = 75 of critical, f_c = 0.06.....136

Table A.8 Measured particle size distribution for ball size 30 mm, feed size (-600 +425 μm), U = 0.75, J = 20 %, ϕ_c = 75 of critical, f_c = 0.06.....136

Table A.9 Measured particle size distribution for ball size 30 mm, feed size (-425 +300 μm), U = 0.75, J = 20 %, ϕ_c = 75 of critical, f_c = 0.06.....137

Table A.10 Breakage function values calculated using the BII-method from laboratory data and later used to determine breakage function parameters.....137-138

Table A.11 Breakage parameters as scaled-up to industrial mill.....149

Table A.12 Measured versus scaled-up particle size distributions.....149

Chapter 1 Introduction

1.1 Background and Motivation

Milling is an operation widely used in the mineral, metallurgical, power generation and chemical industries. One of the primary reasons for choosing to mill materials to smaller sizes is to liberate valuable components that are dispersed in the host matrix. Once the material has been broken and sufficient of these components have been liberated, they are separated from the valueless remainder by downstream processes such as flotation. The effectiveness of the downstream process is therefore dependent on the milling process. That is the reason why it is necessary to tailor the milling parameters to obtain products that are best suited to the requirements of the downstream process concerned. For instance flotation, the particle size range has to be such that over-grinding is avoided on one hand which is a waste of energy and on the other under-grinding that leaves most mineral value unliberated resulting in low mineral recovery during the separation process is also undesirable. The application of comprehensive mathematical milling models is useful in targeting the flotation size requirements better.

The most commonly-accepted milling model follows the Population Balance Model (PBM) framework (Yekeler, 2007), which is based on the first-order law of kinetics. In this model, particles in a narrow size interval are assumed to break proportionally to their mass fraction (Reid, 1965; Kelsall and Reid, 1965; Austin, 1971; Mika, 1975). By performing a size-mass balance in narrow size intervals, it is possible to describe milling in a time domain (Koka and Trass, 1988), which makes it possible to determine the product size distribution after a given grinding time.

The assumption of first-order breakage suggests that ball milling can be represented in a mode similar to the expression of chemical reactions (Khumalo *et al.*, 2006 – 2008). Consequently, an analytical tool known as the Attainable Region (AR) can be used to study milling. Initially proposed for the analysis of

chemical engineering systems, the AR technique has been successfully extended to comminution (Khumalo, 2007; Khumalo *et al.*, 2006 – 2008; Metzger, 2011; Metzger *et al.*, 2009 & 2011; Katubilwa *et al.*, 2011, Chimwani *et al.*, 2012).

The successful use of the AR technique to determine the set of all achievable distributions for the process conditions has already been demonstrated. Although most of the work done so far has been laboratory-based, the results have been encouraging. That is why the present thesis seeks to extend the methodology to full scale milling. To accomplish this, data collected from batch grinding tests was scaled up to an industrial mill that had been surveyed and the data were explored further to arrive at best milling option that met the flotation size requirements. The intention was to determine a milling circuit that would produce optimal flotation sizes in the milled ore. The sampling work of the referred industrial mill was published before (Makokha, 2012). It is shown that improved milling efficiency could be achieved through optimal residence time.

1.2 Problem statement

The most common processing challenges encountered when liberating Platinum Group Mineral (PGM) ores are generally associated with the fineness and gangue association of mineral species (Cramer, 2001). In a typical South African scenario, PGM ores are milled before being sent for flotation. In such a case, one of the reasons for a low flotation recovery could be the failure of the last stage of milling to generate a sufficient percentage of particles within the floatable size range. It is therefore understood that optimizing the milling stage could be one way of improving flotation efficiency. However, in order to optimize milling, it is necessary to start by establishing the optimum flotation requirements in terms of floatable particle sizes. Then, using the AR technique, this information can be used to determine how the milling can be adapted to provide a more appropriate feed for the flotation section. The key issue is therefore to develop a robust AR framework applicable to continuous milling. Having achieved this, the final task will be to ascertain whether the laboratory-based findings can be extended to full-scale milling.

It has been shown at the laboratory scale using the AR technique that a substantial amount of energy can be saved, while still ensuring effective grinding, through controlled classification (Khumalo *et al.*, 2008). Common practice, however, continues to follow the assumption that the higher the energy consumption, the higher the milling rate (Austin *et al.*, 1984; Wills and Napier-Munn, 2005). It has also been shown that less powder and fewer grinding balls can bring about more effective grinding (Metzger *et al.*, 2011). Conventional practice, on the other hand, favours mills with high ball loading J and powder filling U close to unity (that is $U \cong 1$) (Tangsathitkulchai, 2003; Latchireddi and Morrell, 2003). Finally, low-speed mills have been shown to bring about a high product fineness at the same rate as (and sometimes at a higher rate than) high-speed mills (Metzger, 2011); whereas, once more, traditional practice proposes speeds nearing 75 % as critical to guarantee high power draw and therefore more grinding at a faster rate (Austin *et al.*, 1984; Wills and Napier-Munn, 2005).

All of the above suggests that the innovations prompted by the AR approach contradict the milling conditions under which most of the concentrators operate. The main problem is that all of the AR-related claims have so far been based on laboratory batch investigations (Khumalo, 2007; Khumalo *et al.*, 2006 – 2008; Metzger, 2011; Metzger *et al.*, 2009 & 2011; Katubilwa *et al.*, 2011), and as such, their validity has been limited by the scale factor. In addressing this issue, a convincing answer has to be provided to a key question: Can the attainable region technique be extended to industrial conditions of a full scale mill and be used to optimise flotation feed size distribution? If this can be answered in the affirmative, then the corollary to this question would be to propose the AR as an alternative and complementary analytical tool for the optimization of milling circuits.

1.3 Research objectives and envisaged contribution

This research was intended to apply various aspects of industrial ball milling that could be used to control and optimize the performance of a milling circuit. The desired end result was to generate the maximum production of preselected sizes

for flotation or floatable particle sizes. The AR approach was used to optimize the operational parameters as well as the residence time of a full-scale industrial mill. The breakage and selection function parameters of a PGM ore were measured by means of laboratory batch grinding tests, and the resultant parameters were scaled up using empirical scale-up models (Austin *et al.*, 1984). After that, the influence of the various milling parameters on the mill circuit and on size distribution of the final product was assessed by simulation.

The research set out in this thesis is expected to provide information on the milling characteristics of PGM ores in general. This is important, since these data have not been generally available to the public at large. The milling data can be used for simulation and optimization purposes, and may lead to further investigations of PGM milling. In addition, the research establishes a precedent for the use of the AR technique in the minerals industry as a tool of choice for the analysis and optimization of mineral processing circuits.

1.4 Layout of the dissertation

The thesis is organized into eight chapters, including the introduction. In the introductory chapter, the background and motivation are presented as well as the problem statement and research objectives on which the thesis is based.

The second chapter presents a review of the studies accomplished to date regarding comminution modelling. It reviews the population balance modelling of ball mills. It also gives a description of the attainable region approach, to provide a context for the research work reported in the chapters that follow.

The third chapter comprises a detailed description of the experimental equipment, the data collection methods used in the work undertaken, and the simulation strategy used to assess whether the objectives of this study had been met.

Chapter four recounts how a set of batch milling parameters were established for the platinum group mineral ore. Some of the breakage parameters were measured directly in the laboratory, while the remaining breakage parameters were back-

calculated within the population balance model framework. These parameters provide a basis for simulation and optimization of the milling process in the subsequent chapters. Validation of these parameters is also done in the same chapter.

Chapter five records the process by which the batch milling parameters were scaled up from laboratory to full operation. The data generated was validated against industrial mill data before the AR technique was used to optimize a range of industrial milling conditions. These included ball filling (J), mill speed (ϕ_c), ball size (d) and powder filling (U). The optimization was centred on the production of a particle size amenable to efficient flotation.

Chapter six introduces the optimization of residence time as a function of mill speed (ϕ_c), ball filling (J), slurry filling (U) and ball size (d). Two mill transport models are considered: the plug flow model and the perfectly mixed mill model. Using these simple models, it is possible to determine how a variation in each of the milling conditions considered affects the production of floatable mill product from an AR point of view.

Chapter seven is an extension of the sixth chapter. It contains a description of the application of AR methodology to determine the optimal residence time of a full-scale mill that incorporates a more realistic transport model based on data concerning residence time distribution collected from a full-scale mill; attempts made to optimise the mill product relative to flotation requirements; and assessment of the energy requirements of the optimized mill. The results are taken to underscore the power of the AR method as an optimization tool.

Chapter eight contains a summary of the major findings and conclusions drawn from the work described in this thesis. Recommendations for future work are also listed.

Chapter 2 Literature Review

2.1 Introduction

The designers of industrial mills used for mineral extraction aim to create operational conditions that guarantee high mineral recovery and low costs. In order to achieve these ends, they normally consider two objective functions: the energy consumption and the product size relative to a chosen downstream process. The key aspects of meeting these requirements, as far as grinding and flotation are concerned, would be the effective control of the desired mill product without overgrinding or under-grinding.

McIvor and Finch (1991) showed that the relationship between particle size and flotation performance can be used as a basis for both technical and economic analyses of the viability of a plant. In terms of particle size, the population balance model provides a robust formulation of the milling process, and years of experimentation have confirmed its value (Herbst and Fuerstenau 1980; Herbst *et al*., 1981; Austin *et al.*, 1984; Rajamani, 1991; King, 2001). More recently, the AR concept has been introduced as a graphical technique for the analysis of milling, and has already proved its relevance as an optimization tool. The technique can be used to highlight the overall picture of what the data is saying and help in identifying opportunities that can lead to optimisation. While it is recognised that flotation is a complex process that is affected by many factors, as far as milling is concerned, controlling the size distribution of the feed to flotation is a key role of the milling process.

To provide a perspective on how milling should be tailored to flotation, the work done by previous researchers on milling was reviewed, and the variety of technical models they have introduced for analytical and evaluative purposes. These include the population balance model, the batch grinding equation and the scale-up procedure for batch grinding data. The product size requirements for optimal flotation was also discussed, and a detailed introduction to the attainable region technique given.

2.2 Theory of milling

In comminution, mathematical relations between feed size and product can be developed by applying a size mass balance to the milling operation. This is made possible by the definition of two actions taking place simultaneously inside the mill: the selection of particles for breakage and the breakage distribution of 'children' particles as a result of broken 'parent' particles (Gupta and Yan, 2006). The selection and breakage function are used to investigate the kinetics of size reduction in tumbling mills (Austin, 1971; Lucky *et al.*, 1972). These two functions have led to the establishment of the population balance model, which provides the basis for the modelling of the grinding process. It describes material breakage in mills based on size-mass balances on narrow size intervals of the particulate mass. The particulate masses are subjected to breakage in the mill and are formulated in terms of the selection and the breakage function parameters (Koka and Trass, 1988). These two actions are discussed in detail in the sections that follow.

2.2.1 Selection function

The selection function, also called the breakage rate, can be defined as the rate at which material is broken out of a particular discretized size class.

To explain the concept more fully, a wide range of particle sizes is split into a number of size intervals following a $\sqrt{2}$ sequence of sieves. The top size interval is numbered size class 1, the second is class 2, and so on down to the n^{th} interval, which is the final size interval. Now, when one considers the breakage rate of size class 1 to smaller size classes in a fully mixed batch mill, if the disappearance of particles per unit time and unit mass due to breakage is proportional to the instantaneous mass fraction of particles of that size fraction that are present inside the mill, the breakage is said to follow the first-order law of kinetics.

This can then be expressed as follows (Austin *et al.*, 1981):

$$\frac{dw_i(t)}{dt} = -S_i.w_i(t) \qquad \textbf{(2.1),}$$

where S_i is the rate of disappearance of particles or the selection function;

w_i is the mass fraction present in the size interval *i* after grinding time *t*; and

i is an integer defining the different size intervals, the largest being 1.

If the breakage rate function (S_i) is constant over time as the contents of the mill become finer, Equation 2.1 integrates to what is known as the "first-order rate model of grinding" (Napier-Munn *et al.*, 1996):

$$w_1(t) = w_1.e^{-S_1.t} \qquad \textbf{(2.2),}$$

where w_1 is the mass fraction present in the size interval 1 after grinding time *t*.

Equation (2.1) has been found to apply to different types of materials and has worked well for many materials over a wide range of operations (Austin *et al.*, 1976; Austin *et al.*, 1984, Bilgili *et al.*, 2006). However, several researchers have also reported and investigated departures from the first-order breakage pattern. The following non-exhaustive list of references provides a detailed description of non-first-order milling kinetics: Austin *et al.*, 1973; Austin *et al.*, 1977; Bilgili and Scarlett, 2005; Bilgili *et al.*, 2006; Bilgili, 2007; Capece *et al.*, 2011. Suffice it to say that non-first-order grinding generally occurs when coarse particles are being milled. In that case, the breakage is referred to as abnormal.

Austin *et al.* (1977) studied abnormal breakage and postulated that during grinding, some material that is initially soft breaks down into a component resistant to further breakage. They proposed the following non-first-order model:

$$w_i(t) = \frac{m(t)}{m(0)} = (1-\psi_i).e^{-S_{soft}.t} + \psi_i.e^{-S_{hard}.t} \qquad \textbf{(2.3),}$$

where $\psi_i = \dfrac{b_{ii}'.S_{soft}}{S_{soft} - S_{hard}}$

S_{soft} is the selection function of the easy-to-break component of the material;

S_{hard} is the selection function of the hard-to-break component of the feed.

The system behaves as if the material consists of a fraction 1 - ψ of soft component and a fraction ψ of the hard component. The mean value of the effective selection function is given by:

$$S_i = \frac{1}{\frac{1}{S_{soft,i}} + \frac{b_{ii}}{S_{hard,i}}} \qquad \textbf{(2.4).}$$

Figure 2.1 below illustrates a good agreement between the first-order breakage model and laboratory batch grinding results for a given material, while Figure 2.2 summarizes the types of non-first-order kinetics that have been reported in the literature. Austin *et al.* (1984) further argued that a number of physical causes can slow down the expected breakage rate, thereby violating the assumption of first-order kinetics.

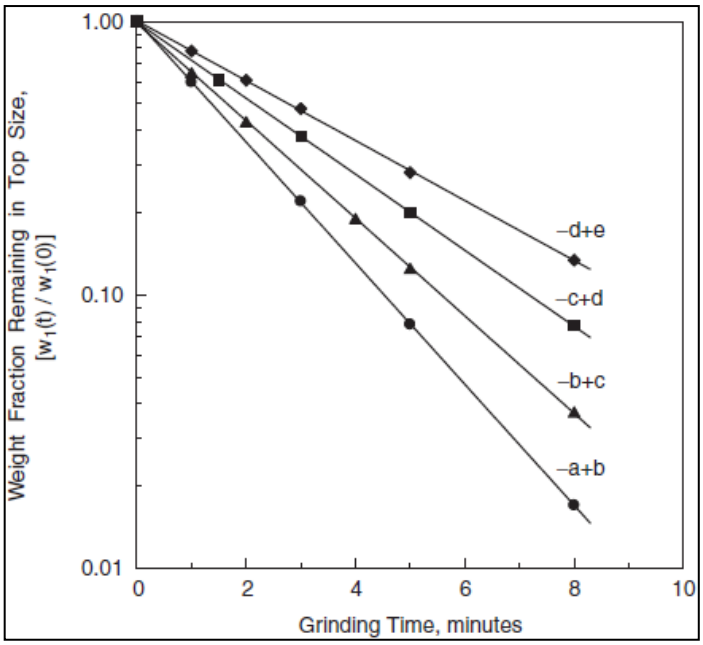


Figure 2.1 Schematic illustration of first-order plots (Yekeler, 2007).

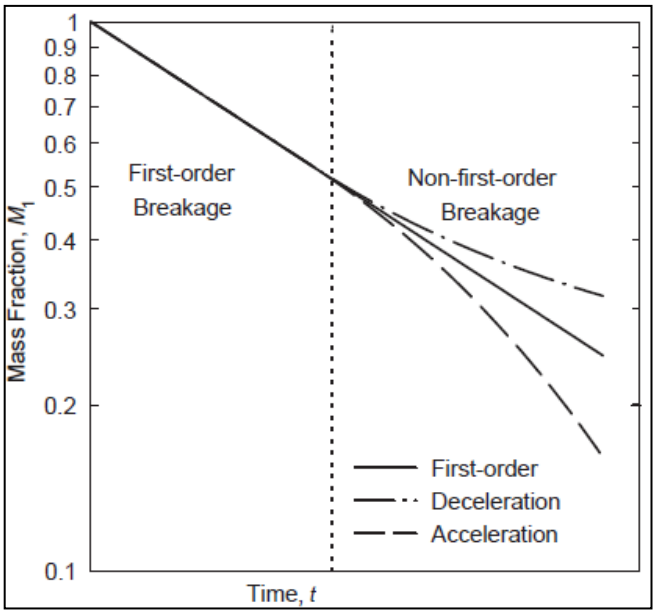


Figure 2.2 Non-first-order grinding of a narrow-sized feed (Bilgili *et al*., 2006).

In order to define the variation of the selection function with particle size, Austin *et al*. (1984) proposed the following empirical model:

$$S_i = a.x_i^{\alpha}.Q_i = a.x_i^{\alpha}.\frac{1}{1+\left(\frac{x_i}{\mu}\right)^{\Lambda}} \qquad \textbf{(2.5),}$$

where x_i is the maximum limit in the screen size interval i in mm;

Λ and α are positive constants which are dependent on material properties;

a is a parameter dependent on mill conditions and material properties, which indicates how fast the grinding is (Makokha *et al*., 2006);

μ is a parameter dependent on mill conditions; and

Q_i is the correction factor accounting for abnormal breakage.

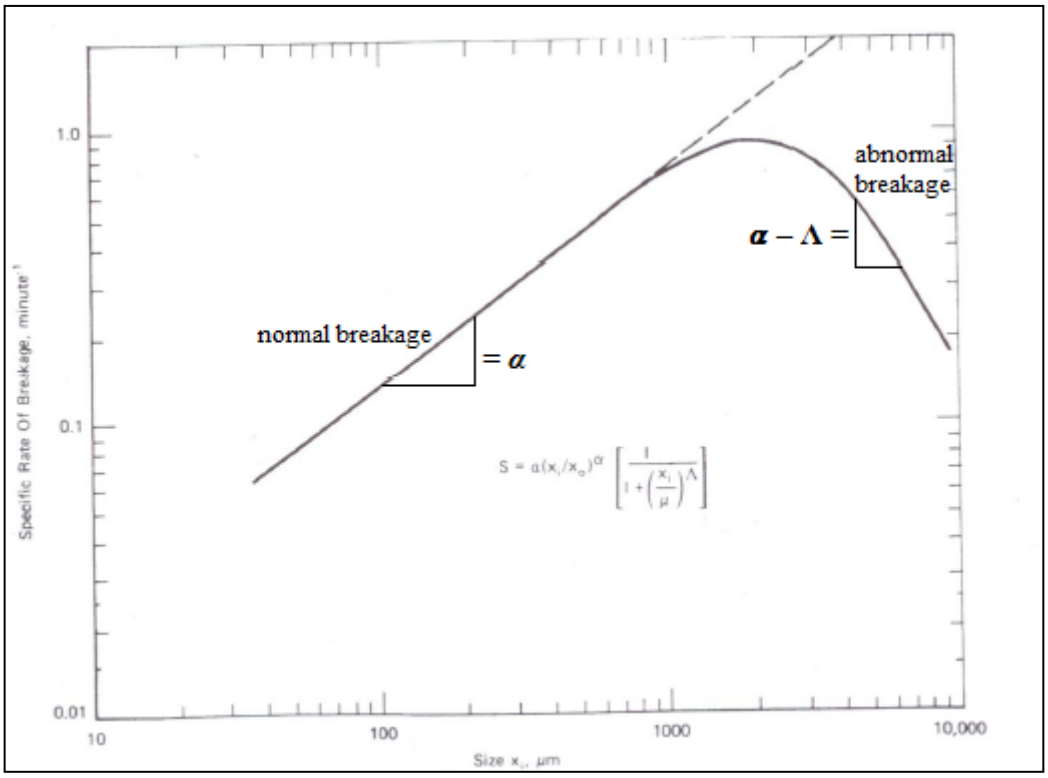


Figure 2.3 Variation of the selection function with particle size.
(Austin *et al*., 1984)

Equation (2.5) is valid for a material milled at constant speed with a charge of balls of the same diameter. For fine material, Equation (2.5) can be approximated to

$$S_i = a.x_i^{\alpha} \qquad \textbf{(2.6).}$$

2.2.2 Breakage function

The primary breakage distribution function can be defined as the average size distribution produced from a single breakage (Kelly and Spottiswood, 1990). It is considered good practice to measure the size distribution of progeny fragments after a breakage event before they are reselected for further breakage. That is why researchers like Gupta and his colleagues (2006) recommend that a sieve analysis should be carried out on a product sample from a single-sized feed that has been batch milled for a short period.

The distribution of fragments produced by breaking size *i* before re-breakage occurs is called the primary daughter fragment distribution b_{ij}. It is the ratio of mass from size class *j* reporting to size class *i* (Austin *et al*., 1984):

$$b_{ij} = \frac{mass\ of\ particles\ from\ class\ j\ broken\ to\ size\ i,\ \ t\to 0}{mass\ of\ particles\ of\ class\ j\ broken,\ \ t\to 0}\text{, where } i < j \qquad \textbf{(2.7).}$$

A more convenient way of describing the breakage function is to represent it in cumulative form:

$$B_{ij} = \sum_{k=n}^{i} b_{kj} \qquad \textbf{(2.8),}$$

where B_{ij} is the sum of the fraction of material that is less than the upper size of size interval *i* resulting from breakage of size *j* material.

The duration of grinding over which the breakage function can be measured accurately is determined by the requirement that only 20 – 30 % breakage occurs in the top size interval, to minimize the re-breakage of particles. The breakage function is then calculated following the B-II method proposed by Austin *et al.* (1984):

$$B_{ij} = \frac{Log\left[\dfrac{1-p_i(0)}{1-p_i(t)}\right]}{Log\left[\dfrac{1-p_{j+1}(0)}{1-p_{j+1}(t)}\right]} \text{ with } i > j \qquad \textbf{(2.9),}$$

where $p_i(0)$ is the weight fraction of material in the mill less than size x_i at time 0;

$p_i(t)$ is the weight fraction of material in the mill less than size x_i at time *t*; and

B_{ij} is the cumulative mass fraction of particles passing the top size of interval *i* from breakage of particles of size 1.

An empirical model relating the cumulative breakage function to particle size has been formulated by Austin *et al*. (1984):

$$B_{ij} = \Phi_j \left(\frac{x_{i-1}}{x_j}\right)^{\gamma} + (1-\Phi_j)\left(\frac{x_{i-1}}{x_j}\right)^{\beta} \qquad \textbf{(2.10)},$$

where β is a parameter characteristic of the material used, the value of which is generally greater than 2.5;

γ is a material-dependent parameter, the value of which is typically found to be greater than 0.6; and

Φ_j is a material-dependent parameter representing the fraction of fines that is produced in a single fracture step. Its value ranges from 0 to 1.

Equation 2.10 conforms to mass balance considerations such that when a large particle breaks, the mass of the daughters produced adds up to the mass of the initial large particles.

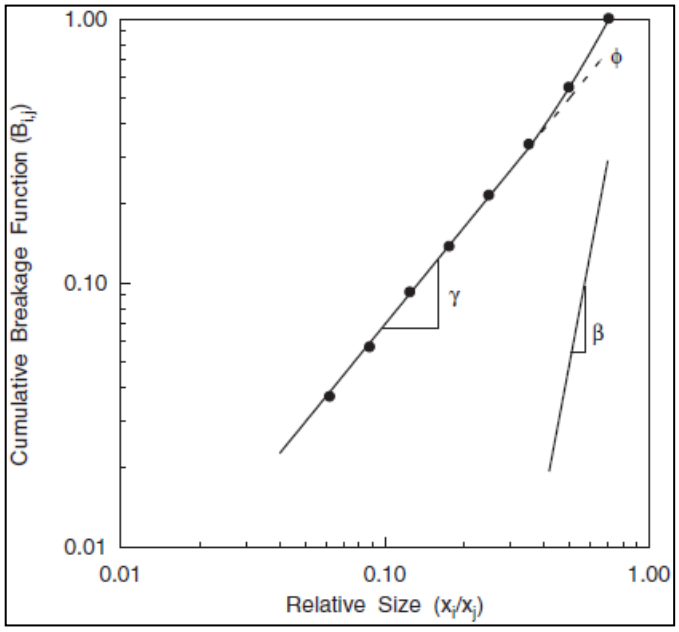


Figure 2.4 Breakage function of typical material (after Yekeler, 2007).

Model parameters (β, Φ_j, γ) define the distribution and the characteristic material properties of a given ore. The breakage distribution function can be considered as independent of the initial particle size (normalizable breakage function) where Φ_j is a constant, and not a function of the parent size j. Although this assumption is arguable in essence, it has proved acceptable for many materials and for simulation purposes (Austin *et al*., 1984; King, 2001).

2.2.3 Batch grinding equation

The batch grinding equation is formulated by using the concept of a size-mass balance, which is simply a rate-mass balance, on each particle size interval. The equation is primarily used to measure and characterize the material in terms of the breakage and selection functions, which in turn enable the investigation of the kinetics of the breakage. A procedure known as the one-size-fraction test is used to perform these tests in a laboratory mill (Austin *et al.*, 1984).

If a size-mass balance is performed for a particular size *i*, the rate of production of size *i* material equals the sum of the rate of appearance from breakage of all larger sizes minus the rate of the disappearance by breakage. This is symbolically expressed as follows (Austin *et al.*, 1984):

$$\frac{dw_i(t)}{dt} = -S_i.w_i(t) + \sum_{j=1}^{i-1} S_j.b_{ij}.w_j(t) \qquad \textbf{(2.11),}$$

where $S_j b_{ij} w_j(t)$ is the rate of appearance of size *i* material produced by the fracturing of size *j* material;

$S_i w_i(t)$ is the rate of disappearance of size *i* material by breakage to smaller sizes;

S_i is the selection function of the material considered to be of size *i*;

$w_j(t)$ is the mass fraction of size *i* present in the mill at time *t*; and

b_{ij} is the mass fraction arriving in size interval *i* from breakage of size *j*.

Equation (2.11) can then be used to predict the particle size distribution of the material being milled for any grinding time.

2.3 Population balance model applied to a continuous mill

Austin *et al.* (1984) were able to demonstrate that the population balance model applied to a steady state continuous plug flow mill with no classification at the exit discharge is similar to the batch grinding equation. Using this model when solving Equation (2.11), the size distribution of the product discharged after the mean residence time τ can be determined.

With the assumptions of plug flow and no size classification at the mill exit, if the initial feed is $w_j(0) = f_j$, and the final product is $w_i(t) = w_i(\tau) = p_i$, the general solution to Equation (2.11) is given by (Reid, 1965):

$$p_i = w_i(\tau) = \sum_{j=1}^{i} d_{i,j}(\tau).f_j \qquad \textbf{(2.12),}$$

where $d_{i,j}$ is physically interpreted as the fraction of feed size j transferred to size i in the product via the repeated steps of the breakage process over time τ. The set of $d_{i,j}$ values is the mill transfer function between feed and product. Austin *et al.* (1984) presented the following expression for the mill transfer function:

$$d_{i,j} = \begin{cases} 0, & i < j \\ e^{-S_i.t}, & i = j \\ \sum_{k=j}^{i-1} c_{i,k}.c_{j,k}.\left(e^{-S_k.t} - e^{-S_i.t}\right), & i > j \end{cases} \qquad \textbf{(2.13),}$$

$$\text{with } c_{i,j} = \begin{cases} -\sum_{k=i}^{j-1} c_{i,k}.c_{j,k}, & i < j \\ 1, & i = j \\ \frac{1}{S_i - S_j}.\sum_{k=j}^{i-1} S_k.b_{i,k}.c_{k,j}, & i > j \end{cases} \qquad \textbf{(2.14).}$$

Equations (2.12 – 2.14) provide a comprehensive expression of the relationship between feed and product on the assumptions that the mill is a plug flow mill with no classification at the exit discharge.

An analysis similar to that of a plug flow mill with no post-classification is also possible for the other simplified residence time distribution (RTD) model, that is, a steady-state, fully mixed, continuous ball mill. When they applied a size-mass balance to the latter flow model, Austin and Gardner (1962) derived the following:

$$p_i = f_i + \tau.\left(\sum_{\substack{j=1 \\ i>1}}^{i-1} b_{i,j} S_j w_j\right) - S_i w_i.\tau \qquad \textbf{(2.15).}$$

Equations similar to Equations 2.13 and 2.14 have also been proposed for a perfectly mixed mill with no post-classification. In this case, the mill transfer function is given by (Austin *et al.*, 1984):

$$d_{i,j} = \begin{cases} \dfrac{1}{1+S_j.t}, & i = j \\ \displaystyle\sum_{k=j}^{i-1} c_{i,k}.c_{j,k}.\left(\frac{1}{1+S_k.t} - \frac{1}{1+S_i.t}\right), & i > j \end{cases} \qquad \textbf{(2.16).}$$

$$\text{with } c_{i,j} = \begin{cases} -\displaystyle\sum_{k=i}^{j-1} c_{i,k}.c_{j,k}, & i < j \\ 1, & i = j \\ \dfrac{1}{S_i - S_j}.\displaystyle\sum_{k=j}^{i-1} S_k.b_{i,k}.c_{k,j}, & i > j \end{cases} \qquad \textbf{(2.17),}$$

Equations 2.18 and 2.19 below were proposed for a full-scale mill, which comprises one large fully mixed reactor followed by two smaller, equally fully mixed, reactors and a dead time with no post-classification:

$$d_{i,j} = \begin{cases} \dfrac{e^{(-S_j\tau_d)}}{(1+S_j.\tau_1)(1+S_j.\tau_2)^2}, & i = j \\ \displaystyle\sum_{k=j}^{i-1} c_{i,k}.c_{j,k}.\left(\frac{e^{(-S_k\tau_d)}}{(1+S_k.\tau_1)(1+S_k.\tau_2)^2} - \frac{e^{(-S_i\tau_d)}}{(1+S_i.\tau_1)(1+S_i.\tau_2)^2}\right), & i > j \end{cases} \qquad \textbf{(2.18),}$$

$$c_{i,j} = \begin{cases} -\displaystyle\sum_{k=i}^{j-1} c_{i,k}.c_{j,k}, & i < j \\ 1, & i = j \\ \dfrac{1}{S_i - S_j}.\displaystyle\sum_{k=j}^{i-1} S_k.b_{i,k}.c_{k,j}, & i > j \end{cases} \qquad \textbf{(2.19).}$$

2.4 Scale-up procedure for batch grinding data

The scale-up is done on material the properties of which are known, or the breakage and selection function parameters of which have been determined in the laboratory. In order to develop the scale-up successfully, it is necessary to distinguish between parameters that are material-specific and those that depend on

the conditions and geometrical scale of the mill that is to be used (King, 2001). The breakage function parameters do not need any scale-up if the material is considered to be normalisable, that is, if parameter Φ is constant for all breaking sizes. The empirical equations, which predict how the selection function values change with ball and mill diameters, ball filling, powder filling and rotational speed, are combined as follows (Austin *et al.*, 1984):

$$S_i(d) = a_T\left(\frac{x_i}{x_0}\right)^{\alpha} . \frac{1}{1+\left(\frac{x_i}{C_1\mu_T}\right)^{\Lambda}} . C_2 . C_3 . C_4 . C_5 \qquad \textbf{(2.20),}$$

where $C_1 = \left(\frac{D}{D_T}\right)^{N_2} . \left(\frac{d}{d_T}\right)^2$ **(2.21),**

$$C_2 = \left(\frac{d_T}{d}\right)^{N_0} \qquad \textbf{(2.22),}$$

$$C_3 = \begin{cases} \left(\frac{D}{D_T}\right)^{N_1} & , D \geq 3.8\,m \\ \left(\frac{3.81}{D_T}\right)^{N_1} . \left(\frac{D}{3.81}\right)^{N_1-\Delta} & , D < 3.8\,m \end{cases} \qquad \textbf{(2.23),}$$

$$C_4 = \left(\frac{1+6.6J_T^{2.3}}{1+6.6J^{2.3}}\right) . \exp\left[-c(U-U_T)\right] \qquad \textbf{(2.24),}$$

$$C_5 = \left(\frac{\phi_c - 0.1}{\phi_{cT} - 0.1}\right) . \left(\frac{1+\exp\left[15.7\times(\phi_{cT}-0.94)\right]}{1+\exp\left[15.7\times(\phi_c-0.94)\right]}\right) \qquad \textbf{(2.25).}$$

The subscript *T* refers to the laboratory test mill conditions and results, while a_T and μ_T are selection function parameters obtained from batch grinding data dependent on mill conditions, whereas N_0, N_1, and N_2 are parameters dependent on mill diameter: their default values are 1, 0.5, and 0.2 respectively. *J* is the fractional ball filling of the industrial mill whilst J_T is the fractional ball filling of the test mill. As for Δ, it represents the wear rate model for ball diameter. It has a value between 0 and 2, with 0.2 being Bond's default value (Austin *et al.*, 1984). Parameter *c* is used to account for the changes from dry to wet milling between laboratory and industrial mills. Austin *et al*. (1984) reported that a value of 1.32 was adequate when scaling up dry batch grinding results to wet full-scale milling.

Equations (2.20 – 2.25) enable one to predict the selection function of particle size class i for a given ball diameter d and a given geometry of the full-scale mill based on batch grinding results. This is known as the scale-up of batch laboratory data. Correction factors are also used: C_1 accounts for the change in mill diameter from a laboratory mill D_T to industrial mill D. Similarly, C_2 accounts for the change in ball diameter used during laboratory testing d_T to those balls actually used in the plant d. Coefficient C_3 accommodates the design of the mill; in other words, it adjusts the scale-up based on whether the industrial mill has a pancake or a tube design. Coefficient C_4 is an adjustment to the difference in slurry filling considered in the laboratory U_T and that used in the plant U. Finally, C_5 is the correction factor that allows for the mill speed to be changed from laboratory ϕ_{cT} to industrial ϕ_c.

Since a and μ depend on the conditions and the geometrical scale of the mill, their values have to be scaled up to the conditions of the mill to be simulated. The scaled-up value of a_T in Equation (2.26) for the new mill condition is a^*, and the conversion from test conditions to those in another mill is given below (Austin *et al*., 2007):

$$a^* = \begin{cases} a_T . \left(\frac{D}{D_T}\right)^{0.5} . \left(\frac{1+6.6J_T^{2.3}}{1+6.6J^{2.3}}\right) . \exp\left[1 - c.(U - U_T)\right] & , D \geq 3.8\,m \\ a_T . \left(\frac{3.8}{D_T}\right)^{0.5} . \left(\frac{D}{D_T}\right)^{0.3} . \left(\frac{1+6.6J_T^{2.3}}{1+6.6J^{2.3}}\right) . \exp\left[1 - c.(U - U_T)\right] & , D < 3.8\,m \end{cases} \quad \textbf{(2.26)}$$

In a similar fashion and for a different ball diameter, the value of μ^* is converted to the following (Austin *et al*., 2007):

$$\mu^* = \mu_T . \left(\frac{d}{d_T}\right)^{\eta} \quad \textbf{(2.27),}$$

where d_T is the diameter of the balls used in the laboratory mill; and

d is the ball diameter of the simulated industrial mill.

The exponent value η varies between 1 and 2 depending on the material used. Kelsall *et al.* (1967), for instance, proposed the value of 2 based on experiments

they did using quartz. Yildirim *et al.* (1999) later found the value of 1 was most suitable to simulate a quartz grinding circuit. Austin *et al.* (2006), on the other hand, used 1.2 in their analysis of an iron ore grinding circuit. By the same token, Austin *et al.* (1984) and Napier-Munn *et al.* (1996) both reported the value of 2 to be the best default value as far as η is concerned. It is also worth noting that Katubilwa and Moys (2009) found that $\eta = 2$ was a reasonable value for a South African coal tested in the laboratory.

2.5 Factors affecting the breakage rate

Grinding materials in a manner conducive to obtaining the desired product is the key to good mineral processing. The engineer who controls the milling operation therefore needs to strike a balance between reducing the size of the particles and minimizing over-grinding (to maximize efficiency). Under-grinding yields a product that is too coarse and has a degree of liberation too low to be economically feasible when the downstream separation process has been completed. Over-grinding, on the other hand, tends to reduce the materials below the size required for most efficient separation and additionally resulting in unnecessary waste of energy.

These considerations have prompted a number of researchers to investigate the milling process in detail, studying milling parameters such as ball size, slurry filling, residence time distribution, grinding media filling and media shape, and subsequently to make various recommendations to ensure the efficient operation of ball mills. These systematic studies were carried out by Kelsall *et al.* (1968 – 1973) and other pioneers in the field, whose recommendations established a basis that researchers such as Austin *et al.* (1984) and Yekeler (2007) have built upon by proposing models that describe the effects of typical grinding parameters on the milling process. In tumbling ball mills, the rate of breakage and overall mill performance are affected by fractional ball filling (J), fraction of critical speed (ϕ_c), fraction of the mill volume filled by powder (f_c), powder filling (U) and ball diameter. All of these factors are briefly discussed in the sections below.

2.5.1 Ball filling

Fractional ball filling (J) is conventionally expressed as the fraction of the mill volume filled by the ball bed at rest, assuming a formal bed porosity of 0.4. It can be expressed as:

$$J = \frac{\left(\frac{\text{mass of balls}}{\text{ball density}}\right)}{\text{mill volume}} \times \frac{1.0}{(1-0.4)} \qquad \textbf{(2.28).}$$

Shoji *et al.* (1982) proposed an empirical equation that relates milling rate to ball filling. The equation was produced using the results obtained from different researches on small mills with a fixed ball filling. Shoji showed that the effects of ball filling on milling kinetics could be expressed as follows:

$$S_i(J,U) \propto a \propto \frac{1}{1+6.6J^{2.3}}.e^{-c.U} \qquad \textbf{(2.29),}$$

where c is a constant, given the value of 1.32 and assuming $0.2 \leq J \leq 0.6$

The rate of breakage has been found to depend primarily on the grinding ball filling. As the mill rotates, the movement of the grinding media reaches a peak before the balls are either thrown into the air to fall freely, or tumble in a rolling motion on the surface of the bulk charge. In the former case, their motion is referred to as cataracting, whereas in the latter they are described as cascading. In general, during the course of milling, both cataracting and cascading will take place (Austin *et al*., 1984).

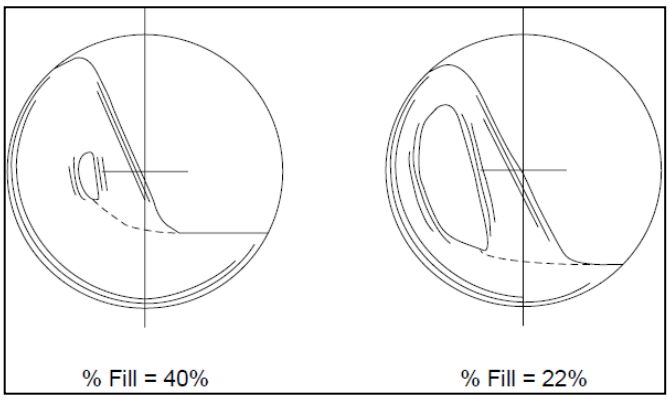


Figure 2.5 Illustration of the difference in load behaviour for different ball charge levels but rotating at the same mill speed (after Fortsch *et al.* 2006).

Fortsch *et al.* (2006) used Figure 2.5 to describe how the production rate is affected by an under-loading multiplier which is pronounced by the hole or gap in the middle of the charge as it is turned by the mill. His team reported that operating a ball mill at 75 % critical speed and a 22 % charge level creates a higher cataracting region than at 75 % critical speed and 40 % charge level. They also observed that cascading action provides the highest grinding efficiency because of the high total surface area exposed to contact. Finally, Fortsch and his colleagues argued that as the ball filling is increased, the breakage rate initially rises to a maximum and then decreases. This is on account of a widely held belief that as the mill draws maximum power, the rate of breakage also gets to maximum. That is why in practice, ball fillings usually range between 20 and 40 %; however with today's ball mills, 35 % charge fillings is considered to be ideal.

2.5.2 Mill filling by powder

The fraction of the mill filled by powder (f_c) is expressed as the function of the mill volume filled by the powder bed, using a formal bed porosity of 0.4. This is calculated by means of Equation 2.30. The fraction of the mill filled by powder (f_c) has to be determined for every mill operation in which a different J is used, since the mill should not be under- or over-filled. Under-filling the mill leads to energy wasted in steel-to-steel contacts, which produces little breakage, but instead, unwanted material wear. Over-filling the mill, on the other hand, leads to an effect called powder cushioning, which impedes the efficiency of the breakage action. That is why it is imperative to fill the mill with an appropriate volume of powder. The fraction f_c of the mill to be filled by powder can be calculated as follows:

$$f_c = \frac{\left(\frac{\text{mass of powder}}{\text{powder density}}\right)}{\text{mill volume}} \times \frac{1.0}{0.6} \qquad \textbf{(2.30).}$$

A similar definition applies to slurry, provided that density of powder in Equation 2.30 is replaced by an appropriate density of slurry.

In order to relate powder loading to ball loading, the formal bulk loading of powder is compared to the formal porosity of the ball bed (Austin *et al.*, 1984). This way, the notion of powder filling can be introduced, that is, the fraction of the spaces between the balls, at rest:

$$U = \frac{f_c}{0.4J} \qquad \textbf{(2.31).}$$

Austin *et al.* (1984) reported that powder fillings U between 0.6 and 1 will generally give the most efficient breakage in the mill. They attributed the small breakage rates obtained with a low powder filling to the little collision spaces between the balls that would be filled with powder. Austin and his team then demonstrated an improvement in breakage rates with an increase in powder, but a drop in breakage rates as the amount of powder filling was raised further. The explanation they suggested for the list of these findings was the expansion of the ball-powder bed to give poor ball-ball powder nipping collisions. Katubilwa (2012) recommended the operation of ball mills with a slurry filling of close to unity, based on the graphical analysis he had carried out on laboratory batch results. His conclusions complemented those of Latchireddi and Morrell (2003) and Tangsathitkulchai (2003), who proposed $U = 1$ as the way to ensure efficient milling. Katubilwa (2012) also suggested operating ball mills at high ball fillings with a slurry filling of unity as the way to guarantee efficient milling if the objective is to generate as much fine material as possible (that is, particles of less than 106 μm).

Shoji *et al.* (1980) used the results of different studies of small mills at fixed ball filling to propose an empirical equation that relates milling rate to powder filling:

$$S(U) \propto a \propto \left(2.80e^{-4.1U} + e^{-0.8U}\right) \text{ for } 0.3 \leq U \leq 2 \qquad \textbf{(2.32).}$$

The investigations done by Shoji *et al.* (1980 & 1982) of milling rate on dry milling and those conducted by Tangsathikulchai (2003) on wet milling demonstrated that ball filling and slurry (or powder) filling affect the milling rate regardless of whether milling is done dry or wet.

2.5.3 Critical speed

The critical speed of the mill is the theoretical rotational speed at which balls centrifuge on the mill case and do not tumble. This is given by:

$$\text{Critical speed } \phi_c, \text{ rpm} = \frac{42.2}{\sqrt{D-d}} \qquad \textbf{(2.33),}$$

where D is the internal mill diameter and d is the maximum ball diameter loaded into the mill, both expressed in metres.

The rotational speed of the mill is normally specified as a fraction of the critical speed ϕ_c. It has effect on the product size distribution and how fast shell liner wear. Shoji *et al.* (1982) found that the industrial mill rotational speeds in use were 70 – 80 % of critical speed for a ball mill with effective lifters. The typical operational philosophy is to run the mill at the speed at which the trajectories followed by the balls are such that the descending balls fall on the toe of the charge and not on the liners. This is attributable to concordant studies that demonstrated that low speeds give rise to abrasive grinding owing to the cascading of the balls, which in turn results in finer grinding and increased liner wear. At higher speeds, cataracting tends to dominate the grinding process, resulting in coarser end products and reduced liner wear. Further increase of the mill speed to close to 100 % leads to centrifuging; the media are carried around in an essentially fixed position against the shell (Wills and Napier-Munn, 2006). Figure 2.6 below illustrates the motion as the balls cascade and cataract inside the mill, and Figure 2.7 shows how the flow of media changes as the mill speed increases.

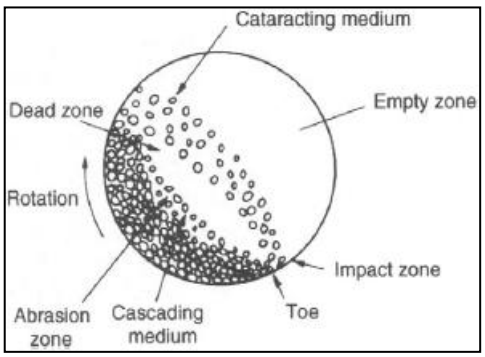


Figure 2.6 Motion of charge in ball mills (Wills and Napier-Munn, 2006).

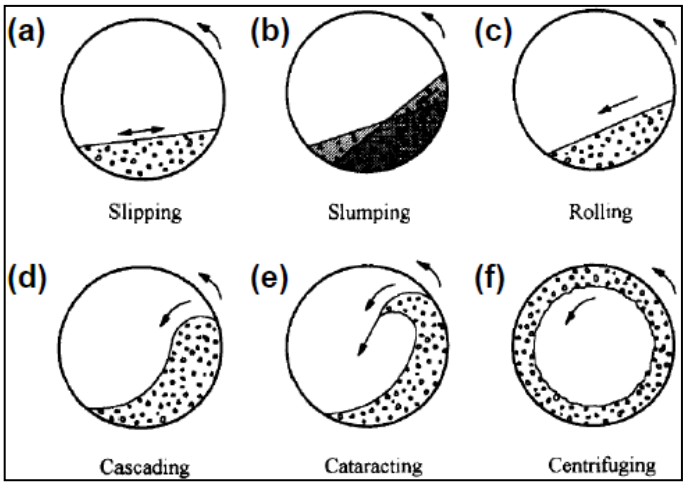


Figure 2.7 Ball mill flow regime as a function of increasing speed (after Boateng and Barr, 1996).

Austin *et al*. (1984) showed similarities between the variation of net power with mill speed and that of specific breakage rates with speed. He proposed an empirical model that relates the breakage rate of a narrow-sized feed S_i to the fractional speed of the mill, thus giving an indication of the effects of mill speed:

$$S_i \propto (\phi_c - 0.1)\left(\frac{1}{1+\exp[15.7(\phi_c - 0.94)]}\right) \qquad \textbf{(2.34),}$$

where ϕ_c is the fraction of the theoretical critical speed N_c of the mill.
This equation is valid only for mill speeds in the range $0.4 < \phi_c < 0.9$.

2.5.4 Ball diameter

A number of published research studies have shown concordance in finding that fine particles are ground effectively by small balls, because of the increase in the rate of ball-on-ball contacts per unit time (Austin *et al*. 1984; Napier-Munn *et al.* 1996; King, 2001; Katubilwa *et al.* 2009; Deniz 2012). Also, if a representative unit volume of the mill is considered, the number of balls in the mill increases, as $1/d^3$. On the other hand, larger balls have been found to do a better job as far as the milling of hard ores and coarser feeds is concerned, since high impact energy is required to break them (Napier-Munn *et al.*, 1996). Katubilwa *et al.* (2009) investigated the effect of media sizes on the breakage of coal, and found a

relatively small variation in breakage for large grinding media sizes, whereas grinding smaller media sizes increased the yield of fines.

Austin *et al.* (1984) used their findings from experiments he and his colleagues carried out on the dry grinding of quartz to show that the specific rate of breakage decreases as the ball sizes become larger. Small media are at present shunned in industry because of the cost, yet they offer the desired higher breakage rates. However, those ball sizes that ensure maximum grinding efficiency ought to be selected in view of the higher profits to be obtained from a better yield.

An empirical rule that relates the particle size x_m to the maximum ball diameter d has been proposed (Austin *et al.*, 1976 and Napier-Munn *et al.*, 1996) as follows:

$$x_m = K.d^2 \qquad \textbf{(2.35),}$$

where K is the maximum breakage factor, reported to be 0.7×10^{-3} for soft to hard materials by Austin's group and in the order of 0.44×10^{-3} by Napier-Munn's group and x_m is equivalent to the particle size at which maximum breakage occurs. Impact and attrition breakage mechanisms are assumed to predominate above and below sizes of x_m respectively.

In an empirical model that defines the variation in selection function with particle size (see Equation 2.5), parameter μ is a function of ball diameter. Since parameters Λ and α are constant for a given material, there is a relationship of proportionality between x_m and μ. This then implies that μ is a function of ball size, and gives an indication of the effectiveness of breakage of a given ball size (Austin *et al.*, 1984). The equation relating the value of x_m to μ is as follows:

$$x_m = \mu.\left(\frac{\alpha}{\Lambda-\alpha}\right)^{\frac{1}{\Lambda}}, \text{ on condition that } \Lambda > \alpha \qquad \textbf{(2.36).}$$

Kelsall *et al.* (1967/68) and Austin *et al.* (1984) proposed two equations to express the dependency of the breakage rate on the ball diameter. The set of correlations are given below:

$$a = a_0 \cdot \left(\frac{d_0}{d} \right)^{\xi} \quad \textbf{(2.37)}$$

$$\mu = \mu_0 \cdot \left(\frac{d}{d_0} \right)^{\eta} \quad \textbf{(2.38),}$$

where a_0 and μ_0 are the reference breakage parameters corresponding with the ball diameter d_0;

ξ and η are constant exponent factors; and

a and μ are the predicted breakage parameters for ball diameter d.

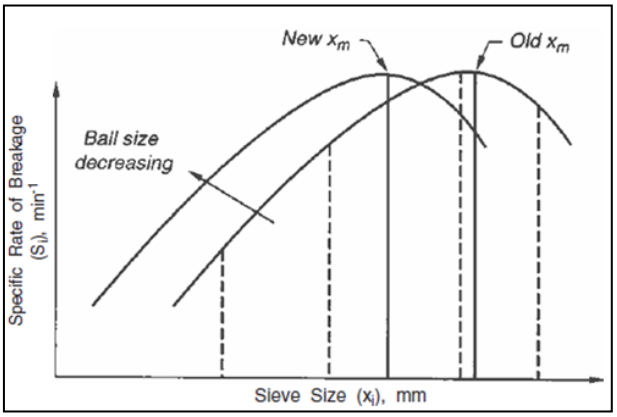


Figure 2.8 Variation of specific rate of breakage with ball diameter (Napier-Munn *et al.* 1996)

The effect of ball size on the selection function can be predicted by combining Equations 2.36, 2.37 and 2.38 as well as the correction factor in Equation 2.5. An example of the predictions is illustrated in Figure 2.8.

Austin *et al.* (1984) presented results which showed B_{ij} parameters (see Equation 2.10) as the function of ball size, taken from the dry grinding of quartz. The results showed that the parameter γ decreased with an increase in ball diameter of the media. The authors suggested that this trend was caused by the greater impact force of collisions involving larger balls, resulting in a higher proportion of fines. They also suggested that in an abnormal breakage, the value of γ decreases as the ball sizes increase for larger sizes to the right side of the maximum in *S*-values, and attribute it to the mean breakage action in this region caused by the chipping and abrasion of bigger components, leading to a relatively greater amount of fine material.

The breakage function parameter γ is an indication of the relative amount of fines produced from the breakage of the top size material, and relates to the efficiency of grinding. Higher γ means grinding is taking place at a slow rate and lower values indicate more effective breakage action with a high production of fines. Parameter Φ depends on the material used, and is the fraction of fines produced in a single fracture. Thus the lower specific rate of breakage found with larger balls is partially compensated for by the production of a higher proportion of fine fragments.

2.6 Axial flow through a ball mill

2.6.1 Residence time distribution

A continuous ball mill can be seen as a tubular reactor. One end of the tube is the inlet for the feed, while the other is the outlet through which the product is discharged. Depending on the feed flow-rate, the material in the mill may stay there for a longer period, undergo more breakage and hence come out finer. Alternatively, the material may flow quickly through the mill and not reach the degree of fineness required. It appears that the residence time (also called retention time) of particles is important for the characterization of continuous milling.

The residence time distribution (RTD) concept, first mooted by MacMullin and Weber in 1935 (Fogler, 1992), was then presented in a more definitive form by Dankwerts (1953) and further developed by other researchers (Austin *et al.*, 1983; King, 2001; van Nierop and Moys, 2002) to model the RTD of rotary mills. A brief explanation of RTD is a probability distribution function that describes the amount of time particles spends in the mill. It has proved an indispensable tool for charting the transport of material over a wide range of engineering processes.

Tracer response and salt tests are the RTD methods most commonly used. When a tracer is injected into the feed stream to the mill over a very short period, it is possible to monitor the concentration of traced material at the mill discharge outlet. While some particles may leave the mill almost immediately, others may

stay for longer. In statistical terms, this is known as a distribution of residence time. Figure 2.9 illustrates the tracer response of a typical ball mill from which the RTD can be inferred.

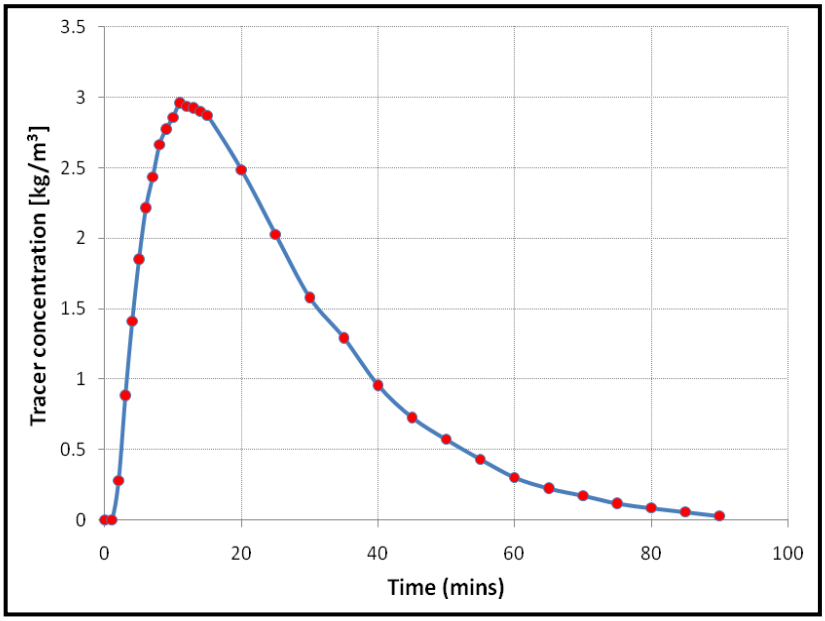


Figure 2.9 Example of tracer response of a full-scale mill: ball filling J = 25 % and slurry at 67.3 % solids concentration (after Makokha *et al.*, 2011).

The tracer concentration (in kg/m^3) is plotted in Figure 2.9 as a function of time (in minutes). The conversion of Figure 2.9 to an RTD profile is done by normalizing the graph with respect to the area under the curve. In other words, if $C(t)$ represents the tracer concentration exiting the mill at time t, the RTD can be defined as follows (Levenspiel, 1971):

$$\varepsilon(t) = \frac{C(t)}{\int_{t=0}^{+\infty} C(t).dt} \qquad \textbf{(2.39).}$$

It is also common to represent the RTD as a cumulative plot of the total fraction of the tracer $E(t)$ that has left the mill, graphed against time t. Symbolically, this is given by the equation:

$$E(t) = \int_{t=0}^{t} \varepsilon(t).dt \qquad \textbf{(2.40).}$$

Perhaps the most important point to make is that the mean residence time τ can be determined from the cumulative RTD plot. It represents the average time spent by particles inside the belly of the mill:

$$\tau = \int_{t=0}^{+\infty} t.\varepsilon(t).dt \qquad \textbf{(2.41).}$$

2.6.2 Simplified flow through a ball mill

One of the simplifying assumptions concerning the flow of material through the mill is to consider particles as behaving on a first-in-first-out basis (that is, the particles that come in first also leave the mill first). It is therefore logical to say that all particles spend the same amount of time inside the mill, counted from the moment at which they enter. There is also no forward or backward mixing as the material moves along the mill. Such a model of flow is referred to as a plug flow. It is understood that all traced feed will exit the mill after the mean residence time τ. This can be expressed as follows:

$$E(t) = \begin{cases} 0 \text{ for } t < \tau \\ 1 \text{ for } t \geq \tau \end{cases} \qquad \textbf{(2.42),}$$

where $E(t)$ is the cumulative fraction of traced feed that has emerged at time t after it has been fed into the mill, and τ is the mean residence time.

At the other extreme is a fully mixed ball mill, which is assumed to mix the traced material into the bulk of the charge immediately. The RTD of a perfectly mixed mill is therefore given by:

$$E(t) = 1 - \exp(-t/\tau) \qquad \textbf{(2.43).}$$

The mean residence time τ is here defined by W/F, with W being the mass of powder material in the mill (also called the hold-up of the mill) and F the feed rate.

The three models of mill transportation most widely used in the description of the flow of material through a ball mill are illustrated in Figure 2.10. Note that the

flow model of a real full-scale mill is intermediary between two extremes: the plug-flow and the well-mixed distributions.

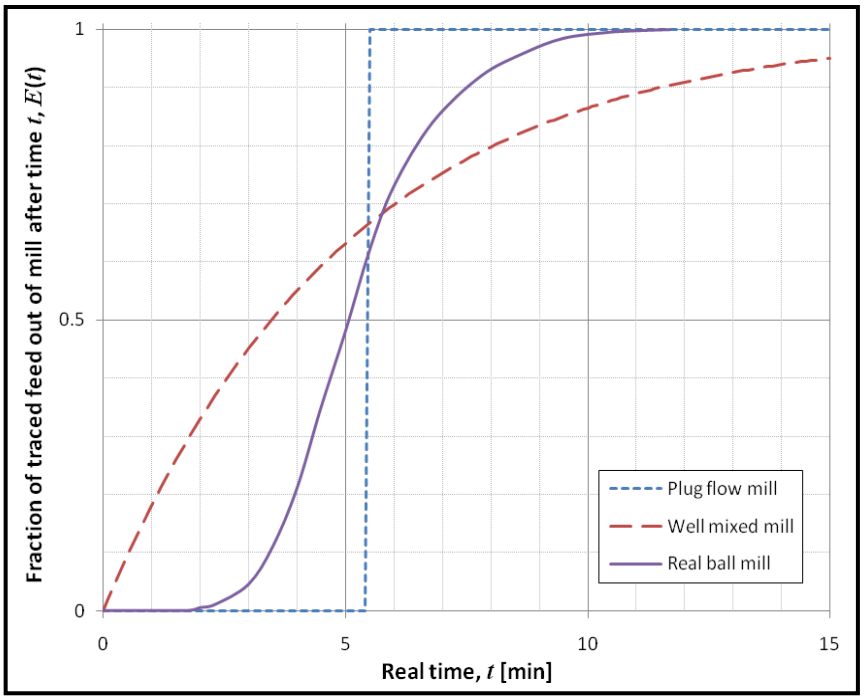


Figure 2.10 RTDs of a plug-flow, a perfectly mixed and a real ball mill.

2.7 The Attainable Region technique

In 1997, Glasser and Hildebrandt proposed the Attainable Region (AR) as a new way of analysing reaction systems in chemical engineering. The tool worked well on the laboratory and pilot scales. Then, appreciating the similarities between comminution and chemical reactions, Khumalo *et al.* (2006 – 2008) extended the AR technique to comminution process studies. Since then, AR analysis has been successfully used to optimize comminution of different types of ore in the laboratory. It is a flexible tool used for graphical analysis of data. It overlooks milling parameters but instead focuses on the fundamental breakage process and determines the set of all achievable distributions under the process conditions. This provides the designer with the best pathway to achieving a specific objective function from the system feed (Khumalo *et al.*, 2006).

The power of AR lies in its ability to define process targets accurately, which in turn permits the engineer to measure the actual process efficiency against a theoretical target. Khumalo *et al.* (2006) were able to validate their AR predictions by showing a good fit between their calculations and their experimental results. They then investigated the theoretical implications of their basic model for different specific energy inputs (Khumalo *et al.*, 2007), and successfully used AR analysis to optimize milling circuits that also include classification of particle sizes (Khumalo *et al.*, 2008). The main focus of the work done by Khumalo and his colleagues (2006 – 2008) was on achieving a desired product with an optimal use of energy. Metzger *et al.* (2009) used the same AR analysis technique, but applied it to a different parameter – optimizing the total time of operation. They found that the AR could be used to determine optimal polices to reduce milling processing time. Katubilwa *et al.* (2011) also used the AR to analyse the effect of ball size on milling, based on the experimental data they had collected from milling coal. They confirmed the generally accepted trend that grinding balls of small diameter tend to promote the production of fine particles at a higher rate than can be achieved by large balls.

As has been shown above, a considerable amount of work has been done by researchers in the Centre of Materials and Process Synthesis (COMPS) at the University of the Witwatersrand over the last eight years to apply the AR methodology to comminution processes. The more detailed examples of its use given below start with the demonstration by Metzger *et al.* (2009) that from the grinding of a single charge constituting single size class feed for different grinding durations, it is possible to generate product size distributions for those grinding times and to develop grinding profiles for each size class produced. Figure 2.11 below is an illustration of how experimental data can be represented for both cases. The grinding profiles can then be grouped into mass fractions m_1, m_2 and m_3, where m_1 is termed the feed size class, m_2 the middling size class and m_3 the fines size class. The margins of the mass fractions are dependent on the objective function to be achieved. For example, if we consider m_1 to consist of size class 1 and 2, m_2 to be made of size class 3 and 5 while size class 6 constitutes m_3, we can clearly define our objective function.

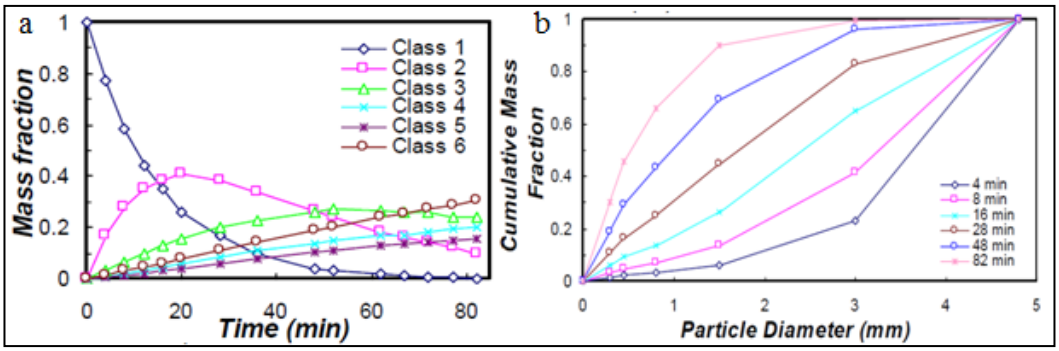


Figure 2.11 (a) Grinding profiles of all six class sizes versus time. (b) Cumulative mass fraction versus average particle size (Metzger *et al.* 2009).

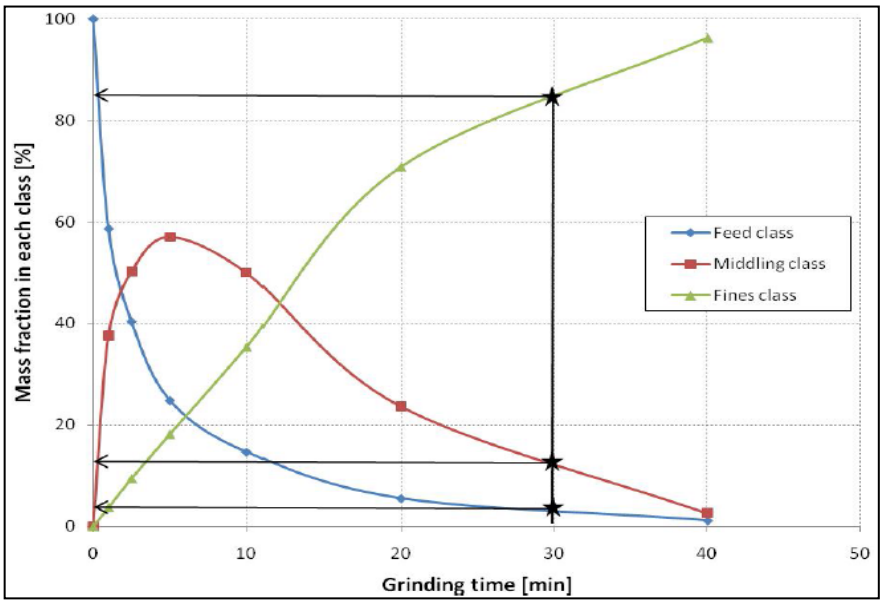


Figure 2.12 Grinding kinetics as plotted for the three size classes m_1, m_2 and m_3 (Katubilwa *et al.*, 2011).

Figure 2.12 illustrates the mass fractions of m_1, m_2 and m_3. If the objective is to maximize the production of the middling (m_2), then from the AR analysis illustrated here, we can interpret the graph to determine the optimal grinding time. We can then extend this analysis to compare the discrete maxima of m_2 obtained under different specified operating conditions. An example of different maxima of m_2 obtained with dissimilar media charges (J) at a single speed is illustrated in Figure 2.13.

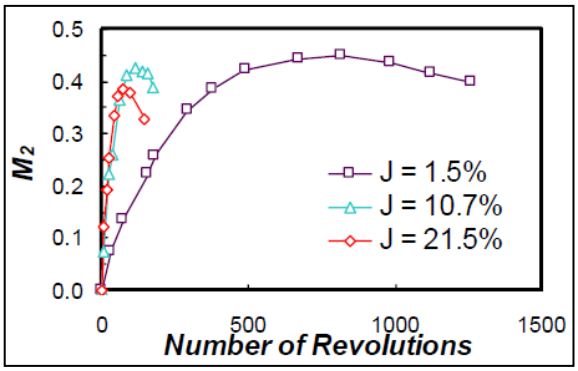


Figure 2.13 Mass fraction of size class two versus number of revolutions (Metzger *et al.*, 2009).

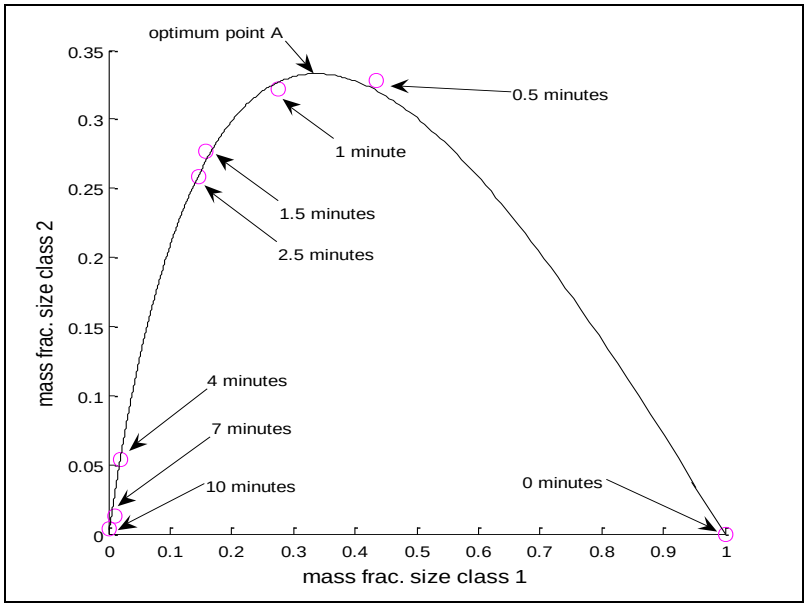


Figure 2.14 Representation of particle size distributions as a single trajectory in the AR space (Khumalo *et al.*, 2007).

Now that mass fractions at different grinding times have been clearly explained, the next step is to present the data in a final AR format. Figure 2.14 shows how particle size distributions (PSD) can be connected with grinding time. In this plot, the boundary curve describes the processes used, and can be interpreted in terms of pieces of equipment (implicitly identifying the equipment required for best performance). The turning point of the curve isolates an optimum solution when the objective is to maximize the mass in size class 2 (m_2). This solves the optimization problem, and provides the process control policy needed to achieve that objective.

2.8 Optimal floatable particle size

Flotation is widely used for physically separating particles that are hydrophilic and that are hydrophobic. The ability of air bubbles to selectively adhere to specific hydrophobic mineral surfaces in a mineral/water slurry allows them to be removed from the slurry phase and recover them in the froth phase.

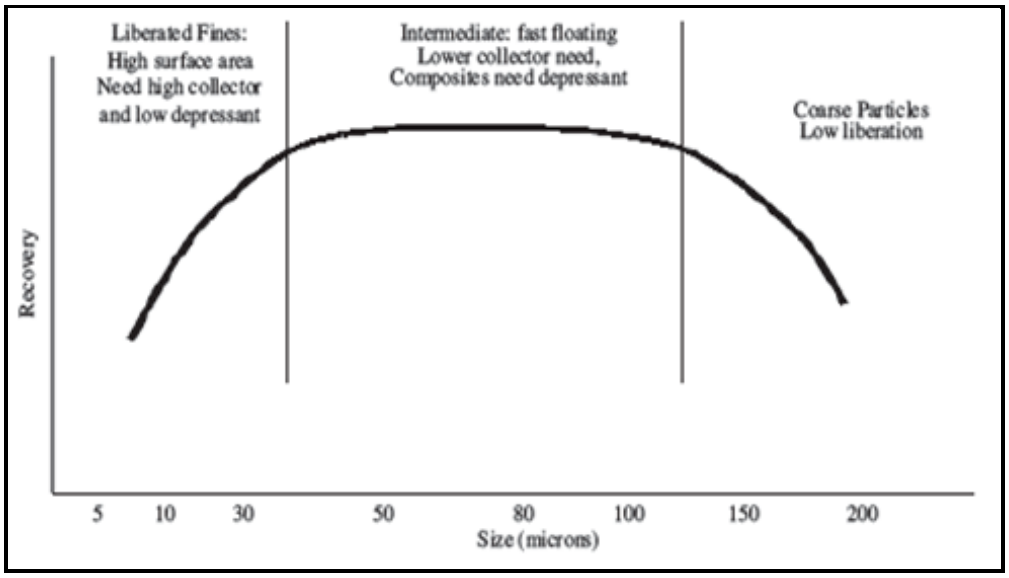


Figure 2.15 Typical flotation size/recovery curve (Rule and Anyimadu, 2007).

The first detailed study of the effect of particle size on flotation was done by Gaudin *et al.* (1931) who found that the best recoveries of lead, zinc and copper sulphides were obtained for particles with diameters between 10 – 50 µm. Recovery falls sharply above 100 µm, but only gradually below 20 µm, as shown in Figure 2.15. Using other mills and laboratory tests, Trahar *et al.* (1975) concluded that recovery is best for particles of an intermediate size. Rule and Anyimadu (2007) showed that with the flotation equipment currently available, 10 µm for PGM ore can float very well. These authors announced that work was in progress to identify better ways of improving ultra-fine flotation (for particles of less than 5 µm), but until that has been achieved, engineers will have to control milling to maximize the production of the intermediate size, with 9 microns as the lowest allowable size.

Because PGMs require fine grinds to liberate the maximum amount of valuable components (Rule, 2008), the fine size of the resultant particles (less than 10

microns) and gangue association poses processing challenges (Cramer, 2001). Over-grinding leads to a reduction in the amount of platinum group minerals recovered (Bryson, 2004), and sets a physical constraint on the flotation of fines, owing to the energy requirements necessary to enable a very small particle to attach to a bubble.

Decreased recovery in the fines region is attributable to a lower probability of particle-bubble collision, since viscous and electrostatic forces have a strong influence on ultrafine particle attachment. The low flotation rates in this region will largely dictate the total retention time required (which has to be borne in mind by the designer of the circuit). Particle recovery by water entrainment is also a factor in the fine size range.

Particles in the intermediate size range are the most readily floated. The relative position of the highly floatable size range for two minerals with different degrees of hydrophobicity is a key factor in selective floatation. Lower recovery in the coarse region may be related to floatation kinetics as a function of particle size itself, but it is also in this region that the locking of mineral gangue is most probable (McIvor *et al.*, 1990). McIvor and his co-researchers pointed out that the relationship between floatation performance and particle size itself can be used as a basis for both technical and economic analyses of plant performance.

2.9 Power draw in ball mills: The Morrell model

Mill power has attracted a great deal of attention over the past century, since it is one of the parameters that determine the feasibility of any mineral processing plant. Interpretation of the load behaviour enabled Hogg and Fuerstenau (1972) as well as Arbiter and Harris (1982) to propose mill power equations. Moys *et al.* (1996) proposed mill power relations based on the torque-arm approach, which can be used for different shapes of the load. In this approach, the shape of the load is considered as a rigid circular segment inclined at an angle equal to the dynamic of repose of the mill load, from which the centre of gravity is determined. The

torque of the load at the centre of the rotation of the mill is then calculated, which in turn can be used to determine the mill power.

The torque-arm approach considers the load as locked in a circular segment, which many other researcher considered a shortcoming. Moys (1990) and Fuerstenau *et al.* (1990) proposed semi-phenomenological models in which the former proposed the division of load into cascading and centrifuging fractions, while the latter suggested dividing the load into cascading and cataracting fractions. These models are based on a mechanistic description of the load behaviour in conjunction with physically meaningful milling parameters that have been determined through the empirical results of experiments (Wills and Napier-Munn, 2005).

Morrell (1993) proposed an energy balance approach which enabled him to develop a power model based on the motion of the charge. This model proved superior to the earlier empirical models. He formulated the power draft of the mill as given by:

$$P_{net} = 2\pi gL\rho.\int_{r_i}^{r_m} dr.\int_{\theta_T}^{\theta_S} N_r.r^2 \cos\theta.d\theta \qquad \textbf{(2.44),}$$

where r_i is the inner radius;

r_m is the mill radius;

θ_S is the shoulder angle in radians;

θ_T is the toe angle in radians;

N_r, is the angular speed of upward- and downward-moving balls;

L is the length of the mill; and

ρ is the bulk density of charge.

Integrating Equation (2.44) to find a mathematical expression of the net power while considering the crescent shape and velocity of the load, Morrell (1993) came up with the following power model, which is applicable to both grate and overflow discharge mills:

$$P_{net} = \frac{\pi g L N_m r_m}{3(r_m - z r_i)}\left[2r_m^3 - 3z r_m^2 r_i + r_i^3(3z-2)\right]\times\left[\rho_c(\sin\theta_S - \sin\theta_T) + \rho_p(\sin\theta_T - \sin\theta_{TO})\right] + L\rho_c\left[\frac{N_m r_m \pi}{(r_m - z r_i)}\right]^3\left[(r_m - z r_i)^4 - r_i^4(z-1)^4\right] \quad \textbf{(2.45),}$$

where ρ_p is the density of the slurry;

ρ_c is the average density of the grinding charge;

θ_{TO} is the slurry toe angle for overflow discharge mills, which will be equal to θ_T for grate discharge mills;

r_m is the internal radius of the mill;

r_i is inner surface radius charge, which marks the boundary between the active part of the charge and the inactive kidney-shaped media charge;

$z.r_i$ (the product) is the normalised radial position corresponding to the first inner concentric layer of the charge which is entrained by the mill, determined from photographs of the mill charge in motion. The z parameter was found to be a function of the fractional mill filling J_t. The definition of z is established in such a way that as J_t increases, z tends to zero and hence the rotational speed at any radial position r, that is, N_r tends to N_m;

N_m is the rotational speed of the mill in revolutions per second;

L is the length of the mill; and

g is the constant of gravity.

The Morrell model is adequate, especially for ball mills, which are operated at speeds where there is no centrifuging.

2.10 Net power draw and milling efficiency

Austin *et al*. (1984) presented a typical variation of the net power required to turn the mill with rotational speed. The results showed that the work input to the mill increases linearly with the rotational speed to a point at which the maximum power draw is reached. A further increase in rotational speed leads to a reduction in power, as the mill starts to centrifuge. The maximum power is usually found in

the range of 70 – 80 % of critical speed (Wills and Napier-Munn, 2005), or 70 – 75 % for mills of large diameter with a full ball loading ($J \approx 40$ %) (Austin *et al*., 1984). This made it possible for engineers to use speed to modify mill power, especially in the case of dry grinding, where the effect of powder filling is insignificant. For wet milling, Tangsathitkulchai (2003) showed that mill power rises steadily with an increase in slurry filling, and reaches a maximum at a slurry filling of approximately 1.0 before starting to decline. Katubilwa (2012) used kinetic milling profiles (AR graphs that show the evolution of mass fraction in each class in relation to the energy consumed) to investigate the effect of powder filling on mill power. He found that a powder filling of $U = 1.5$ achieved the maximum desired size class (-75 +9 μm) at a lower energy input than $U = 3.0$.

Metzger (2011) used the AR to investigate the effect of media size on energy, and showed that smaller media require much more energy while producing a smaller amount of product in the desired size class. He recommended the use of larger media under optimal conditions for industries where energy saving is a primary concern. He also showed that less energy is used when operating on larger amounts of grinding media (higher J) than smaller amounts, although it does not obtain as much of the desired product as when the combination of larger grinding media, at the slowest rotation and lower J, is used.

2.11 Classical configuration of milling circuits

Milling circuits play an important role in achieving desired product size distributions and product properties since it has a direct link to the energy consumption of the whole process. The production chain can be made up of grinding mills connected to classifiers. The way in which the grinding mills and classifiers are connected determine the type of a circuit they form. There are generally four single stage circuits (Austin *et al.*, 1984) used in practice:

- Grinding circuits employing mill in an open circuit
- Normal closed circuit
- Reverse closed circuit
- The combined closed circuit

Figure 2.16 is an illustration of a combined closed circuit in which all the circuit feed material is subjected to the classification action before entering the mill. The course product from the pre-classifier is the actual make up feed G to the mill. The undersize by-passes the mill and flows into the circuit product. The makeup feed G is milled and flows out of the mill as the mill product and subjected to the second classification in the post-classifier. The coarse particles from the post-classifier is fed back to the mill and is mixed with feed G before being subjected to the milling action again, while the undersize size product flows into the circuit product stream (Austin *et al.*, 1984).

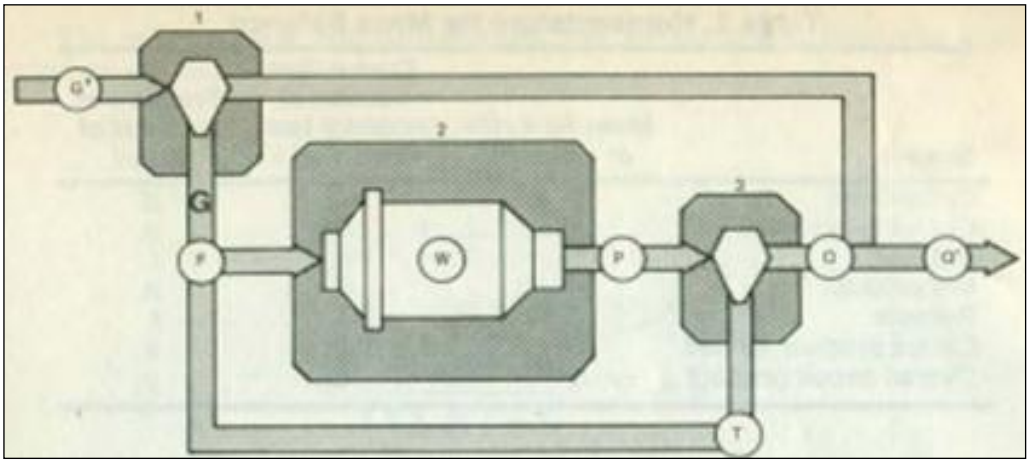


Figure 2.16 The combined closed circuit (from Austin *et al.*, 1984).

Depending on the presence of the first classifier, the second, or both as well as their corresponding loops (streams), the combined circuit can reduce to an open, a normal closed, or a reverse closed circuit. In the case of an open circuit, the mill is operated without being directly influenced by a classifier. The normal closed circuit does not have the first classifier and therefore the make-up feed G is the actual feed stream. Conversely, the reverse closed circuit keeps only the first classifier. There are advantages and disadvantages associated with each specific configuration. Suffice it to say that the general motivation is to optimise the production of material of a specified fineness of a grinding mill hence the desire to limit this study to an open circuit.

2.12 Summary

In this chapter, the mathematical models that best describe the breakage process in mills were reviewed. Because of its simplicity and flexibility, the population balance model is applied in most comminution processes and is the preferred method for our investigations. The model is based on defining two fundamental concepts: the selection function and the breakage function. The empirical description of the two concepts has shown that four selection function parameters and three breakage function parameters are required to predict mill product size distribution, which in turn can be used to set the operating conditions of the mill as well as the objective function to be optimized.

The attainable region, which complements the analysis of milling by the PBM framework as a graphical technique, was also reviewed in this chapter. The success of subsequent research work applying AR methods to comminution has shown that the AR is a novel analysis technique that can be used to optimise laboratory scale milling. However, it is generally believed that at this stage, the AR technique is not sufficiently robust to be applied to industrial milling.

It was also apparent from the background information given that the milling of PGM ore to achieve the product size which ensures maximum recovery during flotation is a challenge. This makes further study of the situation difficult since competition among the various processing industries has severely restricted the amount of scientific information concerning PGM available. As a contribution towards alleviating this problem, information is provided in this thesis that can be used for simulation and optimization purposes, which in turn will lead to further development in the milling of PGM ores. Greater recognition of the AR technique as the tool of choice in the analysis and optimization of mineral processing circuits is expected to result from this study, which will use the AR and PBM approaches in a complementary fashion to ascertain the operating conditions under which a preselected industrial mill will be able to optimize product size distribution for flotation purposes.

Chapter 3 Experimental programme, equipment and simulation strategies used

3.1 Introduction

In this chapter, the experimental methods and simulations used to fulfil the objectives of this investigation are set out. The information provided comprises a description of the laboratory mill used for batch testing, the experimental conditions, and, after that, the details of the experimental design, the materials used and the procedures followed.

The experimental programme consisted of feed sample and ball size preparation, batch grinding tests and particle size analysis. All of the milling runs were performed in a dry environment.

3.2 Experimental equipment and programme

3.2.1 Description of the laboratory grinding mill

During the first part of the experimentation, the milling kinetics of PGM ore were examined in order to determine the breakage and selection function parameters that would later be used for modelling purposes. All the batch grinding tests on the ore were carried out on a laboratory scale batch mill in the Department of Chemical Engineering at the University of the Witwatersrand. Figure 3.1 is a photograph of the mill set-up.



Figure 3.1 View of the laboratory ball mill.

The laboratory batch mill is installed on a steel structure that also carries all the control and measurement facilities required to run the mill. Manipulation of the mill speed is achieved through an electronic speed meter that enables one to set and control the motor speed. The power of the mill can be measured through a load beam that converts the force exerted onto it into the corresponding voltage. One of the ends of the load beam is attached to a piece of rod which generates a force attributable to the rotational torque of the mill. The mill is fitted with eight symmetrically-spaced lifters (see Figure 3.2), and is driven by a variable speed motor. The internal dimensions of the mill are given in Table 3.1, along with the test conditions.

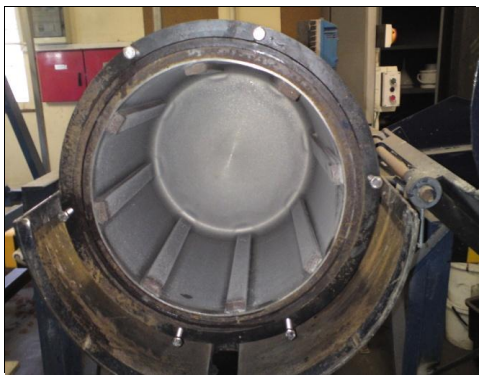


Figure 3.2 Picture of the laboratory grinding mill used for the experiments.

Table 3.1 Specifications of the mill

Mill dimensions	Diameter Length Volume	0.302 m 0.282 m 19.493 litres
Liner configuration	Number Dimensions	8 0.013 m height 0.025 m width 0.272 m length
Test conditions	Ball filling, J_T Powder filling, U_T Mill filling, f_c Mill speed, ϕ_{cT}	20 % 0.75 0.06 75 % of critical speed

$$J = \left[\frac{\frac{mass\ of\ ball}{ball\ density}}{mill\ volume}\right] \times \frac{1.0}{0.6} \qquad f_c = \left[\frac{\frac{mass\ of\ powder}{powder\ density}}{mill\ volume}\right] \times \frac{1.0}{0.6} \qquad U = \frac{f_c}{0.4\ J}$$

The latter are classically defined as follows. The ball filling (J) is conventionally expressed as the fraction of the mill volume filled with grinding balls at rest while assuming an average bed porosity of 0.4. The mill filling (f_c) is represented as the fraction of the mill volume filled by the powder bed, using a formal bed porosity of 0.4. The powder filling (U) is the fraction of the spaces between the balls at rest that is filled with powder. These definitions and the corresponding formulas, which are shown below in Table 3.1, were used to make the calculations necessary before the laboratory tests could be carried out.

3.2.2 Laboratory testing protocol

The experimental programme to investigate the millings kinetics of PGM ore was conducted using a combination of mono-sized balls and narrow-sized feed sizes, as shown in Table 3.2. Dry milling was done in all the experimental tests, which were carried out with a ball filling of J_T = 20 %, a powder filling of U_T = 0.75, and a mill speed ϕ_{cT} = 75 % of critical speed.

Table 3.2 Experimental design

Feed size in μm		Ball diameter d_T		
Upper size	Lower size	10 mm	20 mm	30 mm
850	600	x	x	x
600	425	x	x	x
425	300	x	x	x

3.3 Feed material preparation

The platinum ore used in this work was obtained from the feed to the secondary mill of the Anglo Platinum Waterval mine in the Republic of South Africa. The mine's internal reports indicate that the ore has a density of 3.47 g/cm^3. The platinum ore was collected in batches of 10 kg bags and was split using a Jones riffler in order to obtain a representative sample for use. The individual samples generated from that exercise were then mixed to a large feed sample

After collecting the feed sample, the moisture content was determined by drying a 500 g sample of the platinum ore at 50˚C in an oven overnight. When the difference in weight before and after drying was measured, the moisture content was found to be 1 %.

The next step was to prepare narrow-sized feed samples for batch testing: -850 +600 μm; -600 +425 μm and -425 +300 μm from the -1200 μm sample that was received. Following this, three sizes of grinding media were prepared: 10 mm, 20 mm and 30 mm in diameter. In each case, the mass of the grinding charge was fixed at 17840 g which represents a ball filling J_T of 20 %. A series of batch milling tests were then carried out under different conditions, in order to characterize the breakage properties of the platinum ore fully. More detailed description of the experiments is covered in the following sections.

3.3.1 Feed preparation

The specifications of the mill given in Table 3.1 were used to determine the amount of material needed per test. It was found that a feed sample of 2.771 kg for a density of 3.47 g/cm^3 was required for all the tests. This mass of powder was

calculated for a fractional interstitial filling U_T = 0.75 and a load porosity $\mathcal{E}_L$ = 0.4, which led to the determination that a mass of 17 840 g of steel grinding media and 2 771 g of ore would be loaded per run. The mill speed was set at 75 % of critical speed. (The theoretical critical speed was approximately 59.7 rpm.)

Three narrow-sized feeds were prepared from the feed material with particle size range from below 25 µm to 2000 µm in the following classes (-850 +600 µm, -600 +425 µm and -425 +300 µm). For each size class, 15 kg of material was initially prepared. Then, 2 kg from every 15 kg platinum ore batch was sieved for 50 min in order to ensure that each mono-size feed contained uncontaminated particles within its size class. The above screening time of 50 min was established by sieving 500 g of the platinum ore for 60 min, and stopping at 10-minute intervals to determine the changes in mass retained on the screens of interest. As shown in Table 3.3, the screening time, that is, the time at which the mass stopped changing, was found to be 50 min.

Table 3.3 Mass retained on each sieve at different times

Size	Sieving Time (min)					
	10	20	30	40	50	60
850 µm	46 g	44 g	43 g	43 g	42 g	42 g
600 µm	47 g	46 g	46 g	46 g	46 g	46 g
425 µm	87 g	86 g	86 g	85 g	85 g	85 g
300 µm	75 g	75 g	75 g	75 g	75 g	75 g
pan	246 g	249 g	250 g	251 g	252 g	252 g

Fractions of the platinum ore retained on the screens of interest were stored in appropriately labelled plastic bags. Finally, three samples from each batch of narrow-sized feed material were prepared by splitting the ore using a Jones riffler to make 2 771 g representative feed platinum ore samples ready for batch tests. In total, nine feed samples were prepared; for experiments involving three media sizes as shown in Table 3.2.

3.3.2 Preparation of the grinding balls

The breakage characteristics of the platinum ore were determined using the single ball sizes listed in Table 3.4, which also gives the number and sizes of the balls. Mono-sized grinding media were prepared by sorting the spherical steel balls to predefined size intervals in order to make up the desired quantity.

Table 3.4 Mono-size media charges used

Ball size d_T	Number of balls	Total mass (kg)
10 mm	4 441	17. 8
20 mm	510	17. 8
30 mm	150	17. 8

3.3.3 The batch grinding tests

The experiments were performed in batch mode, using a one-size fraction method (Austin *et al.*, 1984). The feed material was ground for a total of 30 min in all tests. Per batch run, the grinding was interrupted at 0.5, 1, 2, 4, 8, 15 and eventually 30 min intervals. After each interruption, a full-size distribution of the mill product was measured and the material was re-introduced into the mill after the sample was analysed.

Before each batch test, a blank sieving test was carried out on the prepared feed material, after which he loaded the sample to be milled into the mill with media of the appropriate size and weight. The mill was then run and the material milled for 30 seconds and stopped in order to do particle size analysis. The mill powder was offloaded, then split, so as to obtain a representative sample of the mill content. The ground product was removed, then by appropriate sampling technique (using a splitter) a representative sample of the mill content was obtained for sieve analysis.

The representative sample was later used for size analysis after the laboratory procedure described in the next section had been completed. After size analysis, the fractions retained on the sieves were weighed. The fractions were recombined and added back to the mill with rest of the unscreened sample for the next milling

interval. This procedure was repeated until the grinding routine mentioned above was completed.

3.3.4 Particle size analysis

A complete size analysis of a sample of platinum ore collected from the mill was carried out using a nest of sieves arranged according to $\sqrt{2}$ screen sequence with the top sieve being 850 µm. The following sieves were used: 850, 600, 425, 300, 212, 150, 106, 75, 53, 38 and 25 µm. The minus 25 µm were collected in a bottom pan.

Before sieving, a test was conducted to determine the optimum screening time that would enable the material to be screened without the retention of fines on the coarser sieves (contamination) or over-sieving, which would lead to pre-breakage of the material before the milling had taken place. Having determined the optimum sieving time, a 100 g sample of platinum ore from the mill was dry screened for 50 minutes, and after that, each sieve was weighed to ascertain the mass of material retained. The sieves were then restacked in order, but without a pan at the bottom, and wet washed to recover the residue dust on each screen. The washed through sample was dried in the oven at 50˚C. Then, the dried material was weighed and the recorded weight added to the -25 µm pan fraction.

The process described above for all the grinding experiments were repeated. The same nest of sieves was used throughout the experiments in the interests of maintaining consistency. The masses of material on each sieve were added together, and the total sum was subtracted from the initial mass of the sample before the wet sieving had taken place. The difference in mass was added to the mass of materials in the pan to achieve mass balance.

3.3.5 Data collection and processing

Raw data collected from the experiments were used to determine the breakage function parameters (β, γ, Φ from Equation 2.10) and the selection function parameter (α from Equation 2.6) by means of the progeny fragment distributions

from the breakage of the mono-size classes -850 +600 µm; -600 +425 µm and -425 +300 µm.

3.4 Estimation of the breakage characteristics of the ore

A Matlab® code was written to execute the population balance model and the relevant equations discussed in chapter 2 were incorporated in the scheme. All three breakage function parameters (β, γ and Φ from Equation 2.10) as well as one selection function parameter (α from Equation 2.6) were the input parameters determined from the experimental tests. The remaining selection function parameters (a_T, Λ and μ_T from Equation 2.2) were estimated by letting the simulator search for the best combination of all the parameters that is most successful in minimizing the sum of squared errors between the predicted and experimental product size distributions. Once the parameters were determined, it was possible to predict product size distribution for any given grinding period. A flow sheet for the scheme is shown in Figure 3.3 below

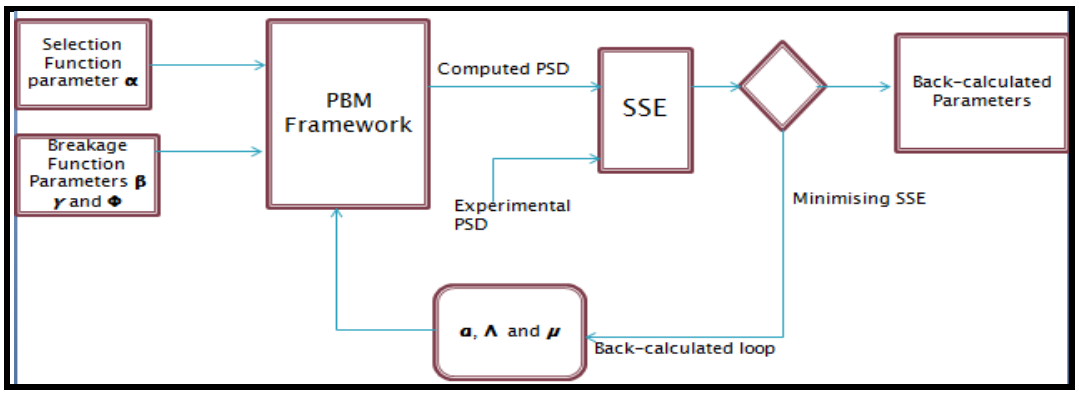


Figure 3.3 Diagrammatic representation of the simulator used.

The calculation procedure makes use of the Matlab® function "fmincon" which uses a sequential quadratic programming method. This function basically solves a quadratic programming sub-problem; an estimate of the Hessian of the Lagrangian is updated after each iteration by globally converging all the unknown parameters simultaneously and not adjusting them one at a time.

Once all the selection and breakage functions had been estimated, the milling evolution of size range (-106 +25 µm) were simulated, and then extrapolated to 300 min. Finally, additional experiments were done by grinding the ore for 60, 90,

120 and 240 min, to enable a comparison between the simulation results and the experimental data (refer to Chapter 4).

3.5 Scale-up Methodology

3.5.1 Batch test data

In the previous section, the breakage function and selection function parameters were measured and estimated from laboratory batch experiments. This section describes how these parameters were extended to full-scale milling.

Before that, the reader of this dissertation is asked to recall that the batch tests were done in a laboratory scale ball mill with an internal diameter (D_T) of 0.30 m, and a length (L_T) of 0.28 m. The mill was fitted with eight lifters, the dimensions of which are a height of 13 mm, a width of 25 mm and a length of 272 mm. Mono-sized balls and narrow-feed size classes were used in each test. The media sizes (d_T) considered were 10 mm, 20 mm and 30 mm steel balls and the feed size classes used were (-850 +600 µm, -600 +425 µm and -425 +300 µm) of the PGM ore. The test conditions were as follows: ball filling J_T = 20 %, slurry filling U_T = 0.75 and the mill speed ϕ_{cT} = 75% of critical speed. All breakage function parameters (β, γ and Φ) and the selection function parameter (α, a_T, Λ and μ_T) were based on the laboratory batch mill tests.

3.5.2 The industrial mill

The specific rates of breakage obtained from the test conditions in the laboratory mill were converted to the operating conditions of a typical industrial mill by means of a methodology recommended by Austin *et al.* (1984). An open circuit mill which had already been comprehensively studied and characterised by Makokha *et al.* (2011) was the source of industrial data used for the research work described here. The mill was a secondary grinding unit of the UG2 Platinum Waterval concentrator situated in Rustenburg, in the North West province of the Republic of South Africa. It has an overflow discharge design with an inside

diameter (D) of 7.312 m and length (L) of 9.6 m, and is run in an open circuit. It is fitted with 44 rubber lifter bars 100 mm high, and is loaded with forged chromium steel balls 40 mm in diameter (d). The wet overflow mill processes fine (less than 1 mm) platinum feeds, grinding the material to less than 106 µm to meet flotation requirements. However, slimes (that is, material less than 10 µm in size) have to be avoided, because they may compromise the flotation process.

For the purpose of scaling-up and modelling, the mill was initially assumed to behave as a plug flow reactor. Consequently, the grinding time was regarded as the mean residence time of the mill (Austin *et al.*, 1984).

3.5.3 The scale-up procedure

The scale-up methodology proposed by Austin *et al.* (1984) is applicable only to materials the breakage and selection function parameters of which have been determined in the laboratory. In this study, the breakage properties of the platinum ore that had already been established were applied, a decision reinforced by the knowledge that these breakage properties had been measured on a feed sample similar to that of the industrial mill under consideration.

On that basis, a Matlab® script was written to scale up the selection function parameters from the laboratory test conditions to the industrial mill. The ore was assumed to be normalisable, so that the breakage function remained unchanged.

The initial input parameters were those for the selection functions (α, a_T, μ_T and Λ) obtained in the laboratory. Other inputs to the Matlab® code were the grinding conditions pertaining to the batch mill (D_T, J_T, U_T, ϕ_{cT}, d_T) and to the simulated industrial mill (D, J, U, ϕ_c and d). For a given set of user-defined industrial mill conditions, specific rates of breakage for the industrial mill were predicted using Equations (2.20 – 2.25). Once the scaled-up selection function values had been determined, they were incorporated into the population balance model (Equation 2.11) together with the laboratory breakage function parameters. Then product size distributions were generated for different grinding times (also termed mean residence times in a continuous milling setup). Finally, the milling kinetics of the

desired size class (-106 +9 µm) were deduced from the particle size distributions generated for each set of industrial mill conditions under consideration. The effects of each milling factor on the production rate of the desired size class were then explored.

3. 6 Simulation of the residence time

The aim of determining the optimal residence time is to extend the use of the AR technique from batch to continuous milling. However, the scope of the work described in this thesis was limited to the optimisation of the residence time of particles inside the mill. The circuit was treated as an open circuit which was assumed to operate without being directly influenced by a classifier. To fulfil this purpose, a full characterization of both the full-scale mill used for the study and the ore that was being processed had already been given. This provided the material to initiate a simulation programme for the large mill in order to generate data for AR analysis. Initially, the residence time was optimised using the plug flow and perfectly mixed transportation models. This was later carried on to the next stage, using residence time distribution (RTD) transport model which comprises, first, a dead zone, followed in sequence by models of a large fully mixed reactor and two smaller but equally fully mixed reactors, as shown in Figure 3.4. The choice of this transport model has been motivated by the fact that the parameters of the model were previously determined for the industrial mill used in this research by Makokha (2011).

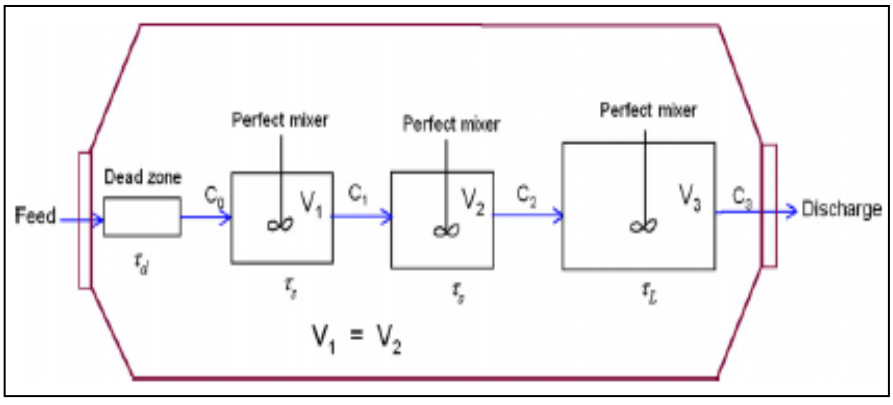


Figure 3.4 Schematic representation of the tanks in series model with dead time. (after Makokha *et al*.,2011)

As far as the properties of the ore are concerned, the breakage and selection function parameters measured in the laboratory were used to characterise the material. These parameters were measured by means of batch tests using the one-size-fraction method described by Austin *et al.* (1984). The parameters correspond to the following experimental conditions: feed size (-850 +600 µm); ball diameter d_T = 20 mm; ball filling J_T = 20 %; powder filling U_T = 0.75; mill speed ϕ_{cT} = 75 % of critical; and mill diameter D_T = 302 mm.

As for the full-scale mill in question, it is an overflow discharge mill, run in open circuit and used in the secondary grinding of UG2 platinum ore. Its technological and operating specifications are as follows: mill power draw is about 9500 kW at 30% mill filling; mill full length L = 9.6 m; mill diameter D = 7.312 m inside liners; mill speed ϕ_c = 75 % of critical; ball filling J ranging from 25 to 33 %; steel ball diameter d = 40 mm. The mill is lined with 44 rubber lifters which have a height of 100 mm. The solids concentration in the slurry is on average 75 % by mass for a 330 tons per hour throughput.

It is important to emphasise that the choice of this industrial mill was motivated by the fact that RTD and milling kinetics have already been comprehensively studied (Makokha, 2011; Makokha *et al.*, 2011). In addition, sufficient data are available for validation purposes.

A Matlab® script for the simulation programme that was based on the solutions of the PBM applied to continuous milling was written. The PBM parameters obtained from laboratory experiments on the same material were scaled up to an industrial mill using Equations 2.20 – 2.25. Next, the PSD of the full-scale mill were generated using Equations 2.12 – 2.19, and finally an AR optimisation routine ran to determine the optimum residence time for both the fully-mixed and the plug-flow mills and the residence time distribution mill models.

3.7 Simulation of the power draw

The Morrell model was used for predicting the net power drawn by the full-scale mill. The Matlab® script written to calculate the net power (P_{NET}) incorporated a set of operational conditions which included mill speed, ball and slurry fillings.

To satisfy the requirements of the Morrell model, the charge density was calculated first, and then the toe angle and the shoulder angle. After that, in-mill parameters such as the charge inner surface radius were worked out before Equation (2.45) could be applied to obtain the net power draw.

3.8 Summary

All the experimental tests were completed using the equipment and techniques described in this chapter. The results of experiments carried out on the Wits laboratory mill, coupled with the back-calculation technique, enabled the determination of the milling parameters of the platinum group minerals ore needed for modelling purposes.

The selection function parameters obtained were used in empirical models to convert specific rates of breakage from the laboratory test conditions to a preselected overflow full-scale ball mill. Data relating to the effects of operational factors such as the mill filling, mill rotational speed, grinding media filling and media size were generated and analysed. In addition, reported data from the same full scale mill were used and compared with those generated using the models. The effects of the operational factors as well as the residence time and net power draw were simulated with the aim of optimizing the product size distribution for flotation purposes.

Chapter 4 Determination of the milling parameters of a Platinum Group Minerals ore to optimize product size distribution for flotation purposes

The results of this chapter have been published in the Minerals Engineering Journal under the reference: **Chimwani, N**., Glasser, D., Hildebrandt, D., Metzger, M.J., Mulenga, F.K., 2012. Determination of the milling parameters of a platinum group minerals ore to optimize product size distribution for flotation purposes. *Minerals Engineering,* vol. 43 – 44, pp. 67 – 78

This is completely my work, i did all the experiments and processing of data as well as writing the paper, the other authors are my supervisor except M.J. Metzger whose contribution was in helping me to structure the paper into a journal format.

Abstract

Most concentrators desire to operate under optimal design configuration that guarantees high mineral recovery and low operational costs. The optimal milling conditions can be determined by studying the material to be milled on a laboratory scale under standard conditions that make it possible for the selection and breakage function parameters to be measured. These parameters provide the basis for the mathematical simulation of grinding for optimisation purposes.

Accordingly, three narrow-sized feeds (-850 +600 µm, -600 +425 µm and -425 +300 µm) of a platinum ore were milled, using three different ball sizes (10, 20 and 30 mm), in a laboratory mill for a range of grinding periods (0.5, 1, 2, 4, 8, 15 and 30 min). The data collected were used to determine the breakage function parameters and some of the selection function parameters. The remaining parameters were back-calculated within the population balance model framework. The parameters were then used to obtain the product size distribution, which was later compared with those determined from the experimentally measured data. The milling kinetics for the desired size class (-150 +25 µm) for grinding times ranging between 60 – 240 min were also measured and compared with the extrapolated simulation.

A good match was found between the predicted and measured size distributions. The results of the milling done for 60, 90, 120 and 240 min grinds to validate the simulation model estimates were also satisfactory. This further confirmed the validity of the determined parameters. The measured selection and breakage function parameters then provided the foundation on which the determination of the grinding conditions for optimal flotation was built.

4.1 Introduction

In PGM recovery, the primary reason for milling materials to smaller particles is to liberate the valuable components dispersed in the host matrix. When the material has been reduced to a size small enough to give sufficient liberation of the valuable components, these components are separated from the host matrix by downstream processes such as flotation. The size reduction operations, especially the final stage of grinding before the separation circuit, constitute the primary feed preparation for the separation circuit (Coleman, 1983).

Liberating PGMs, especially those present in the Upper Group 2 Reef (UG2) from their host matrix, which consists of base metal sulfides, silicates and chromites poses processing challenges (Hay and Roy, 2010). Most of them are attributable to the fineness and gangue association of the PGMs (Cramer, 2001). The valuable minerals in UG2 have significantly smaller average grain sizes and require fine grinds to optimally liberate the valuable components (Rule, 2008). Cramer (2001) anticipated the future of the PGM processing industries would require further development of the processes to address the encountered technical challenges. This confirms that the design and performance of the PGM processing circuits is poorly understood, and hence a topic of interest (Bryson, 2004). Optimizing the milling stage is one way of improving the efficiency of the PGM processing circuits.

In order to optimize the milling stage, requirements of the flotation in terms of particle size have to be fully understood first, since either over-grinding or low liberation leads to the reduction in the amount of PGM recovered (Bryson 2004; Rule and Anyimadu, 2007). This would be followed by understanding the breakage properties of the ore to be used which is modelled by the selection and breakage function parameters as discussed in chapter 2.

These parameters are used to predict the product size distribution, which in turn can be applied in setting the standard operating procedure of the mill. Discrete size classes are usually used, for they provide adequate approximations for practical computation (King, 2001). The parameters describe the breakage and

characterize the objective function that is to be optimized. Examples of objective functions could be to minimize the total energy consumption in a circuit, achieve a specified particle size distribution (PSD), or to shorten the total duration of operation.

The work reported in this chapter helps the engineer to determine the preliminary parameters describing the milling behaviour of PGM ore. This is necessary because the PGM ore processing industries have been unwilling to divulge scientific information concerning their ores, for fear of competition.

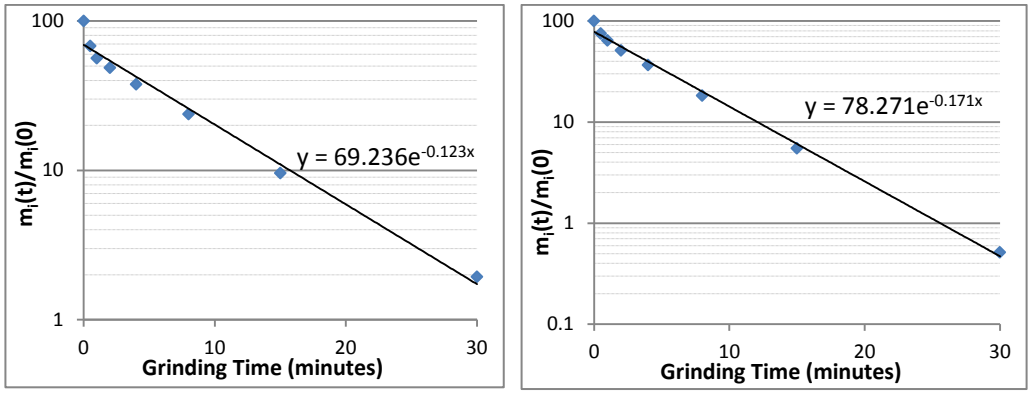
The research therefore seeks to provide information that can be used for simulation and optimization purpose which leads to further development of the milling process of PGM ores.

4.2 Results and discussions

The experimental work discussed in chapter 3 is analysed to obtain the breakage parameters that characterise the PGM ore.

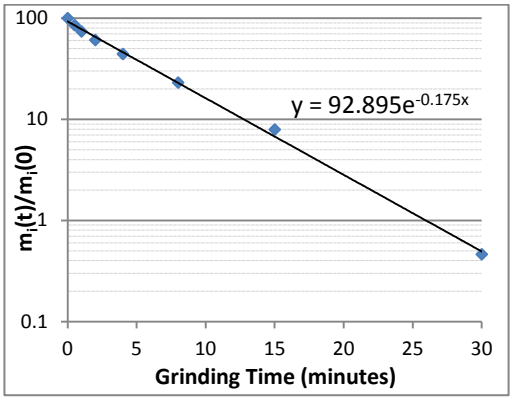
4.2.1 Determination of the selection function parameters

The rate of breakage for PGM ores was obtained numerically using Equation 2.4 as the mean value of the effective selection function. Figure 4.1 shows the experimental results obtained from plotting the mass percentage retained on the top screen against grinding time *t* on a log–linear scale for the feed size -600 +425 µm using three different media sizes, 10 mm in Figure 4.1(a), 20 mm in Figure 4.1(b) and 30 mm in Figure 4.1(c). The graphs do not start at 100 % indicating that the initial sample had undersize material. This indicates that the equations are different from the first order model (Equation 2.2) and therefore, the breakage in the mill has departed from the first-order hypothesis. That is why Equation (2.4) was used to determine the selection function for feed sizes -850 +600 µm, -600 +425 µm and -425 +300 µm when milled with different media sizes.



(a)

(b)



(c)

Figure 4.1 First-order plot for UG2 ore mono-size class (-600 +425 µm) ground with different media sizes (d_T): (a) 10 mm; (b) 20 mm; (c) 30 mm.

The results presented in Table 4.1 show that for the ore feed sizes -425 +300 µm and -600 +425 µm, the magnitude of the selection function is inversely proportional to the ball size. This is because, if the balls of smaller diameter are used for the same J_T to grind relatively small particles, the rate of ball-on-ball contacts per unit time increases. This results in a higher rate of breakage of smaller particle sizes by balls of smaller diameter (Austin *et al.*, 1984). A different trend can be observed if a feed size with bigger particles is used. Austin *et al.* (1984) was able to show that as the diameter of the ball increases, the mill can break a feed containing larger size of particles more efficiently. This is confirmed by the selection function of feed size -850 +650 µm, which rises with an increase in ball diameter, as shown in Table 4.1.

Table 4.1 Selection functions for different feed sizes and media sizes

Mono-sized UG2 materials	Media size (mm)		
	10 mm	20 mm	30 mm
-850+600 µm (S_1)	0.18	0.28	0.29
-600+425 µm (S_2)	0.21	0.20	0.18
-425+300 µm (S_3)	0.16	0.13	0.11

The selection function values in Table 4.1 were plotted against particle size, as shown in Figure 4.2. It can be seen that the increase in selection function with an increase in particle size is linear and almost linear for 30 mm balls and 20 mm balls respectively. The figure also shows that the maximum value of the selection function for the 10 mm balls has been reached, and that the breakage rate decreases with a further increase in particle size beyond 600 µm. The size classes -850 +600 µm and -600 +425 µm are too big and strong to be properly nipped and fractured by the 10 mm balls, hence the drop in the rate of breakage, which is in agreement with Austin *et al.* (1984).

In Figure 4.2(a), the parameter α was determined by the 30 mm ball curve using a power function. The 30 mm curve was chosen because it is considered to be in the linear region, that is, before the x_m (the size at which the maximum value of S occurs). The value obtained for α is 1.40. Figure 4.2(b) shows what a complete selection function curve should look like (King, 2001). The part of the curve that shows normal breakage behaviour is the region where S has not passed through the maximum, and abnormal breakage behaviour is shown by the region where S has passed the maximum. When one compares Figure 4.2(a) and 4.2(b), one can see that Figure 4.2(a) represents only a small portion of the entire curve of the selection function. It follows that it would be unwise to assume that it provides a basis for the accurate determination of all parameters associated with the selection function. However, the value of α (the slope of the linear portion of the curve) can be determined from the 30 mm curve in Figure 4.2(a), and this value was fed into the population balance model for simulation purposes.

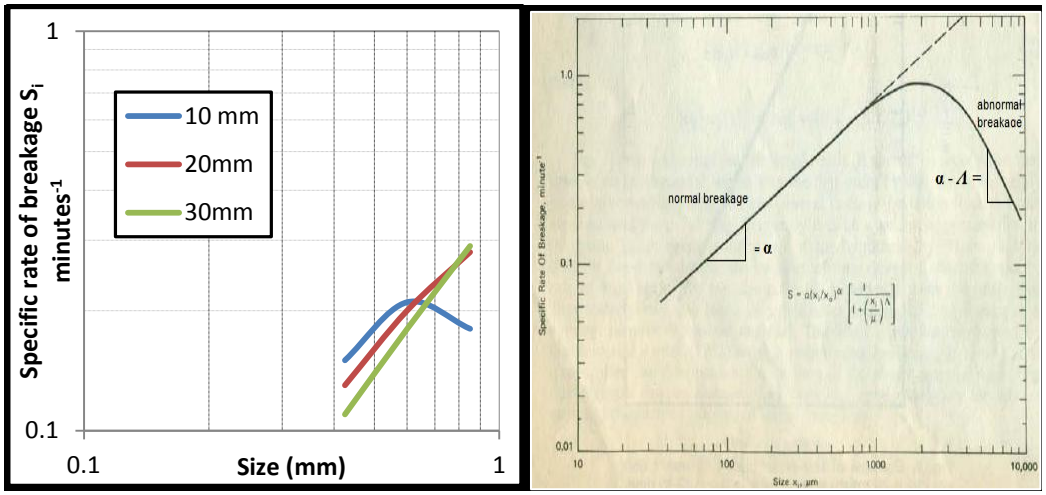


Figure 4.2 (a) Variation of *S* with particle size. (b) Graphical procedure for the determination of the parameters (Austin *et al.* 1984).

4.2.2 Determination of the breakage function parameters

Figure 4.3 shows the primary breakage distribution plots of all the feed size classes for 10 mm, 20 mm and 30 mm media sizes, which were determined using Equation 2.9 (B-II method). Austin *et al.* (1984) recommended that shorter grinding times, which result in 20 – 30 % broken materials out of the top size, should be used in this procedure. Although shorter grinding times give researchers the most accurate estimates of the breakage function, Austin and Luckie (1971) showed that even with 65 % broken material, the procedure remains sufficiently accurate to be used.

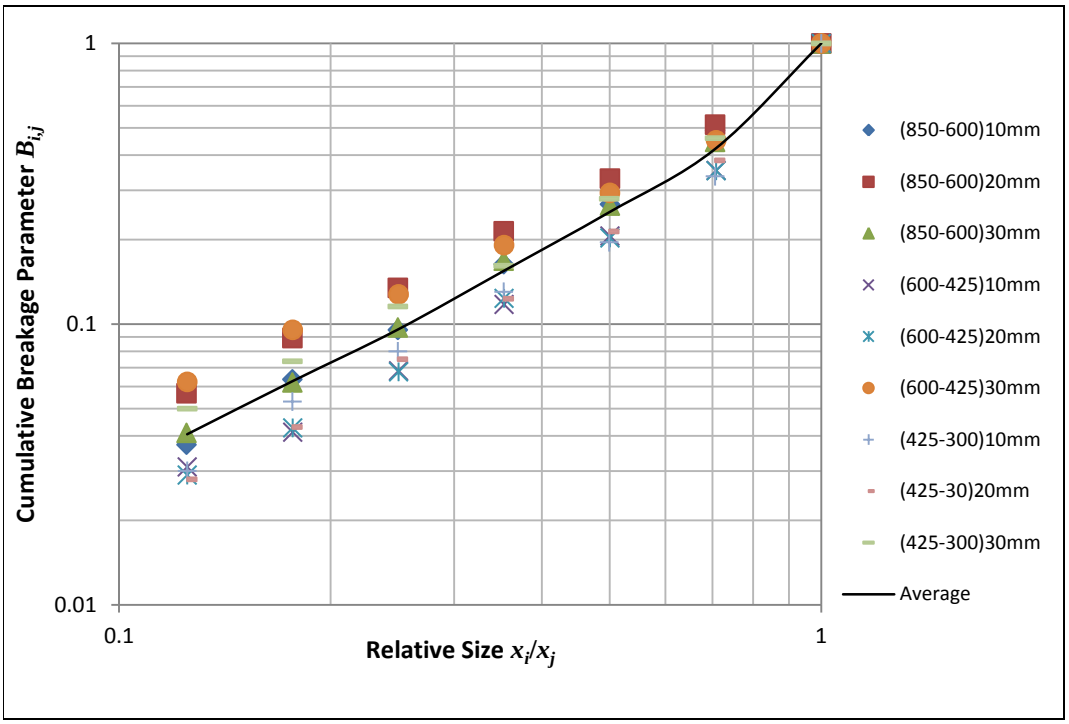


Figure 4.3 Variation of breakage function values with feed size.

The breakage function data obtained were fitted to the empirical model in Equation 2.10 and the breakage function parameters for PGM ore were evaluated. The average breakage function parameters determined for all feed size classes and media sizes used were found to be: β = 6.2, γ = 1.30 and Φ = 0.59. These parameters were then fixed for the rest of the simulations as the breakage function is considered to be independent of milling conditions.

These parameters are close to those obtained by Yekeler (2007) for chromite, which were as follows: β = 7.9, γ = 1.14 and Φ = 0.75. Austin *et al.* (1984) also found values of β = 5.8, γ = 1.30 and Φ = 0.58 for the experiments they conducted on quartz. Though these ores are not identical, the similarity in the results provides confidence in the parameter determination method. Most important of all, the PGM ore was considered to be normalizable, since no specific trend was identified in Figure 4.3.

4.2.3 Particle size distributions (PSD)

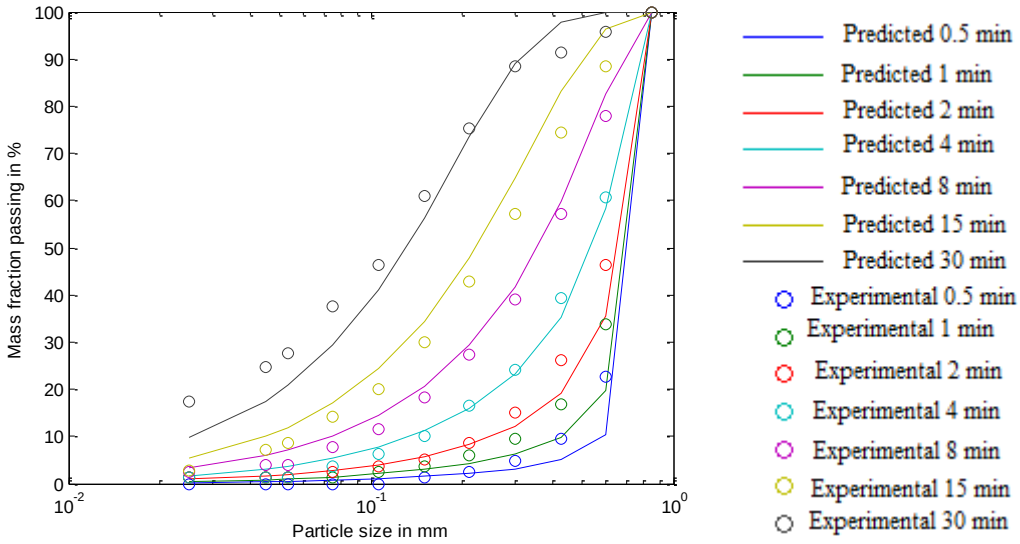
The parameters of the selection and breakage function evaluated from the experimental data were used as initial estimates for the model in the parameter search process. The parameters (a_T, Λ, γ and μ_T) were estimated by the optimization model, which searches for the best combination of these parameters that performs best at minimizing the residual error between the experimental and the predicted product size distributions. Table 4.2 shows the predicted breakage and selection function parameters for all feed sizes using 10 mm ball diameters, which in combination yielded the best fit between predicted and experimental product size distributions. It can be seen that the value of a_T decreased with an increase in feed size. The possible explanation for this behaviour is that the rates of breakage of smaller sizes are higher with balls of smaller diameter, and that the *S* values of feed sizes comprising larger particles will be to the right of the maximum, giving lower rates of breakage (Austin *et al.*, 1984). This was also confirmed by the results given in Table 4.1, which show the drop in *S* values for 10 mm balls as the feed size increases from 600 to 850 µm. The value of γ decreased as the feed size increased, because the value of γ is lower in the abnormal breakage region. The reason is that the mean breakage action in this region is dominated by chipping and abrasion, resulting in the production of more of the finest material, and hence a low value for γ (Austin *et al.*, 1984).

Table 4.2 The UG2 ore selection and breakage function parameters

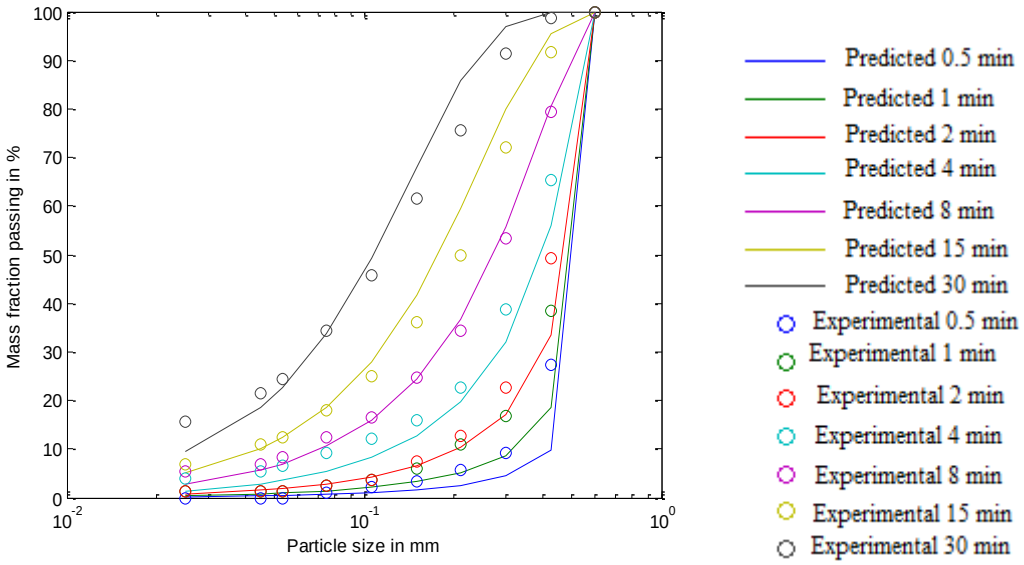
Selection function parameters				Breakage function parameters			
x_i	425µm	600µm	850µm	x_i	425µm	600µm	850µm
α	1.40	1.40	1.40	β	6.2	6.2	6.2
Λ	4.74	4.74	4.74	γ	1.27	1.24	0.79
a_T	0.59	0.42	0.28	Φ	0.60	0.60	0.60
μ_T	2.0	2.0	2.0	Normalizable material			

Figure 4.4 below gives graphical comparisons of the experimental and predicted results of the particle size distributions for the PGM ore, obtained with 10 mm balls and all feed size classes under different grinding durations. The predictions compared reasonably well with the results, considering that the breakage took

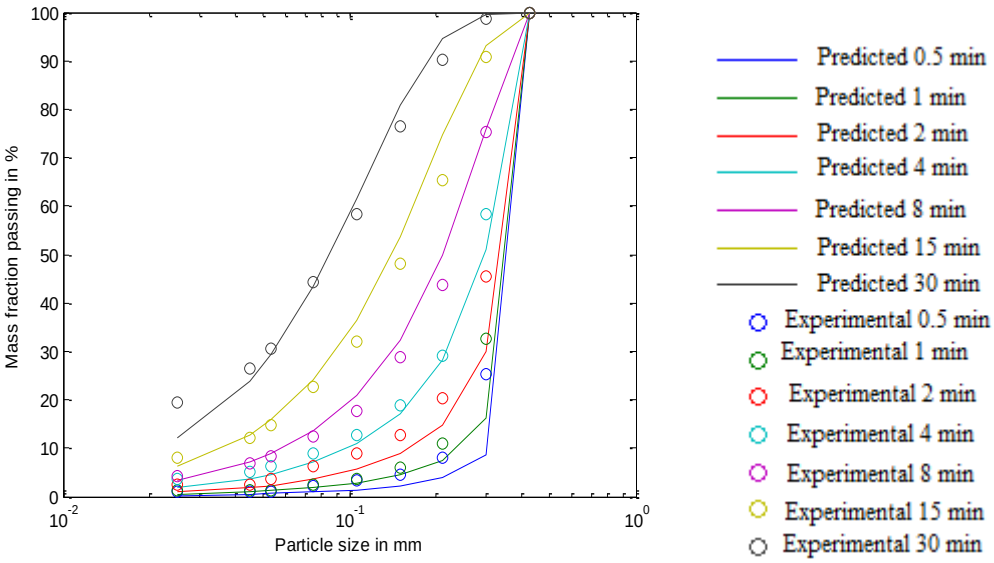
place in the abnormal region, where the kinetics of the breakage follows non-first order behaviour. In all cases, a much coarser product was predicted for the shorter grinding times of 0.5 to 2 minutes. This could have been caused by the non-linear behaviour of the coarser material. In their experiments on coal, Katubilwa *et al.* (2011) reported very similar findings. In the graphs of the three feed sizes, it can be clearly seen that the predictions compared particularly well with the laboratory results for the particle size distribution (PSD) of the feed size -425 +300 µm. The reason might be that this is the smallest of the feed sizes, hence the occurrence of breakage in the normal region. However, with the assumptions made for normal breakage and normalizable material, the simulator was able to perform the task it was intended for, that is, to predict some of the breakage and selection function parameters that could not be determined experimentally, for the purpose of optimizing the PSD.



(a)



(b)



(c)

Figure 4.4 Measured and predicted particle size distributions corresponding to 10 mm ball size and feed sizes: (a) -850 +600 µm (b) -600 +425 µm and (c) -425 +300 µm.

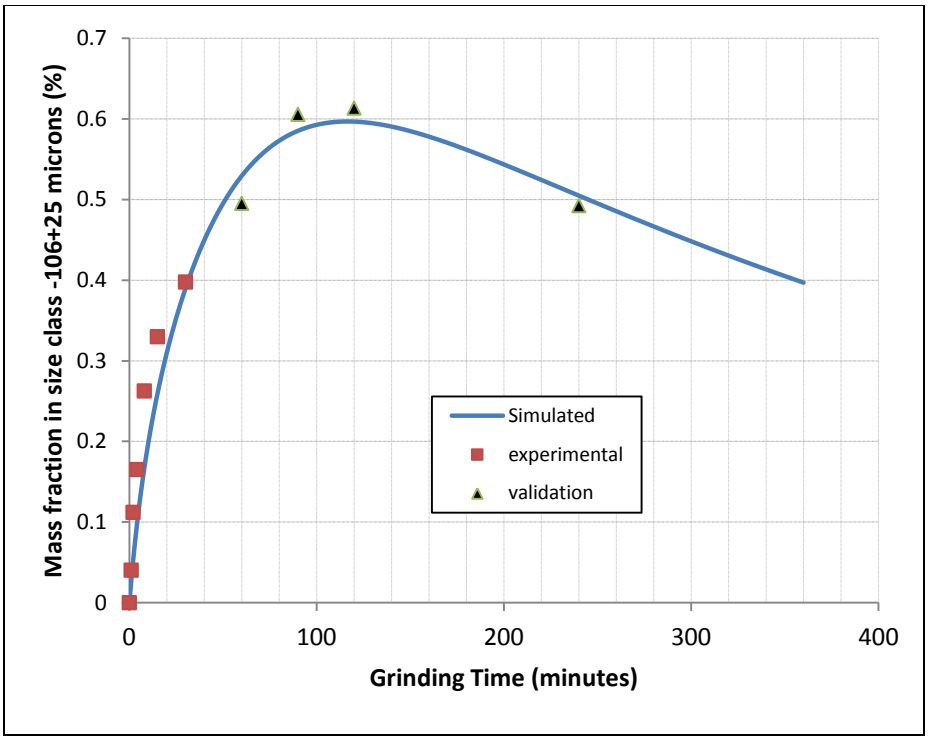


Figure 4.5 Milling kinetics of the desired size class for 20 mm balls and feed size -850 +650 µm.

Figure 4.5 shows a comparison between the simulated and the experimental milling kinetics of the desired size class (-106 +25 µm) of the UG2 ore for 20 mm balls and a feed size -850 +600 µm. The first set (with square markers) was experimentally used to determine model parameters; and the second set (with triangular markers) was used to validate the model. The milling kinetics simulated from the determined parameters were validated by the results of the milling done for further periods of 60, 90, 120 and 240 min, indicated by the last four points with triangle markers on the experimental curve. In these results, it can be observed that the simulated milling results match the experimental data very well.

4.3 Conclusion

In this chapter, experimental results from the laboratory were used to determine the selection and breakage function parameters for a typical PGM ore. These initial parameter estimations were then used to find the missing parameters by back-calculation.

Using the selection and breakage function parameters, the predicted PSD of the PGM ore was compared with the experimentally-measured PSD, with a satisfactory outcome. The results reported in this chapter also reinforce the proposition made by Austin *et al.* (1984) that, if the entire set of selection function parameters is not determined experimentally owing to limited data, some of the parameters can be determined indirectly by back-calculation from the experimental data that are available, in this way reducing the need for additional experimental work.

From the trends of the variation of breakage function values with feed size for all media sizes, it is reasonable to assume a normalizable breakage function. From the simulated parameters, it was noted that a (the selection function parameter) decreases with an increase in feed size and γ (breakage function exponent) shows exactly the opposite behaviour. Using the parameters that have been obtained, a good match was observed between the experimental and the predicted PSD's. There was also a good match between the experimental and the simulated milling kinetics curve of the desired size class (-106 +25 μm) for 20 mm balls, which further confirmed the validity of the parameters that had been determined.

The subsequent chapters will focus on application of these findings to determine optimal grinding times required for yielding the particle size range desired for optimal operation of downstream processes (in this case, flotation), and testing the model parameters at additional scales.

4.4 Summarised findings

In this chapter a scheme used to determine the PBM parameters for a South African PGM ore has been presented.

Following this undertaking, the following parameters have been successfully estimated and validated.

Breakage function parameters	β	6.2
	γ	0.8
	Φ	0.6
Selection function parameters	α	1.40
	Λ	4.74
	a_T	0.32
	μ_T	4.2

This information can be used for simulation and the optimization of milling circuits for PGM ores particularly UG2 ore.

Chapter 5 Scale-up of batch grinding data for simulation of industrial milling of platinum group minerals ore

The results of this chapter have been provisionally accepted for publication in the Minerals Engineering Journal under the reference: **Chimwani, N**., Mulenga, F.K.., Glasser, D., Hildebrandt, D., Bwalya, M., 2012. Scale-up of batch grinding data for simulation of industrial milling of platinum group minerals ore. *Minerals Engineering, Manuscript Number:* MINE-D-13-00424R1

This is completely my work, i did all the simulation and processing of the data as well as writing the paper, the other authors are my supervisors.

Abstract

The attainable region analysis of batch grinding is a graphical method of establishing limits of performance of possible outcomes of any defined process. When applied to batch grinding, the results have often come into conflict with traditionally acceptable milling practice under which most concentrators operate (Metzger *et al.*, 2011). This novel technique has not been tested on an industrial scale and thus, application of the scheme to full scale industrial mill is naturally the next step.

This chapter entailed scaling-up data obtained from laboratory batch milling of a platinum ore using empirical models. Using the parameters obtained in the laboratory tests, a technology pioneered by Austin *et al.* (1984) was applied to predict the selection function and breakage function parameters for an operational industrial mill on which some plant survey had been conducted. It was found that the simulated product size distributions based on this scale up-procedure displayed a close match with the actual obtained from an operational industrial mill.

The attainable region plots from the scaled-up data showed that a finer product is achieved by using small balls. This is in agreement with initial findings based on laboratory batch tests only. It is also anticipated that pilot tests, industrial tests or

simulations should be the next step in the quest for bridging the gap between the attainable region methodology and industrial experience. Also validated on industrial scale was the fact that less powder and grinding balls are needed to incur finer grinding. However, it was interesting to note that the factors that produced a coarser product when analysed from a particle point of view were the same as those that yield the greatest amount of the desired size class when viewed from an attainable region perspective.

5.1 Introduction

In industrial milling, size reduction is commonly known to be a highly energy-intensive process that accounts for a major proportion of the costs involved in operating processing plants. This explains why engineers designing concentrators strive to operate the grinding systems and circuits in the most energy-efficient way. To identify optimal design configurations, researchers have resorted to laboratory batch tests to establish selection and breakage function parameters that enable them to identify optimal design configurations (Herbst and Fuerstenau 1980; Herbst *et al*., 1981; Austin *et al.*, 1984; Rajamani, 1991; King, 2001; Datta and Rajamani, 2002).

The Attainable Region (AR) approach, initially proposed for the analysis of chemical engineering systems, has now been extended to comminution processes (Khumalo *et al.*, 2006–2008), and has already been applied successfully to optimise the milling of different types of ore (Khumalo, 2007; Khumalo *et al.*, 2006 – 2008; Metzger, 2011; Metzger *et al.*, 2009 & 2011; Katubilwa *et al.*, 2011; Chimwani *et al.*, 2012). Research carried out on laboratory mills has demonstrated the capacity of the AR technique to determine the set of all the achievable size distributions under different process conditions. This information provides the engineer with accurate data on the operating conditions required to achieve a specific objective function, such as maximizing the amount of a certain size class or minimising energy consumption for a given feed to the mill (Khumalo *et al*., 2006).

As an illustration of the above claim, the investigation carried out by Khumalo *et al.* (2006 – 2008) used the AR technique to obtain a desired product using a minimum amount of energy. The results from his undertaking showed how the optimisation problem of the level of specific energy to be used in a given equipment, to achieve a certain objective function can be answered. Most important, he and his colleagues pinpointed the stage at which the energy intensity in a comminution process can be controlled in order to develop an optimal energy regime. On similar lines, Metzger *et al.* (2009) researched means of minimizing the total time required for operation. Their results showed how useful AR is in

determining optimal policies to reduce milling processing times. Katubilwa *et al.* (2011) analysed the effect of ball size on milling, and demonstrated clearly the advantage of mixing the sizes of the grinding balls to produce a maximum amount of material in a target size range.

All of the above outcomes of AR were, however, based on laboratory batch testing. The question to be addressed by this research is whether this technique can be successfully applied to the operation of industrial mills, in other words whether it is possible to expand its application from laboratory-scale to full-scale scenarios. The present work seeks to address this question and demonstrate how the tool can explore outputs that can assist in choosing optimal operating conditions. It is envisaged that this technique will serve as a complimentary analytical tool for the optimisation of milling circuits.

In the work described in this chapter, the work that involved standard laboratory batch experiments on a Platinum ore is presented to determine the selection function and empirical scale-up to a full industrial discharge mill. The attainable region approach was used to investigate the extent to which variations in the selection function parameters (μ, a, α and Λ, as symbolically presented by Austin *et al.* (1984)) affect the final product distributions in an industrial set-up. The results demonstrate that the AR technique can be used as a good tool for the design and analysis of mineral processing circuits.

5.2 Results and Discussions

To validate the scale-up procedure, the predicted particle size distributions (PSDs) of mill product arrived at using the scaled-up data were compared with the PSDs obtained from the industrial mill and a good match was observed. Mill speed, ball and powder fillings and ball size were the factors on which the scaled-up data were evaluated, since milling kinetics depend on them.

Having verified the scale-up method and shown that it was applicable to the platinum ore and the full-scale mill considered in this thesis, the mill operating conditions used to describe the industrial mill operation were varied, which made

it possible to use AR approach to optimise the operating conditions by considering the full range of options.

5.2.1 Validation of the scale-up procedure

Since they depend on the operating conditions and the geometrical scale of the mill, the values of a_T and μ_T were scaled up to the conditions of the simulated industrial mill. The scaled-up value of a_T based on Equation 2.20 for the new mill condition is a^*, and that of μ_T in Equation 2.20 is μ^*. The scaled-up parameters are presented in Table 5.1.

Table 5.1 Breakage parameters as scaled-up to industrial mill

Breakage function parameters	β	6.2
	γ	0.8
	Φ	0.6
Selection function parameters	α	1.40
	Λ	4.74
	a^*	3.74
	μ^*	9.65

The validation results of prediction of industrial mill product are given in Figure 5.1. It can be seen that there is a good match between the predicted PSDs and the measured plant data. Having successfully validated the scale-up parameters against real plant data, the model was then used to explore various factors that affect the milling kinetics that are discussed in the sections that follow.

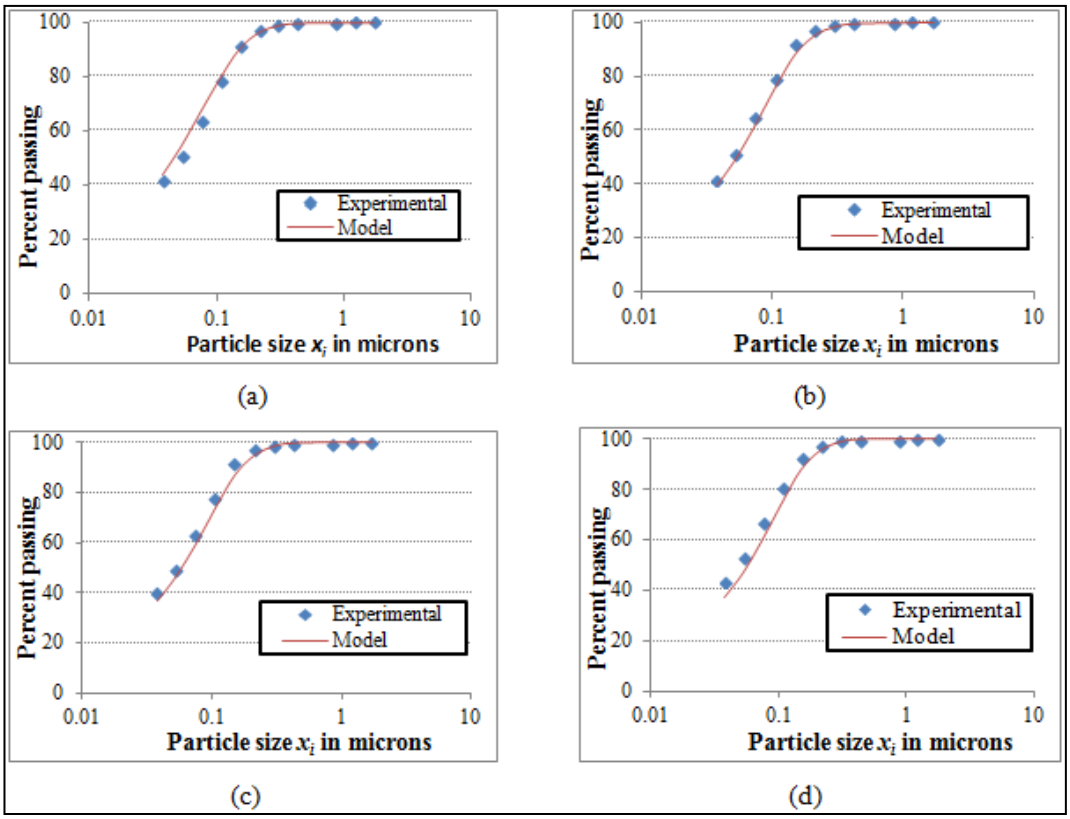


Figure 5.1 Comparison between experimentally measured data and the predicted PSD using the scale up method for the large scale mill:
(a) J = 24.6 % and 74.5 % solids, (b) J = 32.9 % and 67.7 % solids,
(c) J = 32.8 % and 65.1 % solids, (d) J = 32.9 % and 72.1 % solids.

5.2.2 Using modelling to explore effects of varying operational conditions

In the following sections, the model was used to generate large mill outputs under various operating conditions and the AR scheme was used to recommend optimal operating conditions.

5.2.2.1 Effects of mill speed on milling kinetics

Figure 5.2 shows the PSDs generated by the model for four mill speeds (40 %, 60 %, 75 %, and 90 % of critical speed) and for three mean residence times (2, 4, and 15 min). The graph makes clear that finer grinding is achieved as the mill speed

increases from 40 – 75 %, after which the particles become coarser as the speed is increased to 90 % of critical. It is common practice in milling to recommend speeds of around 75 % of critical to guarantee a high power draw and therefore ensure that the grinding is done at a faster rate (Austin *et al*., 1984; Wills and Napier-Munn, 2005). This observation is supported by the PSDs in Figure 5.2, which show that a coarser material is produced at speeds that are both lower and higher than 75 % of the critical speed.

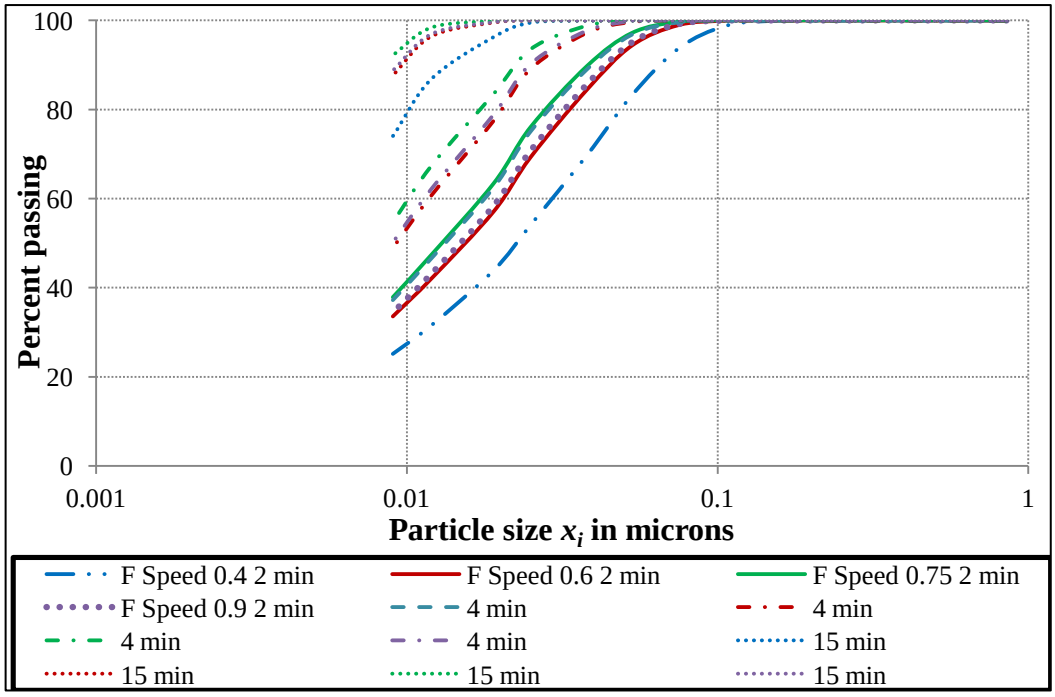


Figure 5.2 Predicted PSDs for four mill speeds: J = 40 %, U = 0.75, d = 40 mm and varying residence times.

The application of the AR method to milling introduced a whole new approach to optimising milling (Khumalo *et al*., 2006 – 2008). Figure 5.3 shows the mass fraction of material in the intermediate (desired) size class termed m_2 (-106 +9 µm) for the following speeds: 40 %, 60 %, 75 % and 90 % of critical speed. The number of revolutions of the mill required to produce the maximum amount of the intermediate size class m_2 was different for different mill speed and in addition, the maximum achievable mass fraction of the desired size class reduced as the mill speed increased. The lowest fractional speed, that is, ϕ_c of 40 % of critical or 6.24 rpm, produced the highest mass fraction of m_2 (74.7 % mass fraction) at a

faster rate, followed by ϕ_c = 60 % (9.38 rpm), which achieved a maximum m_2 of 66.5 %. The speed that produced the lowest maximum amount of m_2 was ϕ_c = 75 % (11.7 rpm), which produced only 62.1 % mass fraction. This is contrary to the widely-held belief in comminution by engineers and designers that industrial grinding mills should be run at ϕ_c = 75 %, though it is not uncommon to find mills being run at speeds as low as 69 % of critical speed to conserve liners.

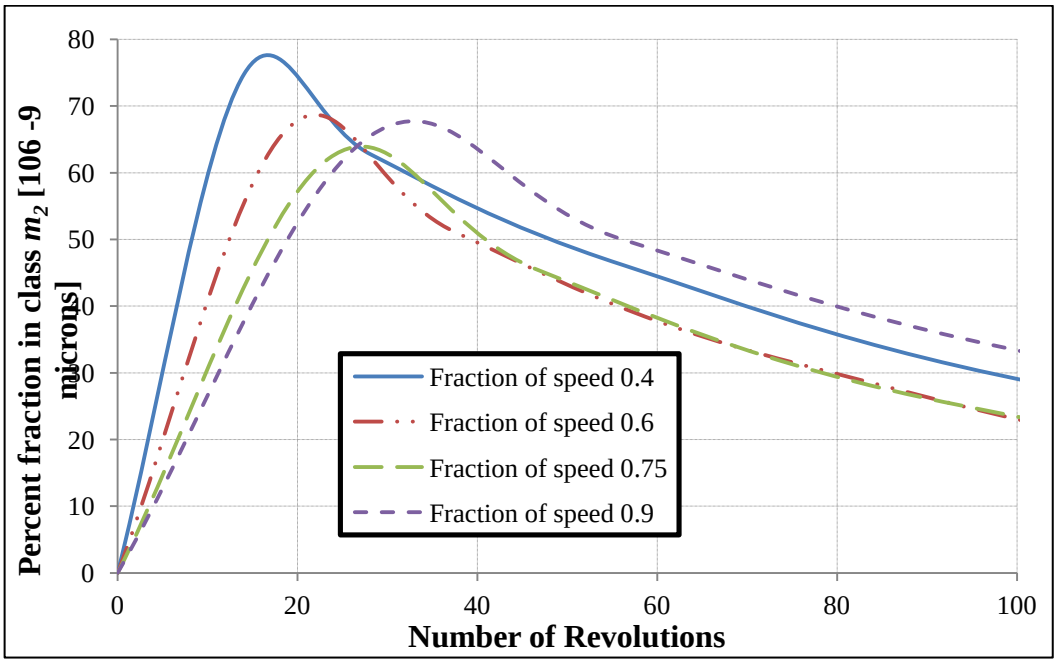


Figure 5.3 Plot of mass fraction of m_2 versus number of revolutions for different speeds ϕ_c; J = 40 %, U = 0.75, and d = 40 mm.

As the mill speed was increased to ϕ_c = 90 % (14 rpm) the maximum mass fraction of the desired product m_2 rose to 65.6 %. This observation confirms the ability of the AR technique to ascertain the optimal operating conditions for a preselected industrial mill. The grinding profiles in Figure 5.3 also support the findings of Metzger *et al*. (2009) that low mill speeds produce more intermediate class material at a higher rate than milling at high speed. Based on the experiments they conducted on silica sand, Metzger *et al*. (2009) also found that operation at the slowest rotation is the best milling policy, because it utilizes energy to the full extent and therefore enables optimal production of the desired size class with the most efficient use of energy. However it has been pointed out that although it is desirable to operate mills at low speeds, a speed that is lower

than optimum may lead to an excessive amount of wear on the shell liners, and produce undesirably large amounts of slimes (Wills and Napier-Munn, 2005).

5.2.2.2 Effect of ball filling on milling

The PSDs achieved for ball fillings (J) of 5 % and 40 % for grinding times of 2, 4, and 15 minutes are shown in Figure 5.4. All the other factors were held constant, with the mill speed at 75 % of critical, ball diameter of 40 mm and U of 0.75. It can be seen from the PSD that coarser grinding is achieved at a higher ball filling (J = 40 %) for all grinding times, possibly because at a given mill rotational speed, a lower media load shows more cataracting action than a higher media load (Fortsch *et al.*, 2006).

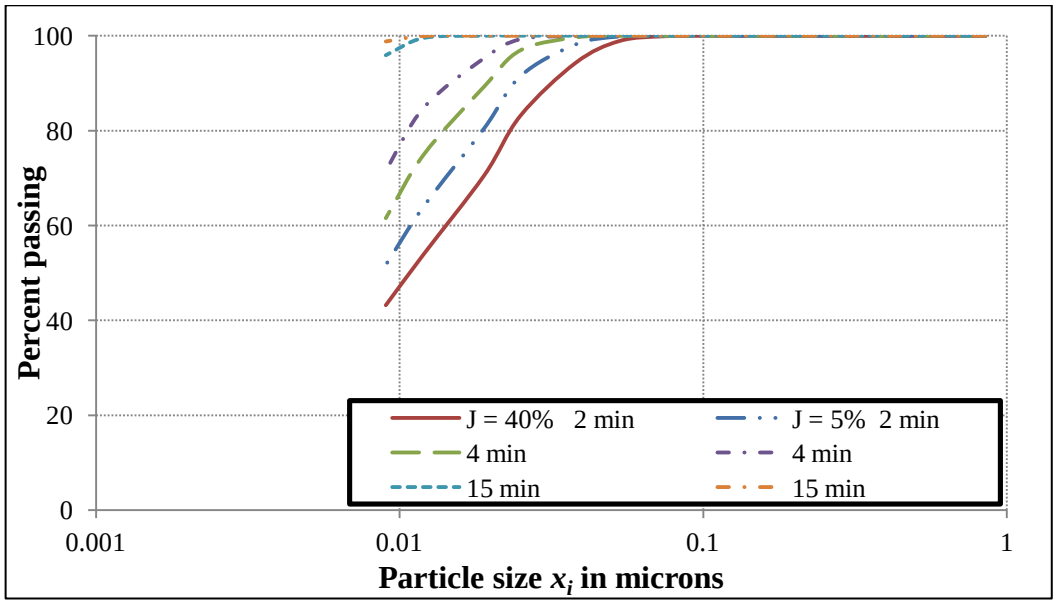


Figure 5.4 Effect of ball filling J on PSD: ϕ_c = 75 %, U = 0.75, d = 40 mm.

An interesting point to note is that J = 40 % produced the maximum amount of the desired size class m_2, as shown in Figure 5.5. This is not very different from J = 35 %, which was proposed by Fortsch *et al.* (2006) as optimal. Metzger *et al.* (2009) suggest that the lowest ball filling produces the highest amount of desired product, which differs from our present observation. Austin *et al.* (1984) also concludes that J = 40 % is the optimal media charge filling.

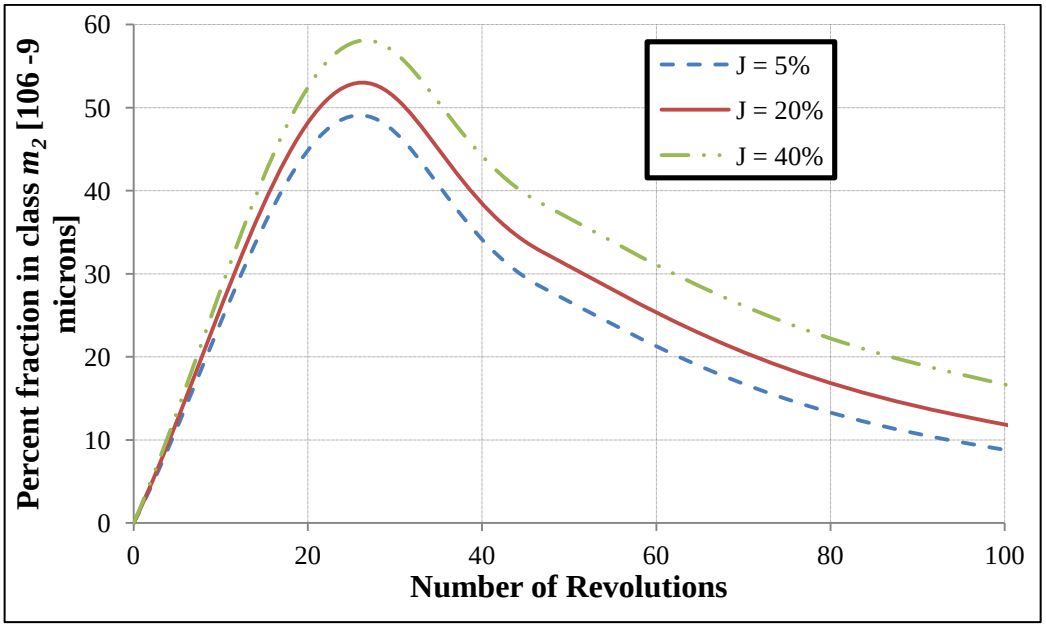


Figure 5.5 Plot of mass fraction of m_2 versus number of revolutions for ball filling J on PSD: ϕ_c = 75 %, U = 0.75, d = 40 mm.

5.2.2.3 Effect of ball diameter on milling

The influence of the size of balls on the breakage rate is shown in Figure 5.6. In general, engineers expect that effective breakage is promoted if bigger balls are used to break coarser particles. Chimwani *et al.* (2012) observed that when grinding a narrow-sized feed of -850 +600 µm, the breakage rate increased with ball size, whereas a decrease was recorded for a feed of -600 +425 µm. As expected, the PSDs in Figure 5.6 show a coarser product for 40 mm balls, and a greater degree of fineness in the product as ball diameter decreases. This is attributable to the fact that, as the diameter of the ball is reduced, the number of balls in the mill increases, which causes a relative improvement in the surface area available for grinding. This in turn leads to a rise in the specific rates of breakage for small particle sizes (Austin *et al.*, 1984).

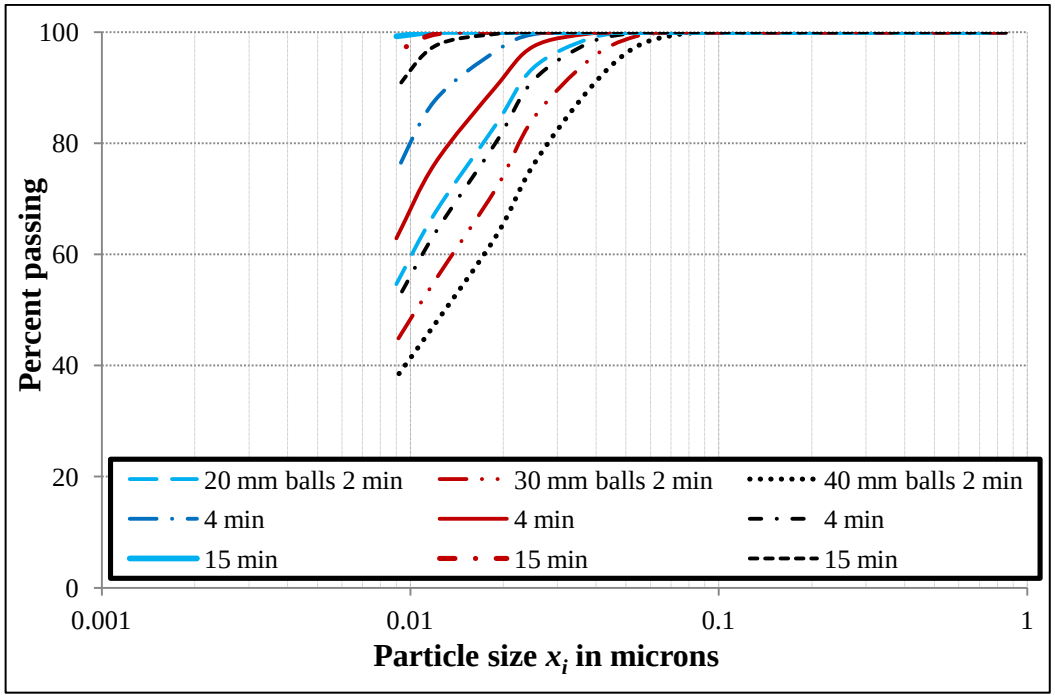


Figure 5.6 PSD for different media sizes; ϕ_c = 75 %, U = 0.75, J = 40 %.

The effect of the ball diameter on the grinding profiles of the desired size class at a constant speed, media and powder load is shown in Figure 5.7. The three ball sizes considered (20 mm, 30 mm and 40 mm) all achieved different maximum amounts of the desired size class. It can be seen that as the ball size becomes smaller, the maximum achievable mass fraction of size class two decreases (see Figure 5.7). The highest maximum amount of the desired size class (62 %) was produced with 40 mm balls; 30 mm balls yielded 55.7 %, while 20 mm balls obtained 45.3 %. The results in Figure 5.7 are also informative from the cost point of view, since the smaller the ball sizes, the more expensive they are to purchase. However, it is worth mentioning that Figure 5.6 shows that the highest breakage rate is achieved by the use of 20 mm balls, followed by 30 mm balls and finally 40 mm balls.

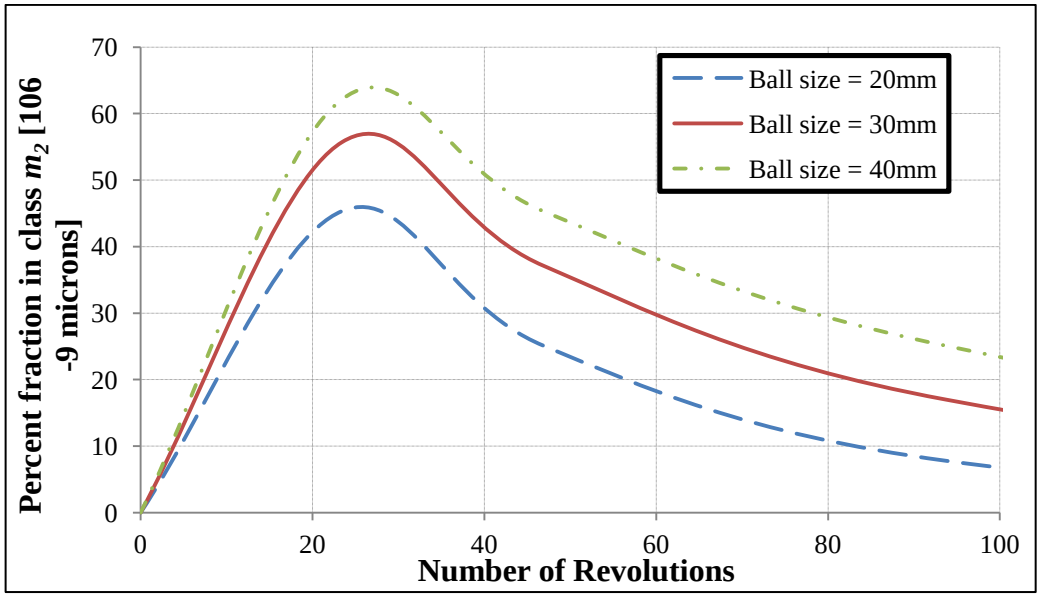


Figure 5.7 Plot of mass fraction of m_2 versus number of revolutions for different ball sizes; J = 40 %, ϕ_c = 75 %, U = 0.75.

5.2.2.4 Effects of slurry filling on milling

The ratio of volume of powder loaded to the volume of the ball interstices available within the bed at rest is called the slurry filling (U). Slurry first occupies the interstices between the grinding balls, and then forms a layer on the bed of balls at rest. Previous research publications on this subject (Shoji and co-workers, 1980 & 1982; Tangsathitkulchai, 2003) have shown that slurry filling affects the milling rate, regardless of whether it is dry or wet milling.

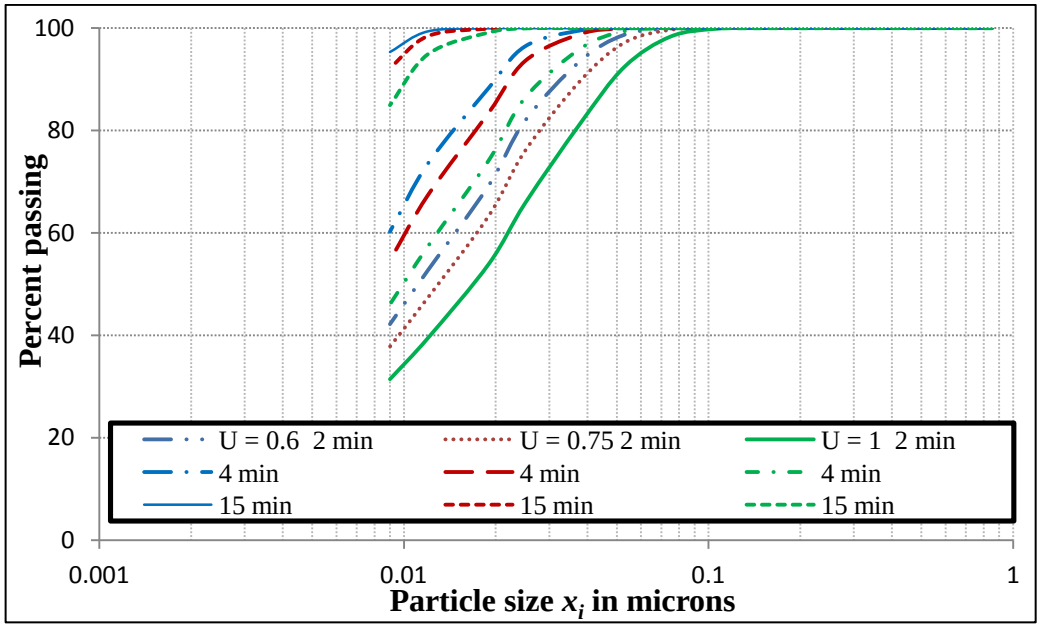


Figure 5.8 PSDs for three slurry fillings; ϕ_c = 75 %, J = 40 %, d = 40 mm.

Figure 5.8 shows the PSD for the slurry fillings U = 0.6, 0.75 and 1, and for mean residence times t = 2, 4, and 15 min. This graph shows that the slurry filling U = 0.6 produced the finest product. As the slurry filling was increased, the product became coarser. This could be attributed to the phenomenon that further addition of slurry increases its mass hold-up, which cushions the collision impacts responsible for grinding, thereby lowering the breakage rate (Austin *et al*., 1984).

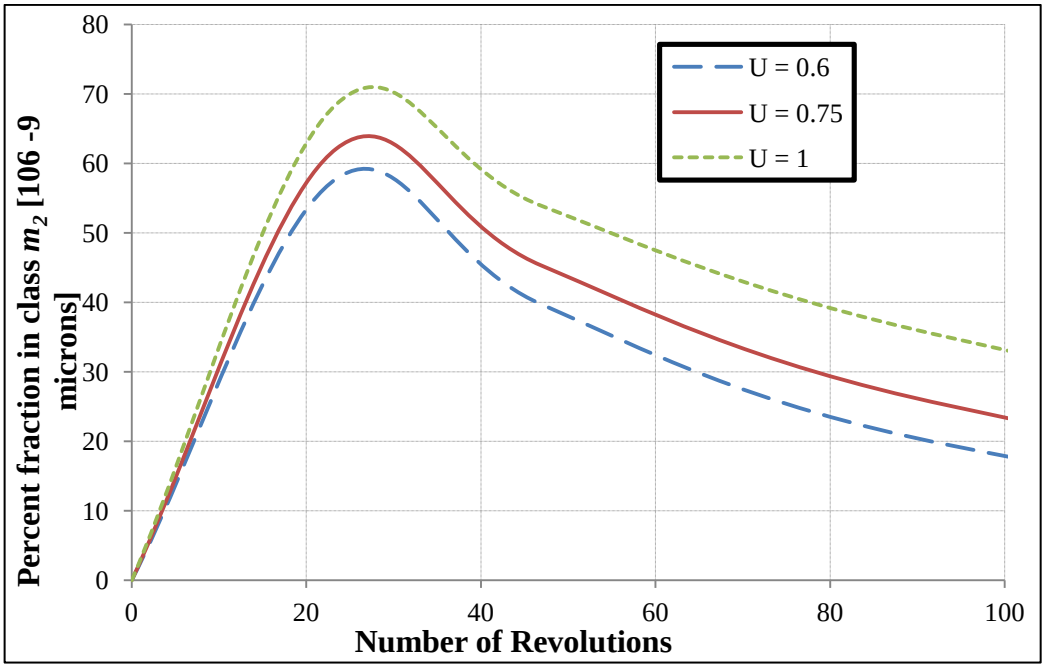


Figure 5. 9 Plot of mass fraction of m_2 versus number of revolutions for different slurry fillings; J = 40 %, ϕ_c = 75 %, and d = 40 mm.

Figure 5.9 shows the effect of slurry filling on the grinding profiles. The grinding profile of U = 1 produced the highest throughput, followed by U = 0.75 and lastly U = 0.6. From this observation, it is clear that operating mills at a higher U maximizes the production of the desired size class, and that any further addition of slurry beyond U = 1 leads to the formation of a slurry pool. After realising that a slurry pool forms around the toe of the media charge once the mill has been supplied with more slurry than the media interstices can accommodate, Katubilwa (2012) concluded that U = 1 was the optimal slurry filling. This was also recommended by Latchireddi and Morrell (2003), who found that the conditions required for the best grinding efficiency corresponded with the maximum slurry hold-up that can be held in grinding media without forming a pool.

Table 5.2 shows the compilation of all the factors examined above, together with the grinding profiles that registered the highest throughput.

Table 5.2 Individual milling parameters and corresponding optimum throughput

Milling parameter	**Optimum value**	**Production of (-106 +9 µm)**
Mill speed	ϕ_c = 40 %	74.75
Ball filling	J = 40 %	56.78
Ball size	d = 40 mm	64.53
Slurry filling	U = 1	68.5

Figure 5.10 shows profiles of the desired size class m_2 for all the operating factors considered in this chapter. Also included is the profile for the operational conditions typically used in industry (ball size d = 40mm, mill speed ϕ_c = 75 % of critical, ball load J = 30 %). Under these typical industrial conditions, the maximum amount of m_2 produced is 63.9 %. However, the diagram shows that a higher rate of production of m_2 per revolution as well as a higher maximum amount of m_2 (74.75 %) can be obtained by using a lower mill speed (ϕ_c = 40 % of critical).

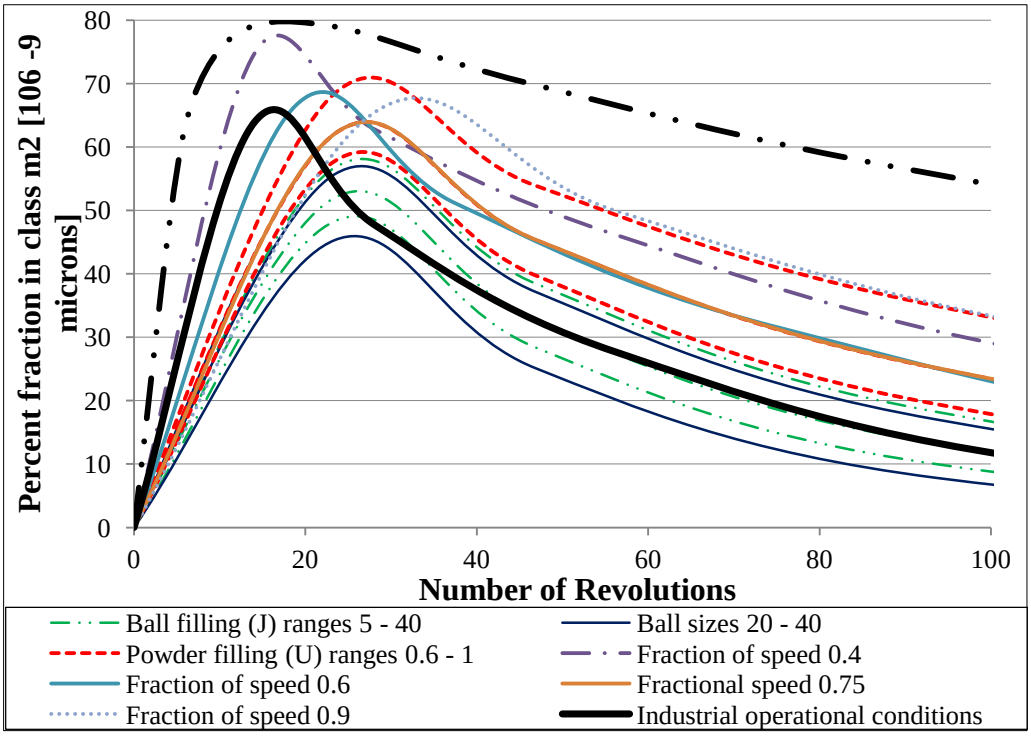


Figure 5.10 Summary of various simulations, optimised solution and industrial operating conditions.

A Matlab® search engine was then used to search for the parameters which would produce the highest amount of the desired size class over the range of $0 < J < 0.6$; $0.3 < U < 3$; $0.4 < \phi_c < 0.9$; $0.01 < d < 0.1$. The optimal set of parameters from the search that maximises the amount of m_2 formed was found to be $J = 0.4$, $U = 1.86$, $\phi_c = 40$ % and $d = 40$ mm; these produced the maximum fraction of 79.1 %.

The Matlab search indicates very clearly that there is more that can be done to improve the throughput, and consequently to maximise the production of the desired size class. The AR graphical analysis tool has shown the conditions under which the mill can be operated to achieve that, but the feasibility of the suggestions made has to be confirmed by tests on the pilot plant in order for the industry to adopt the concept.

To sum up the contents of this chapter, in the tests carried out, when the mill speed was varied, the lowest speed produced the highest maximum amount of the desired size class m_2. This does not agree with common practice, which recommends 75 % of critical speed as optimal. A ball filling of $J = 40$ % produced the highest throughput, which is in agreement with the work of other researchers. A ball size of $d = 40$ mm as well as $U = 1$ was found to maximise the production of the desired size class m_2. It was, however, interesting to note that all these factors, though producing the highest amount of desired product, also produced the coarsest size. The AR analysis also suggested that it is always worthwhile to consider speed as the first factor the engineer should consider adjusting when optimising milling of PGM ore to achieve a given desired size class. In contrast, speed is seldom adjusted in industrial milling.

5.3 Conclusion

In this chapter, empirical models were successfully used to scale-up the breakage rate from laboratory tests to an industrial mill with sufficient validation using both batch experimental data and industrial mill sampling data. Upon validation it was thus possible to use the simulator to explore a number of variables that would affect product size distribution.

The main objective being the maximisation of the m_2 size fraction (-106μm +9 μm). Using the AR technique, a graphical method for exploring output limits of a system, it has been shown that our objective is achieved when the rotational speed ϕ_c = 40 % of critical, ball filling J = 40 %, ball size d = 40 mm and slurry filling U = 1. Though product was coarser, the greatest amount of the desired size class m_2 was produced. The AR can easily be used to determine operational limits once the objective product desired is set and this can be flexibly adjusted if the objectives change. It has thus been demonstrated how the AR can be integrated with population balance modelling to make optimisation of grinding easier. There is no reason why in future this technique cannot be integrated with other models such as grinding liberation models.

The findings described in this chapter regarding AR reinforce the suggestions made by Metzger *et al*. (2009) that running the mill at low speeds saves energy and maximizes the production of the desired size class; however, the throughput dimension was not considered and will be tackled in future. Our findings also suggest that the current operational conditions in industrial mills leave much room for improvement. If the aim is to achieve maximum throughput of the desired size class, much can be done to remedy underperformance and energy inefficiency. The AR technique has been shown to have potential to provide an alternative way of optimizing milling.

For future work, the dependency of the energy requirements of the full-scale mill on operating parameters such as powder filling, media charge filling, mill speed and ball diameter from an AR perspective will be investigated, with a view of determining how the energy consumption can be reduced for a given production rate of the desired size class.

Chapter 6 Use of the attainable region method in determining the optimal residence time of a ball mill

The results of this chapter have been published in the International Journal of Mineral Processing under the reference: Mulenga, F.K., **Chimwani, N**., 2013. Introduction to the use of the attainable region method in determining the optimal residence time of a ball mill. *International Journal of Mineral Processing,* vol. 125, pp. 39 – 50

This is completely my work, i did all the simulation and processing of data as well as writing the paper. F.K. Mulenga is one of my supervisors who sent the paper for publication .

Abstract

The application of the attainable region (AR) technique to the analysis of ball milling is currently limited to batch data. This chapter introduces the use of the technique in continuous milling.

In the earlier chapters of this thesis an investigation into the breakage characteristics of a platinum-bearing ore (less than 850 μm in size) and their measurement by means of standard batch milling tests was described. The breakage parameters were scaled up to the requirements of an industrial mill, which allowed us to extend the AR analytical methodology to full-scale milling. However, the first stage of the analysis was limited to two simple transport models; plug-flow and well-mixed mills without exit classification.

The results of the initial analysis showed the importance of targeting milling conditions to the desired product size requirements, and identified the lower and upper limits at which the maximum production of fines are attainable. The AR plot also demonstrated the importance of controlling the residence time of the mill optimally by recognizing that mill speed is found to be pivotal to managing the retention time of particles inside the mill.

6.1 Introduction

Ball milling is widely used in the mineral, metallurgical, power generation and chemical industries. Its popularity is attributable to its flexibility and versatility in reducing materials to smaller sizes. The degree of milling that can be achieved depends mainly on the time the particles spend inside the mill: a stay that is too short results in a coarse product, whereas one that is too long leads to over-ground particles, and a concomitant waste of energy. It therefore becomes evident that the time needed for the material to travel through the belly of the mill (residence time) is essential to meeting product size requirements. Besides, various researchers have argued that the residence time is pivotal in optimising and constructing accurate models of full-scale mills (Austin *et al.*, 1984; Makokha *et al.*, 2011).

There have been numerous attempts to incorporate the residence time into ball mill models (for example, Austin and Cho, 2002; Cho and Austin, 2002). However, little attention has been paid to its optimisation. In this chapter, an optimisation methodology is proposed that is centred on the AR technique. In essence, the population balance model is used for the formulation of the milling process. At this point the time/rate breakage of particles (or selection function) inside the mill was assumed to follow the first-order law of kinetics (Yekeler, 2007). Finally, the milling data generated were analysed within the AR framework (Khumalo *et al.*, 2006 – 2008). It is to be emphasised that in this introductory study no exit classification process (Cho and Austin, 2004; Austin *et al.*, 2007) was assumed to have taken place.

All the prominent studies on AR so far have been based on laboratory data (Khumalo, 2007; Metzger *et al.*, 2009; Katubilwa *et al.*, 2011; Metzger, 2011; Metzger *et al.*, 2012; Chimwani *et al.*, 2012; Hlabangana *et al.*, 2012). To make the move to full-scale scenarios possible, the batch grinding information needs to be scaled up and integrate it into a continuous system; this is where the transportation modelling becomes necessary.

In an effort to achieve this goal, an ideal open milling circuit was considered with its geometry and ore breakage properties of which are known *a priori*. After that, two flow models were considered: a plug flow mill and a perfectly mixed mill.

This way, it was possible to calculate theoretical residence time boundaries that would guarantee optimal grinding.

6.2 Data collection and analysis

The simulation programme for the scale-up is described in Section 3.5. A Matlab® code (presented in Appendix A.4) was written for the scale-up methodology. The outcomes of the simulation programme initiated in the previous section (Section 6.1) are summarised below. In line with the work done by Makokha *et al.* (2011), simulations were carried out for grinding times below 120 min. In addition, the ball filling *J* was varied from 20 – 35 %. As for the slurry filling, *U*, the volume of slurry was assumed to be that of slurry held up inside the mill at rest without overflow. By using the rule of thumb whereby the trunnion diameter is a quarter of the mill diameter *D* (Morrell, 1993), it was possible to calculate the slurry fillings *U* that were correspondent to any given ball filling *J*. Ball size and mill speed values lay in the ranges 10 – 40 mm and 60 – 80 % of critical speed respectively. The product class m_2 was set between 75 – 9 µm because the platinum industry in South Africa generally requires a product size of less than 75 µm before it is sent to flotation. The latter cut-off size was guided by the poor flotation performance reported for particles of less than 10 µm on average (Rule and Anyimadu, 2007).

Having said that, the initial feed class m_1 considered was -850 +600 µm, while the objective function was to determine the residence time that would result in the maximization of product m_2. The optimisation scheme consisted of plotting the kinetics of material produced in class m_2 as a function of residence time, followed by the identification of the residence time at which the mass fraction in class m_2 was highest.

6.2.1 Effects of ball filling on mill production

Before presenting the findings on the effects of ball filling, it is important to stress the manner in which the actual slurry filling was calculated.

From the definition of the relevant metrics shown in Figure 6.1, one can calculate ball filling J using the approximate formula below (Gupta and Yan, 2006):

$$J \cong \frac{1}{6.\pi.R^2}.\frac{H_B}{W_B}.\left(3H_B^2 + 4W_B^2\right) \qquad \textbf{(6.1),}$$

where $W_B = 2\sqrt{R^2 - H^2}$ and $H = R - H_B$.

The radius of the discharge trunnion radius is a quarter of that of the mill inside liners ($0.25 \times R$), the areas covered by grinding balls A_B and slurry A_{sl} will be given by:

$$\begin{cases} A_B = R^2.\cos^{-1}\left(\dfrac{H}{R}\right) - H.\sqrt{R^2 - H^2} \\ A_{sl} = R^2.\cos^{-1}\left(\dfrac{1}{4}\right) - \dfrac{R^2\sqrt{15}}{16} \cong 1.076R^2 \end{cases} \qquad \textbf{(6.2).}$$

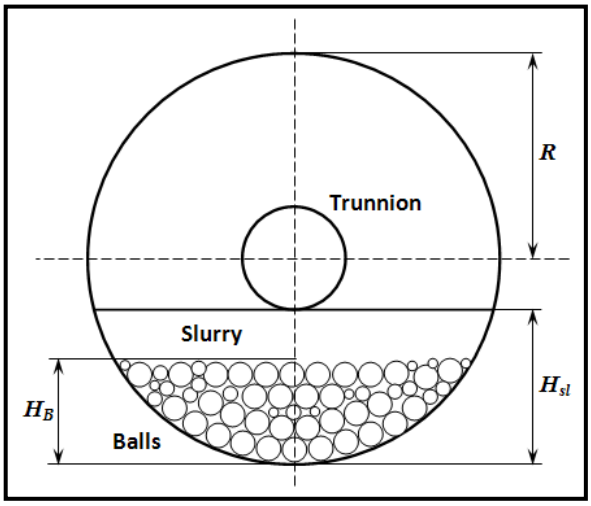


Figure 6.1 Geometric parameters considered for the industrial mill at rest.

If one considers an average bed porosity of grinding balls of $\varepsilon_L = 0.4$, the total volume of slurry contained in the mill unit length will be $A_{sl} - A_B + \varepsilon_L.A_B$. In the end, the slurry filling becomes:

$$U \cong \frac{1.076R^2 - (1-\varepsilon_L).\left[R^2.\cos^{-1}\left(\frac{H}{R}\right) - H.\sqrt{R^2 - H^2}\right]}{\varepsilon_L.\left[R^2.\cos^{-1}\left(\frac{H}{R}\right) - H.\sqrt{R^2 - H^2}\right]} \qquad \textbf{(6.3).}$$

Using Microsoft Excel's solver as the search engine, parameter H_B was back-calculated from Equation 6.1 to correspond to a known ball filling J. After that, parameter H was calculated, and then substituted into Equation 6.3. Table 6.1 provides a sample of ball fillings and their corresponding slurry fillings under the assumption of an industrial mill at rest. Note that slurry U is less than unity (that is, $U < 1.0$) for ball filling $J = 35$ %, suggesting the absence of a pool of slurry.

Table 6.1 Correlation between ball filling J and slurry filling U used

Ball filling J [%]	Slurry filling U [-]
20	2.78
25	1.92
30	1.35
35	0.95
40	0.66

To return to the combined effects of ball and slurry fillings on the production of the size class of interest m_2, Figure 6.2 illustrates the simulation outputs for the two transportation models under consideration (Equations 2.42 and 2.43).

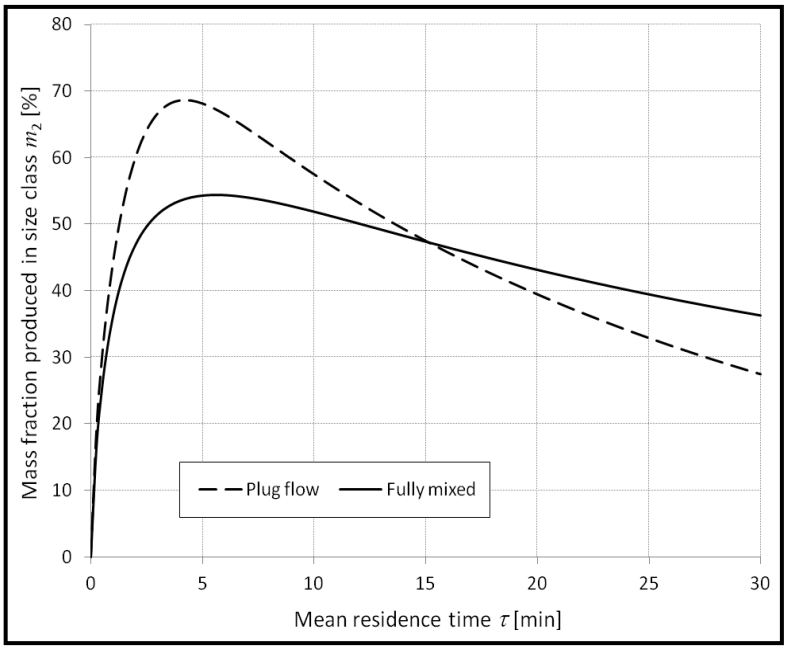


Figure 6.2 Throughput of the mill for the two RTD profiles. Simulation conditions: J = 30 %, U = 1.35, d = 40 mm and ϕ_c = 70 % critical.

One can see that the plug-flow mill model yielded a higher throughput for a lower mean residence time. In Figure 6.2, the throughput and optimal residence time were found to be τ = 4.21 minutes and m_2 = 68.7 % for the plug-flow mill. The fully mixed mill, on the other hand, obtained an optimal time of τ = 5.61 min for a throughput m_2 = 54.4 %.

Next, the effects of ball filling were explored with the help of Equations 2.13 – 2.14 corresponding with the plug flow mill and 2.16 – 2.17 with the well mixed mill. Figure 6.3 shows only the simulation results for the fully mixed mill, and shows that regardless of the level of ball filling, the optimum production of m_2 remains unchanged at 54.4 %. However, an increase in ball filling shortens the mean residence time, which is necessary for the maximum production of m_2.

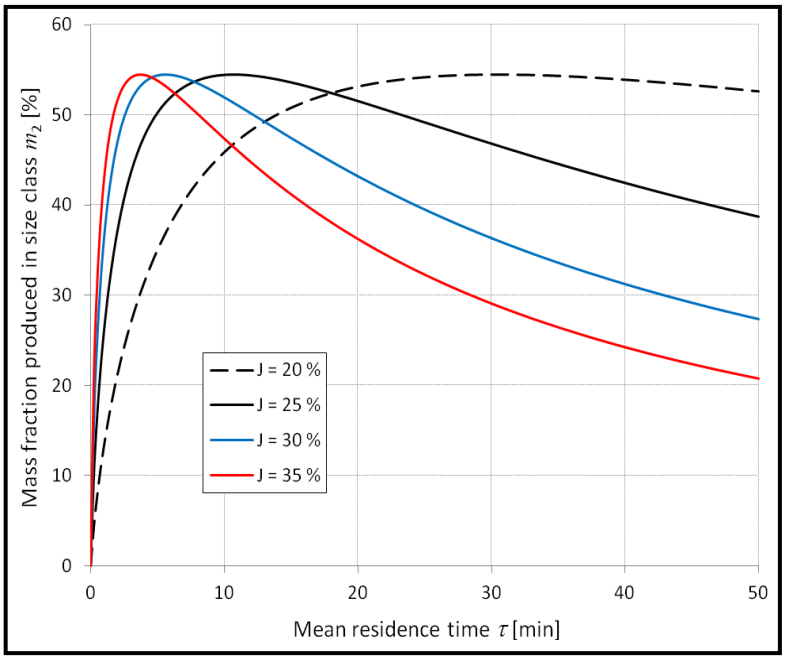


Figure 6.3 Prediction of ball filling effects on mill throughput for a fully mixed mill. Simulation conditions: d = 40 mm and ϕ_c = 70 % of critical.

Similar trends were also noted for the plug flow transport model, with the optimum throughput at 68.7 %.

Table 6.2 provides a summary of the optimum mean residence times corresponding to the two mill flow models for different ball fillings.

Table 6.2 Mean residence times τ_{optim} for d = 40 mm and ϕ_c = 70 % of critical

	Optimum mean residence time τ_{optim} [min]	
Ball filling J [%]	Plug flow	Well mixed
20	22.87	30.45
25	8.04	10.70
30	4.21	5.61
35	2.79	3.72

The general belief among engineers is that a high ball filling leads to faster production of m_2, which agrees with industrially accepted practice (Austin *et al.*, 1984). The problem, however, is that the optimum mean residence time τ_{optim} does not decrease in proportion with an increase in ball filling. In addition, the higher mill power draw required by a raised level of grinding balls may result in

inefficient milling. In other words, unnecessary amounts of power may be drawn for the same production of m_2. Indeed, there is a sharp drop in τ_{optim} when the ball filling rises from 20 % to 25 %, followed by a marked deceleration between J = 30 % and 35 %.

To summarise, running the mill with a high ball filling may indeed be beneficial, as it maximises production of our target size range. Nonetheless, the increased power draw required may force the industry to consider a trade-off between throughput and mill power draw (Austin *et al.*, 1984).

6.2.2 Effects of ball size on mill production

In the second set of simulations, the effects of ball diameter were analysed while keeping the ball filling, slurry filling and mill speed constant. Four ball diameters (10, 20, 30, and 40 mm) were considered.

As depicted in Figure 6.4, the throughput results for d = 10 mm showed that the behaviour of the plug flow model surpassed that of the well-mixed one. In contrast to what was observed while studying the ball filling effects, the mean residence times in this case are closer (1.05 and 1.40 min). Also, in the second set of simulations, the maximum throughputs remained unchanged for the two flow models, at 68.7 % for a plug-flow mill and 54.4 % for a perfectly mixed mill.

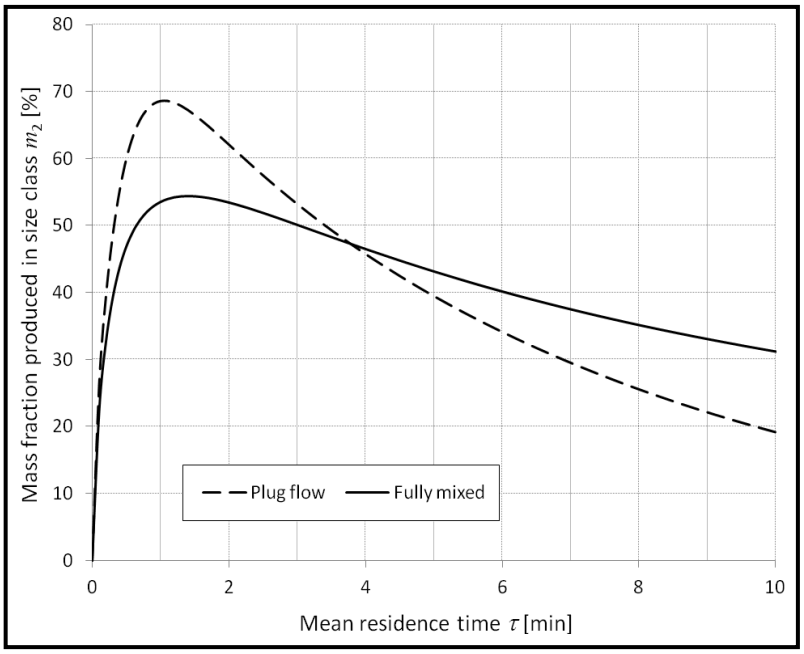


Figure 6.4 Effects of ball diameter on mill throughput for the two RTD profiles. Simulation conditions: J = 30 %, U = 1.35, d = 10 mm and ϕ_c = 70 % of critical.

On the question of the influence of the ball diameter on the optimum mean residence time τ_{optim}, it can be said that more time is required to reach the maximum throughput as the grinding media become larger (Figure 6.5). This implies that smaller balls tend to promote a faster production of the target size range, m_2 or size class -75 +9 µm. Researchers such as Austin *et al.* (1976) and Napier-Munn *et al.* (1996) reported similar findings. The difference between their findings and the present work is that, in addition to having confirmed the widely-accepted theory pertaining to the effects of ball size on milling, the optimum mean residence time τ_{optim} is determined for a full-scale mill in open circuit, by means of two extreme mill transportation models (see Table 6.3 below).

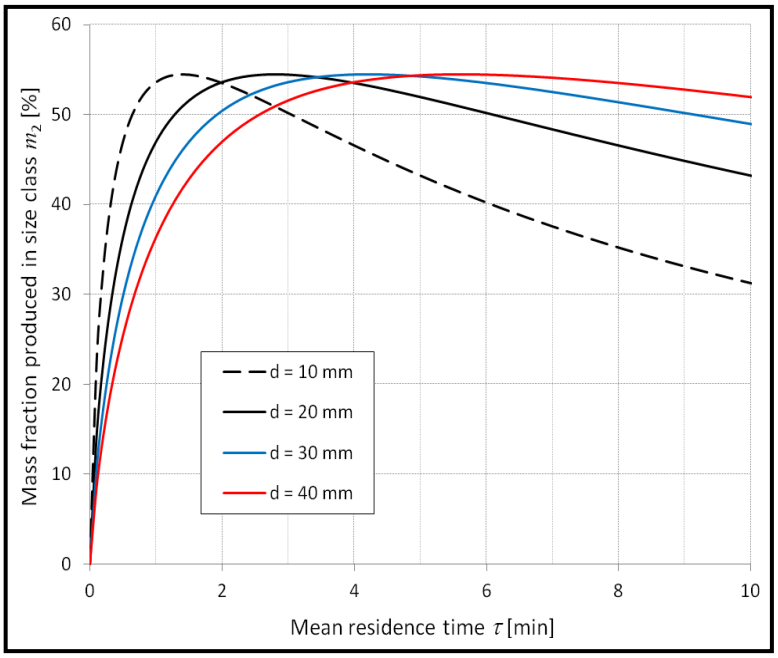


Figure 6.5 Effects of ball size on mill throughput for a well-mixed mill. Simulation conditions: J = 30 %, U = 1.35, and ϕ_c = 70 % of critical.

Furthermore, Table 6.3 shows that there is a linear relationship between mean residence time τ_{optim} and ball diameter d. From a mill power demand point of view, engineers may consider it better to adopt a ball addition policy, in terms of which the graded ball charge comprises a high number of smaller balls. Also, because the mill power draw does not change much with alterations in ball diameter (Austin *et al.*, 1984; Morrell, 1993), it is possible to meet the target throughput faster while using the same amount of power.

Table 6.3 Mean residence times τ_{optim} for J = 30 % and ϕ_c = 70 % of critical

	Optimum mean residence time τ_{optim} [min]	
Ball size d [mm]	Plug flow	Well mixed
10	1.05	1.40
20	2.10	2.80
30	3.16	4.21
40	4.21	5.61

6.2.3 Effects of mill speed on mill production

The last series of tests carried out were aimed at investigating the effects of mill speed on the mean residence time, so as to guarantee maximum production of class m_2. In order to capture the meaningful information, it was decided to expand the speed range from 50 % to 90 % of critical. The results are plotted in Figure 6.6

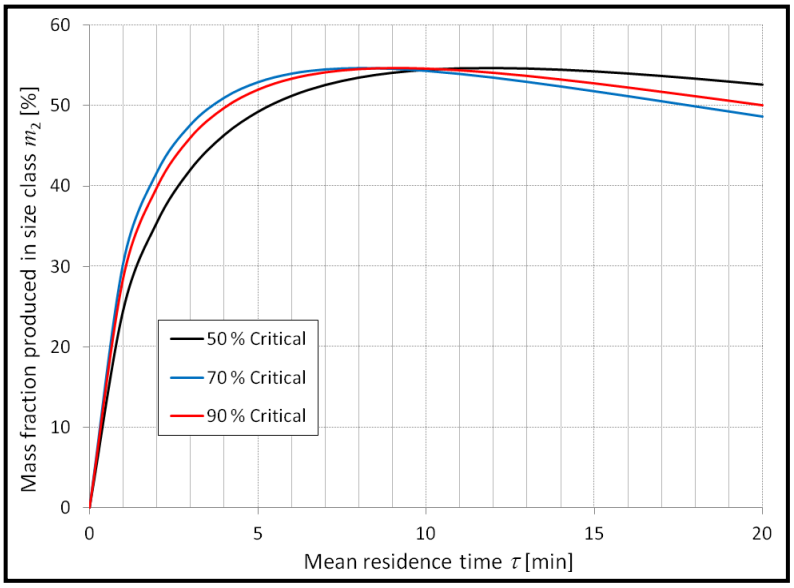


Figure 6.6 Effects of mill speed on mill throughput for a fully mixed mill.
Simulation conditions: J = 25 %, U = 1.92 and d = 30 mm.

The results of this undertaking revealed that in order to reach the optimum throughput, the mill, running at 50 % of critical speed, needs 11.78 min. A shorter time (8.03 min) was recorded at 70 % of critical, while a relatively long time (9.03 min) was taken at a mill speed of 90 % of critical. Values of the optimum mean residence time τ_{optim} for both transport models are listed in Table 6.4 below.

Table 6.4 Optimum mean residence times τ_{optim} for J = 25 % and d = 30 mm

	Optimum mean residence time τ_{optim} [min]	
Mill speed ϕ_c [%]	Plug flow	Well mixed
50	8.85	11.78
60	7.11	9.46
70	6.03	8.03
80	5.61	7.47
90	6.78	9.03

It is evident that there is an optimum mill speed ϕ_c (between 70 – 80 % of critical) at which the mill produces the size class of interest m_2 most rapidly. In contrast, because mill speeds below 60 % of critical are known to produce more abrasion and attrition as far as load behaviour is concerned, engineers expect low-speed grinding to result in more fines. But because the corresponding mean residence times are longer (8.85 and 11.78 min), one could say that abrasion is slow to produce the desired product. It should also be borne in mind that the products of abrasion breakage do not necessarily fall into the targeted class m_2.

Similarly, a high mill speed (90 % of critical) leads to a cataracting load, and consequently to more impact breakage. The figures in Table 6.4 clearly indicate that the product of such a breakage mechanism does not favour the desired class, which is why more time is needed to reach maximum throughput.

6.3 Summarised findings

This section is prefaced by reminding the reader that the aim of the research set out in this chapter was twofold. Firstly, the work sought to propose a data analysis paradigm for continuous ball milling centred on the AR approach. Secondly, it was intended to explore the use of the AR technique in the study of full-scale mills, using simplified flow models.

The next thing to underscore is that the initial exploratory study was built on two flow models: namely, the plug-flow and the perfectly mixed mills. Though models are essentially unrealistic in that they are not directly related to operating parameters such as feed flow-rate and slurry concentration, the two models have important uses. For example, the flow models determine the limiting boundaries of a real full-scale mill. Indeed, the working of a real mill will always fall somewhere between the extremes represented by the two flow models.

The simulation results are discussed in the next few paragraphs, followed by an identification of what these findings imply for future research.

From a throughput perspective, the full-scale mill simulated in this work can generate at least 54.4 % and at most 68.7 % of product in size class m_2. Moreover, the simulated retention time necessary for reaching these targets was found to be 0.70 minutes at best (J = 35 %, ϕ_c = 70 % of critical, plug flow mill) and 44.67 minutes at worst (J = 20 %, ϕ_c = 50 % of critical, fully-mixed mill). The most important insight gained was that the throughput proved insensitive to all the milling conditions considered for both flow models. This needs to be tested on a real RTD model with exit classification, as has been discussed in a number of articles, including those written by Austin *et al.*, 2007; Austin and Cho, 2002 & 2004; and Cho and Austin, 2002.

The next set of simulation outputs suggest that the ball diameter should be tailored to the target product. Figure 6.7 exemplifies this well by giving a broader picture of the effects of ball size on the optimum mean residence time. As can be seen in the figure, every point on each ball diameter curve shows the optimum residence time needed to maximise the production of the desired size class at that particular mill speed. Indeed, it shows that the residence time is largely dependent on ball diameter. In addition, this figure demonstrates that the residence time can be shortened while still meeting the product size requirements by adjusting the ball size appropriately.

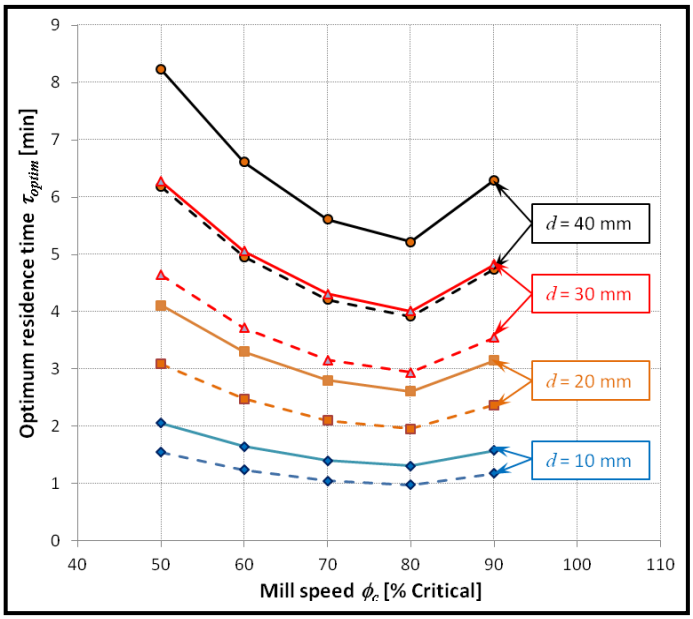


Figure 6.7 Residence time τ_{optim} as a function of mill speed ϕ_c for J = 30 % under varying ball diameters. Solid and dashed lines in the plot area represent the well-mixed and plug-flow mill models respectively.

Finally, mill speed has been identified as an operating parameter that could play a big role in the optimisation of milling. Table 6.4 revealed the existence of an optimal speed ϕ_c situated somewhere between 70–80 % of critical. This finding is further corroborated by Figure 6.7, and signifies that the mill speed should be tuned to the target product m_2. A research study following up this work in the future will need to look at mill speed in an industrial setup while taking into consideration the economics of milling as well as the need to restrict energy usage. At present, mills are generally run at 69 % of critical speed to conserve liners. A more comprehensive simulation model that integrates all the relevant aspects of milling operations needs to be developed to generate the data that will provide a more authoritative set of operational parameters. This of course is beyond the scope of this thesis.

6.4 Conclusion

The attainable region is an elegant and powerful technique of analysis, and its usefulness in milling is only now beginning to be appreciated. However, the

complexity inherent in milling limits AR to a simple description of the data. To put it another way, the AR technique offers a way of looking at the data in hand that yields insights. Hidden information that cannot be picked up otherwise is revealed. In addition, the AR method makes it possible to optimise milling as a single unit process in a complex flowsheet or as a section in a series of unit processes in an integrated fashion. The method, though useful, cannot be used in a situation where 'what-if' analysis is expected. It is merely a visualisation tool that can be used to provide a flexible analysis and an in-depth insight into mineral processing data in general, and milling data in particular. This is the reason why it is believed that the AR technique, as applied to milling, offers an excellent opportunity to optimise milling circuits. The confidence in this method gained by a number of researchers in the Centre for Material and Process Synthesis at the University of the Witwatersrand has, however, been built on laboratory work (Khumalo, 2007; Khumalo *et al.*, 2006– 2008; Metzger *et al.*, 2009; Metzger, 2011; Katubilwa *et al.*, 2011; Metzger *et al.*, 2012; Chimwani *et al.*, 2012). The next step in developing the applicability of the AR technique in milling should be to find ways of validating it using industrial setups. One possible route would be to resort to simulators such as Modsim^{TM} (King, 2001) to generate data that can be optimised with the AR technique.

6.5 Future outlook

The work presented in this chapter is the first step towards the objective outlined above, and it has shown that combining the PBM with the AR technique could provide an alternative route to the analysis of comminution processes.

Projection for further research on this project in the future entails the integration of more realistic RTDs into the analysis of continuous milling. In this regard, plans are already being made to refine the transport models and include the exit classification process. Furthermore, the effects of the following milling parameters will be investigated thoroughly: solids concentration of slurry, feed flowrate, ball size distribution and energy consumption. This will evidently require a validation of the underlying mathematical models as compared against

industrial data. Ultimately, an integrated study of milling circuit configurations will be initiated to consolidate the position of the AR technique as an alternative analysis tool. Indeed, it would be more appropriate to accomplish that by dealing with a problem of milling circuit optimisation, rather than restricting the solution to ideal ball milling. At this stage of the research, it is believed that the merit in applying the AR method and simulation has been demonstrated, and that this technology can be extended to milling circuits.

Chapter 7 Use of the attainable region method to simulate a full-scale ball mill with a realistic transport model

Abstract

In order to achieve optimization and better control of milling circuits, not only a detailed understanding of the process of comminution as carried out in tumbling ball mills is required but also an extensive knowledge of the methods of modelling through which milling data can be analysed. In the previous chapter, the attainable region (AR) approach, complemented by the standard population balance modelling (for size reduction) and transport models, was used to demonstrate that it is possible to define an optimum residence time for tumbling mills. This made it possible to regard throughput as a function of operational mill conditions (Mulenga and Chimwani, 2013). The research was limited to two types of mill transportation modes, the plug flow and fully mixed.

This chapter extends the enquiry to the use of the AR technique to determine both the optimal residence time of ore in an actual full-scale ball mill and the energy requirements of the mill at that residence time setting.

With these purposes in mind, the breakage function and the scaled-up selection function parameters discussed previously were used to simulate the operating conditions required by a real industrial ball mill. This allowed the application of AR methodology to be extended to the design of a real industrial-scale ball mill to link residence time to the production of the desired size class for flotation from a given feed size. This yielded valuable insight for the importance of optimally controlling both the residence time of the material inside the mill and the amount of energy required to maximise the desired size range, in this case -75 +9 μm.

That finding confirmed that the residence time required by a full-scale mill falls between those at which the fully mixed and the plug flow mills operate. The results also showed that operating the ball mill at a lower mill speed and a higher

ball filling saves energy. Mill speed was again found to be a key operational factor for controlling the retention time of particles inside the mill.

7.1 Introduction

Over the years, a great deal of work has been done to develop a well-trodden path towards the understanding and modelling of tumbling mills (Austin *et al*., 1984; King, 2001; Toneva and Peukert, 2007). But owing to the complexity of the process, engineers have yet to explore some aspects of its operating functions. These must be examined if they are to fulfil their ultimate purpose: to develop a robust model of the process.

Residence time is believed to be one of the key factors necessary for the optimisation of the mill product. Several researchers have attempted to relate residence time to the optimization of ball mills (Austin *et al*., 1984; King, 2001; Makokha *et al*., 2011). However, little attention has been paid to actually reaching set optimisation goals. In the previous chapter, a method was develop that could be used to optimise the residence time to overcome a shortcoming in the simulation approach, which was the use of two simple transport models, namely; plug flow and a fully mixed mill. The new method has broken the ground for a new exploration of the concept of using the residence time distribution model in an industrial-scale mill.

In this chapter, the residence time optimisation is expanded from the simple transport models to a more realistic approach, and the analytical methodology developed in the previous chapter is applied. The RTD model comprises a dead zone, two small fully mixed tanks and one large fully mixed reactor (Makokha *et al*., 2011). The resulting flow pattern through these series of tanks describes very well the residence time distribution of slurry in the mill as a function of ball filling, slurry filling, and feed flow-rate.

The PBM framework and the more realistic transportation model made it possible to track the evolution of the mill product size and the amount of energy used in the process. Different mill conditions were explored by simulation and the data generated were analysed using the AR scheme. Practical residence time boundaries were determined for the optimal production of floatable material. It should be noted that no exit classification was considered in the mill model.

7.2 The mill transport model

The RTD model used in this stage of the research was developed by Makokha (2011). It comprises a dead time (τ_d), the residence time (τ_s) of two small fully-mixed reactors of equal volume, and the residence time (τ_L) of one large fully-mixed reactor. A schematic representation of the full mill is shown in Figure 3.4. The equations for the three partial residence times (that is, τ_d, τ_s and τ_L) are given below:

$$\begin{cases} \tau_L = 0.841\tau - 2.531 \\ \tau_S = 0.051\tau + 1.377 \\ \tau_d = 0.046\tau - 0.222 \end{cases} \quad \textbf{(8.1)}$$

where τ represents the total residence time of the full-scale mill.

Equation 8.1 was incorporated into the PBM model and coded in Matlab® (see Appendix A.4).

It is important to also mention that this RTD model can be regarded as an intermediary case between the two extreme models used in the previous chapter.

7.3 Data collection and analysis

Data were generated by means of the simulation programme described in the previous chapter, save for the transport model used. Whereas the plug flow and fully-mixed transport models were used in the previous chapter, the full RTD model for real mills explained above is now applied in this chapter. The energy requirements of the mill were also included in the optimization procedure. This is especially important in that the optimisation of milling process is incomplete unless it is matched by optimized energy usage. The power demand was predicted using the Morrell model, which was coded into a Matlab® script, written to calculate total power (P_{TOTAL}) for a given set of operational conditions (mill speed and ball filling). The corresponding values of slurry filling for different values of ball filling used are given in Table 6.1.

The South African platinum industry normally sets the size requirements of the product for flotation at between 75 and 9 µm (Rule and Anyimadu, 2007). The feed class m_1 considered initially was -850 +600 µm, and the desired product class m_2 set at 75 – 9 µm. The objective function was therefore to determine those residence time and the energy requirements that would lead to the maximum production of m_2.

7.3.1 Effects of ball filling on mill production

Three transport models are illustrated in Figure 2.10; plug flow, fully-mixed and resident time distribution usually modelled by tank-in-series. The graph shows clearly that the tanks-in-series (TIS) mill model is an intermediary case between the plug-flow and perfectly mixed mill profiles. The output of the simulation for the three transport models shown in Figure 7.2 provides confirmation of this statement.

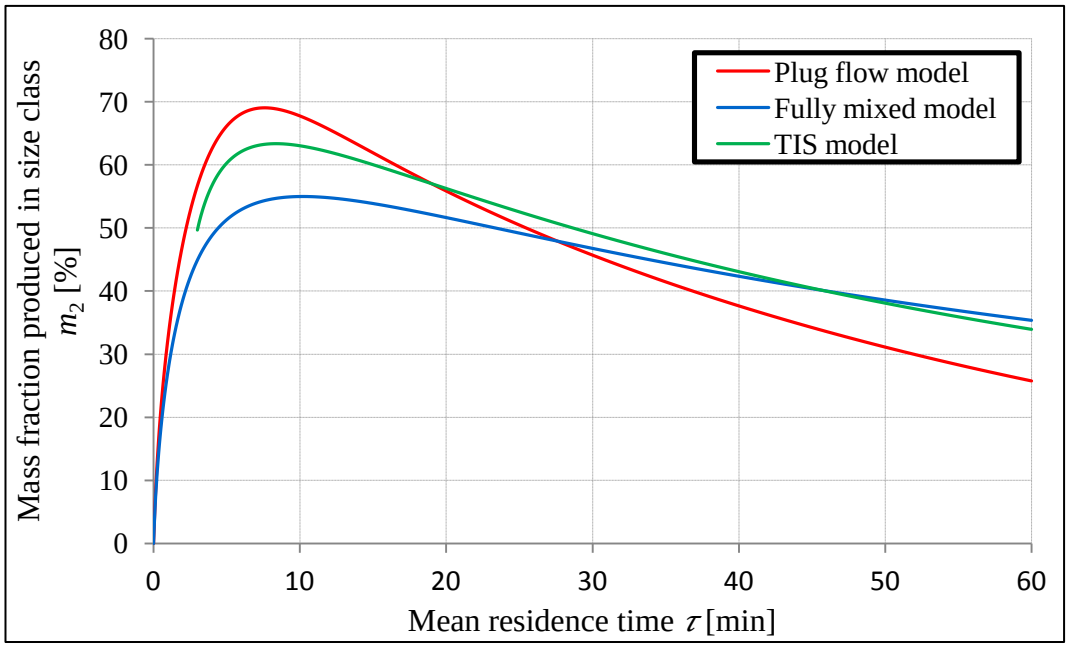


Figure 7.2 Throughput profiles of the mill for the three transport models. Simulation conditions: J = 30 %, U = 1.35, d = 40 mm and ϕ_c = 70 % of critical.

A close inspection of the grinding profiles in Figure 7.2 reveals that both the plug flow and fully-mixed mill models deviates from the ideal transportation model. Therefore, for the remainder of the transport modelling exercise, the TIS model as derived by Makokha *et al*. (2011) was used. The AR was then applied to perform the analysis as in the previous chapter.

Using the RTD Equations 2.18 – 2.19, the effects of ball filling were explored. On the basis of the simulation results for the full residence time scale overflow mill shown in Figure 7.3, it was considered admissible that in spite of the variation in the level of ball filling, the optimum production of m_2 did not change significantly. The reason is that it ranged from the lowest throughput of 61 % for J = 20 % to the highest throughput of 64 % for J = 35 %. However, the mean residence time necessary to achieve the maximum production of m_2 was shown to be inversely proportional to the ball filling.

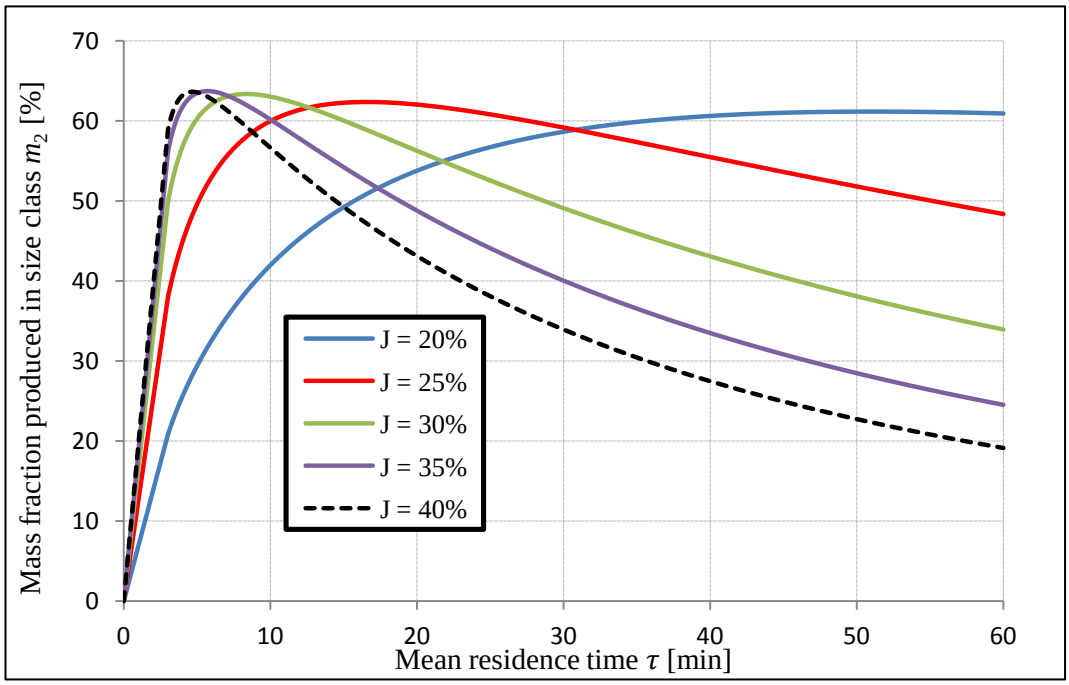


Figure 7.3 Prediction of ball filling effects on mill throughput for the TIS model. Simulation conditions: d = 40 mm and ϕ_c = 70 % of critical.

The trend that could be observed was that a high ball filling leads to faster production of m_2, which agrees with accepted industrial practice (Austin *et al.*, 1984). The power of AR to allow engineers to compare different runs under

varying parameters to determine which provides the optimal production of the desired product is clearly demonstrated for variable ball filling levels in the above figure.

Table 7.1 gives a summary of the optimum values of mean residence times corresponding to the TIS model, and with different ball fillings.

Table 7.1 Mean residence times τ_{optim} for d = 40 mm and ϕ_c = 70 % of critical

Ball filling J [%]	Optimum mean residence time τ_{optim} [min] of full scale mill
20	51.1
25	16.6
30	8.4
35	5.7
40	4.7

From the results presented in Table 7.1, one can see that there is a sudden drop of τ_{optim} when the ball filling is raised from 20 % to 25 %; and a gradual decrease between J = 30 % and J = 40 %. This kind of behaviour was also observed for the results of the plug flow and perfectly mixed mill models in the previous chapter. It was concluded that running the mill with a high ball filling had been found to promote a faster production of the desired size class.

7.3.2 Effects of ball size on mill production

Previous research has shown that a faster production of fine particles is achieved by using smaller balls for smaller particles feed sizes (Austin *et al.,* 1976; Napier-Munn *et al.* 1996; Chimwani *et al*., 2012).

Figure 7.4 shows the effects of varying the ball diameter while keeping the ball filling, slurry filling and mill speed constant. As can be seen in Figure 7.4, the mean residence time needed to reach the maximum throughput increases with the diameter of the grinding media. This means that faster production of the desired size class is promoted by using smaller balls.

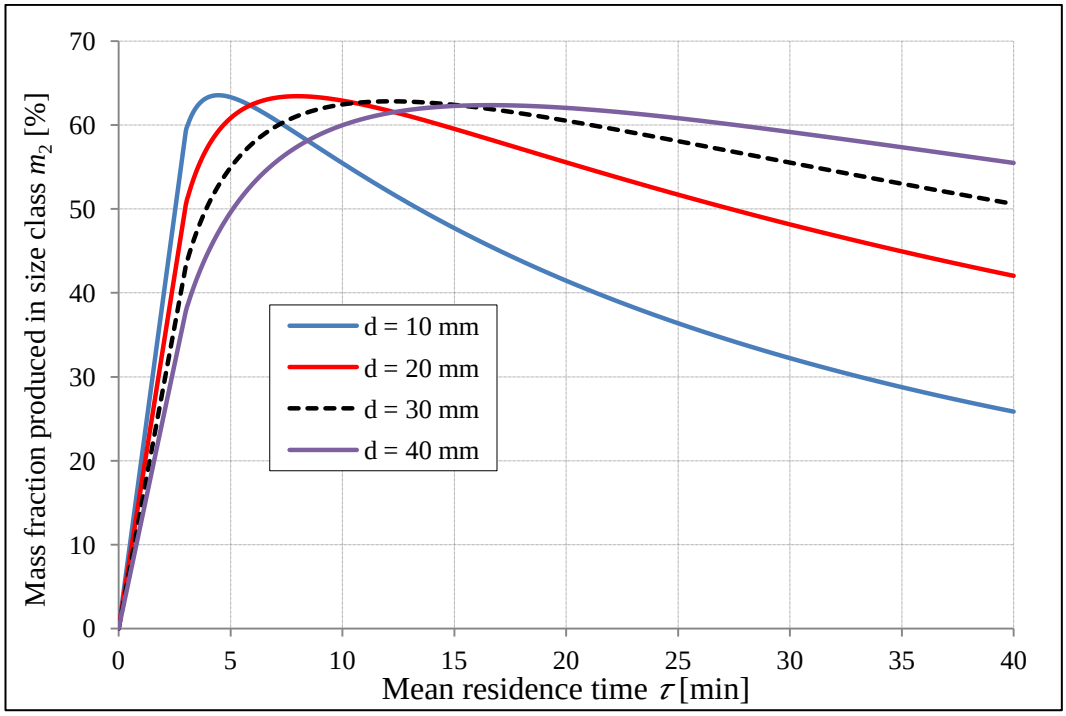


Figure 7.4 Effects of ball size on mill throughput for the TIS model. Simulation conditions: J = 25 %, U = 1.92, and ϕ_c = 70 % of critical.

Table 7.2 shows the optimum residence time for different sizes of balls. It is clearly observable that the mean residence time τ_{optim} rises as the ball diameter d increases. Although smaller balls are preferable for achieving the desired size class at a faster rate, their use may not be favoured because of their relatively high cost, especially when one considers that the mill power draw does not change much with ball diameter (Austin *et al.*, 1984; Morrell, 1993).

Table 7.2 Mean residence times τ_{optim} for J = 25 % and ϕ_c = 70 % of critical

Ball size d [mm]	Optimum residence time τ_{optim} [min] of the full scale mill
10	4.5
20	8.0
30	12.2
40	16.6

7.3.3 Effects of mill speed on mill production

Effects of mill speed on the mean residence time that would guarantee maximum production of class m_2 were investigated. The speed was varied between 40 % and 90 % of critical.

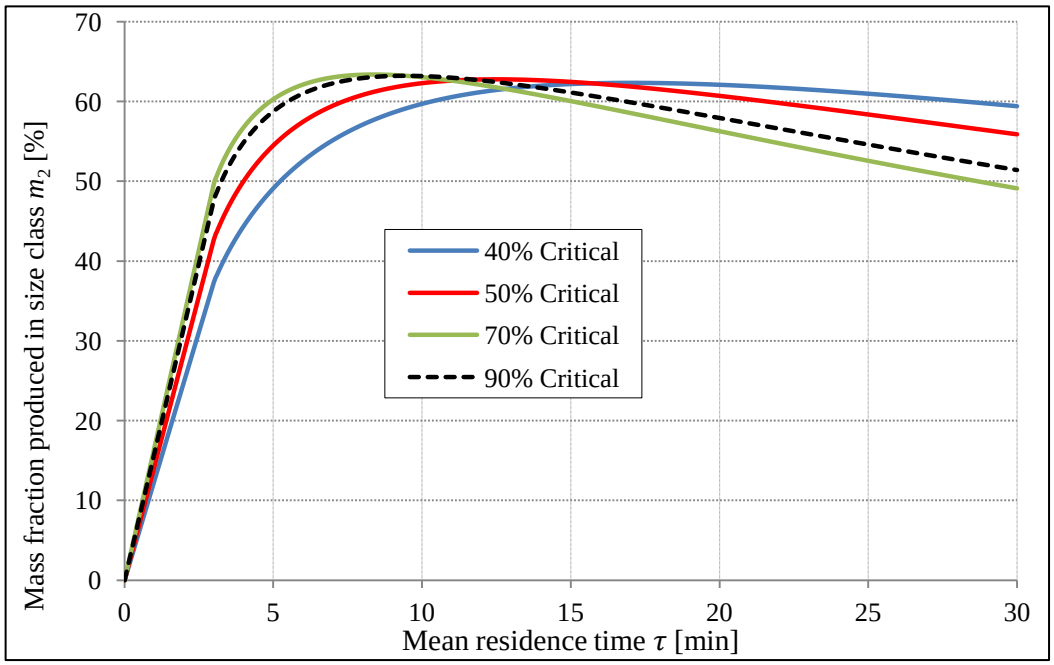


Figure 7.5 Effects of mill speed on mill throughput for the TIS model. Simulation conditions: J = 30 %, U = 1.35 and d = 40 mm.

The results are shown in Figure 7.5. The time required to achieve maximum throughput decreases from 17 min at 40 % of critical speed to 8.4 min at 70 % of critical speed, but later increases to 9.4 min at a mill speed of 90 % of critical. Table 7.3 shows the values of optimum mean residence time τ_{optim}. The desired size class was produced at a fastest rate at an optimum mill speed ϕ_c between 70 – 80 % of critical.

Table 7.3 Optimum mean residence times τ_{optim} for J = 30 % and d = 40 mm

Mill speed ϕ_c [%]	Optimum residence time τ_{optim} [min] of the full-scale mill
40	17.0
50	12.5
70	8.4
90	9.4

The optimum mean residence time started to climb at 90 % of critical speed. This is the result of more of impact breakage in the mill due to cataracting. Operating the mill at such speeds not only prevents the operators from optimising the residence time but also wastes energy. The effect of the latter will be discussed at length in the following sections.

7.4 Energy consumption of the mill

The energy efficiency of ball milling remains one of the most important areas of interest in comminution operations. Because of the size of the milling industry, even a slight increase in the efficiency of comminution processes can result in a significant reduction in energy requirements (Metzger, 2011). The overflow ball mill simulated in this work was comprehensively studied and characterised by Makokha *et al.* (2011). It has a rated power draw of 9 500 kW and an installed power capacity of 11000 kW. Table 7.4 (a to d) presents the optimal residence time, net power and energy needed to yield a maximum throughput of the desired size class for a particular ball size and fraction of speed.

Table 7.4 Optimal residence time, net power and energy of 40 mm ball size for varying fraction of speed and ball filling

(a)

Speed	J = 25 %			
	Time (min)	P_{net} (kW)	Energy (kJ)	m_2 produced (%)
40	34.3	3809	7838922	61.52
50	25.2	5173	7821576	61.84
70	16.6	8165	8132340	62.38
90	18.8	11055	12470040	62.21

(b)

Speed	J = 30 %			
	Time (min)	P_{net} (kW)	Energy (kJ)	m_2 produced (%)
40	17	4171	4254420	62.34
50	12.5	5803	4352250	62.79
70	8.4	9372	4723488	63.38
90	9.4	12573	7091172	63.21

(c)

Speed	J = 35 %			
	Time (min)	P_{net} (kW)	Energy (kJ)	m_2 produced (%)
40	10.9	4440	2903760	62.99
50	8.1	6323	3072978	63.41
70	5.7	10419	3563298	63.75
90	6.3	13746	5195988	63.69

(d)

Speed	J = 40 %			
	Time (min)	P_{net} (kW)	Energy (kJ)	m_2 produced (%)
40	8.4	4632	2334528	63.37
50	6.4	6739	2587776	63.69
70	4.7	11296	3185472	63.65
90	5.1	14534	4447404	63.74

Although (as mentioned above) the real mill has a rated power draw of 9 500 kW, the power requirement predicted by the Morrell model (Equation 2.45) is 10 278 kW for the same operational conditions (J = 30 %, ϕ_c = 75 % of critical, 40 mm ball diameter and 75 % solid content) under which the real mill is operated. The predicted power is greater than the real mill's rated power by 8.2 %, which makes the predicted power draw acceptable, since it is within the 95 % confidence interval quoted by Morrell (1993), that is, $\pm$ 10.6 %.

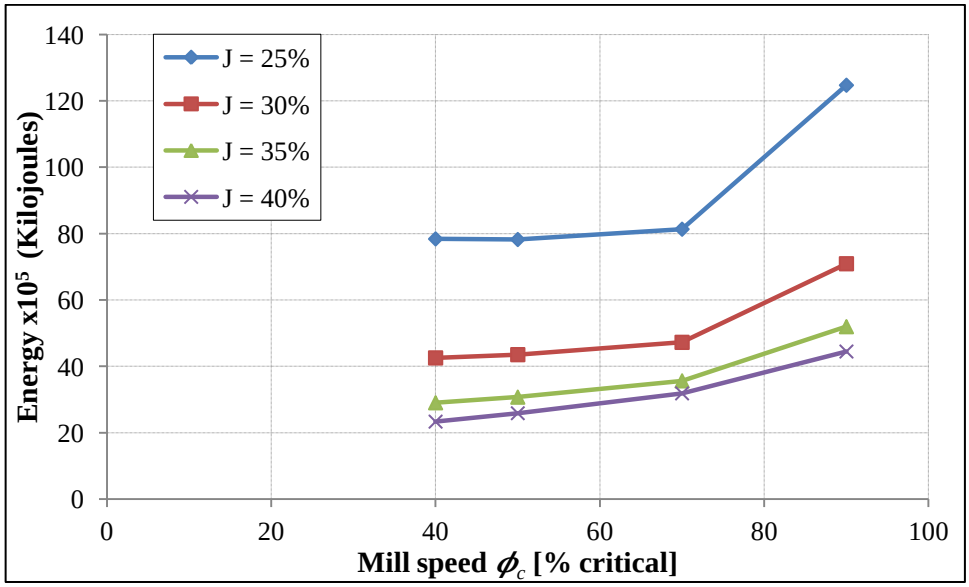


Figure 7.6 Effects of ball filling on energy.

Figure 7.6 represents the effect of ball filling and mill speed on the energy expended. It appears that optimising the residence time is crucial to minimizing energy consumption. As can be seen in Figure 7.6, the energy consumption reduces with an increase in ball filling. This is attributable to the fact that, at a particular rotation rate, lowering the media fill level reduces the total net power draw, whereas an increment in the residence time is required to achieve the maximum amount of the desired size class, as shown in Table 7.5 (a to d). It follows that operating the mill at the lowest grinding fill level is not energy-efficient.

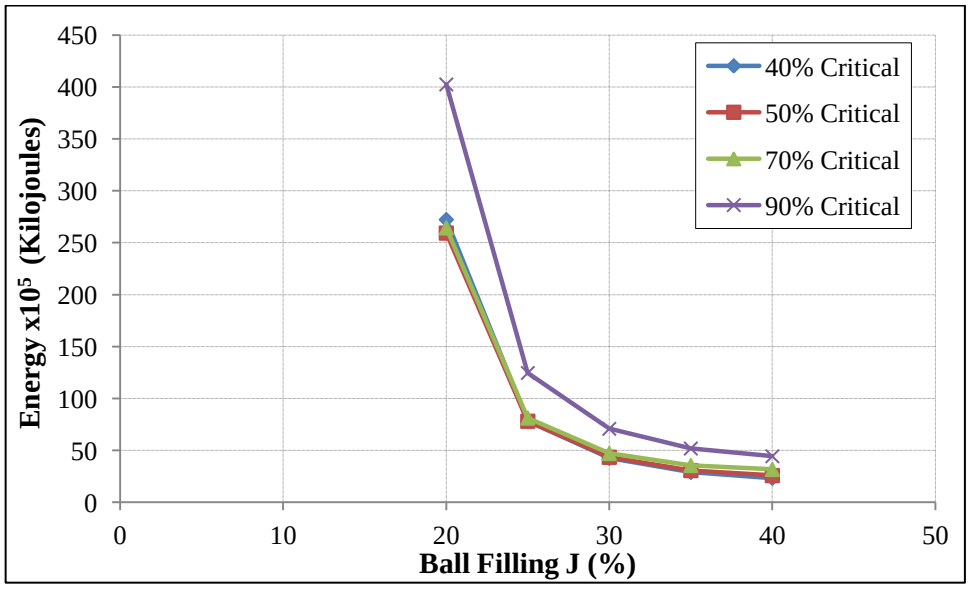


Figure 7.7 Effects of mill speed on energy consumed.

The graph plotted in Figure 7.7 shows the effects of mill speed on energy. As one can see, the energy consumption corresponding to speeds ranging from 40 – 70 % of critical is almost equal, whereas it is high at 90 % of critical speed. This is caused by the reduction in residence time and a corresponding increase in power draw as the speed rises from 40 % to 70 % of critical. A further increase in speed from 70 % to 90 % of critical causes the residence time and the power draw to increase in a similar fashion. Ninety percents of critical corresponds to the highest energy consumption. In the same Figure, one can also see that, as the ball filling increases, the energy consumed at all mill speeds drops. This indicates that the

lowest energy consumption is achieved by combining the highest ball filling with the lowest mill speed.

A *caveat* is entered at this point. Although it has been suggested that lower mill speeds save energy, circuit designers should take care to strike a balance between an additional decrease in mill speed and the risk of lengthening the processing time to an uneconomic level.

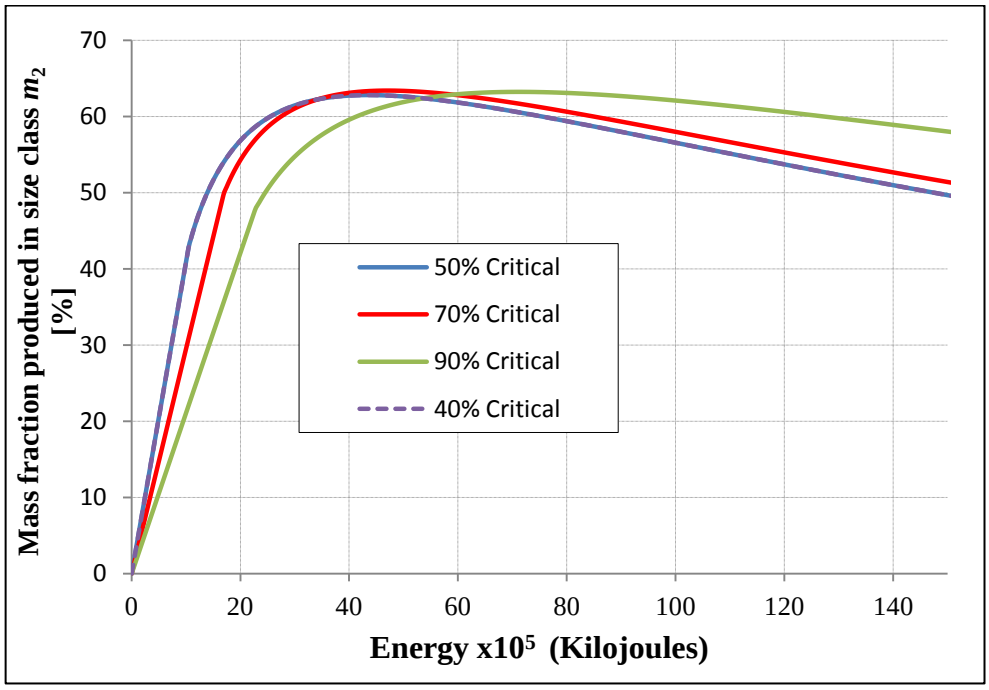


Figure 7.8 Effects of mill speed on mill throughput on the extent of energy draw. Simulation conditions: J = 30 %, U = 1.35 and d = 40 mm.

Further investigations were done on the effects of mill speed on energy demand. These were performed at J = 30 %, with varying mill speeds. According to Figure 7.8, the energy consumption increases linearly with the mill speed. It can also be seen that the slowest rotation rate (ϕ_c = 40 % of critical) produces the optimal amount of the desired size class using the lowest amount of energy, a conclusion also made by Metzger (2011) that operation at the slowest rotation utilizes energy to the fullest extent. This observation is however not in line with that of previous analysts (Ozkan *et al.*, 2009; Austin *et al.*, 1984), which suggest that the most efficient energy usage in large scale industrial ball milling occurs at a speed near 75 % of critical. Our findings as well as Metzger's (2011) differ from

conventional expectations, which aim at maximising throughput, while the main objective in this and Metzger's research is to maximise the fraction of m_2 produced.

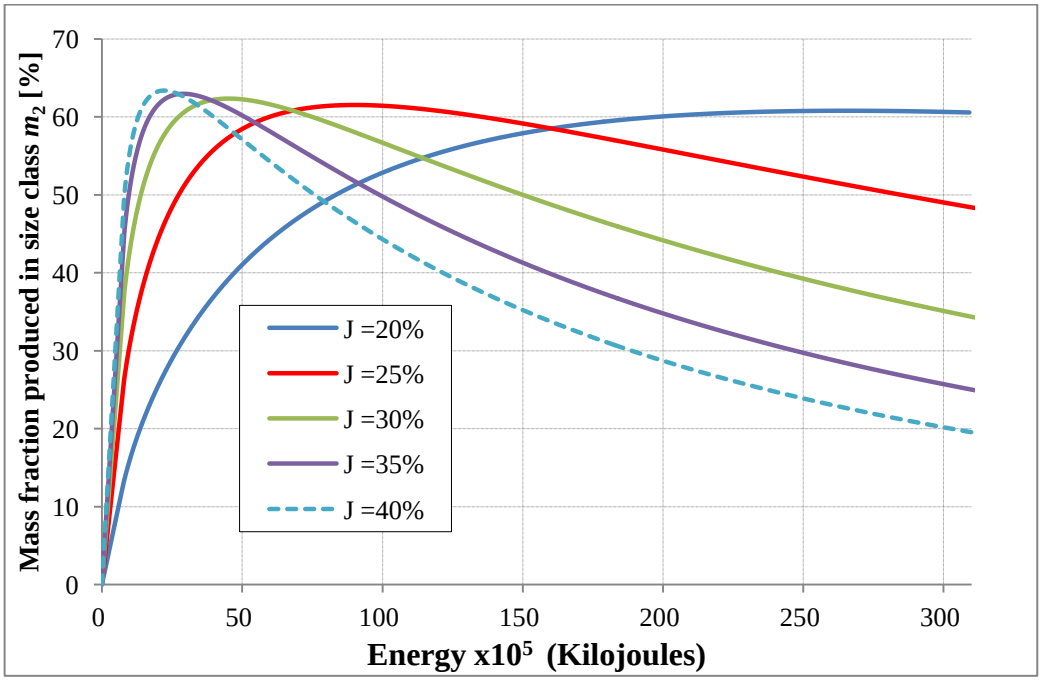


Figure 7.9 Effects of media filling level on mill throughput on the extent of energy used. Simulation conditions: ϕ_c = 40 % of critical and d = 40 mm.

Earlier studies have suggested that the media fill level should be as high as J = 35 % (Fortsch *et al.*, 2006). Austin *et al*. (1984) recommends a level as high as 40 % in order to optimise power consumption. Figure 7.9 simulations results also agree with the need to maximize mill filling to increase energy utilization efficiency. The combination of higher media filling level (J = 40%) and mill speed (ϕ_c = 40 % of critical) not only leads to lower energy consumption but also causes cascading action, which is more suitable for fine grinding.

7.5 Summarised findings

The TIS mill model investigated in this chapter generated the throughput of at least 61.52 % and at best 63.8 % of product in size class m_2. The simulated retention time needed for the maximization of the desired size range was found to

be 5.7 min at best (J = 35 %, ϕ_c = 70 % of critical) and 51.1 min at worst (J = 20 %, ϕ_c = 70 % of critical). It was also observed, as in the previous chapter, that the peak achieved for m_2 did not vary much with the operational conditions. Ball filling J = 40 % yielded 63.7 % of m_2 for 50, 70 and 90% of critical speed with retention times of 6.4, 4.7 and 5.1 min respectively, but using 40 mm ball sizes. It is interesting to note that for all the mill rotational speeds, ball filling is directly proportional to size class m_2 but inversely proportional to retention time and energy used to produce maximum amount of m_2.

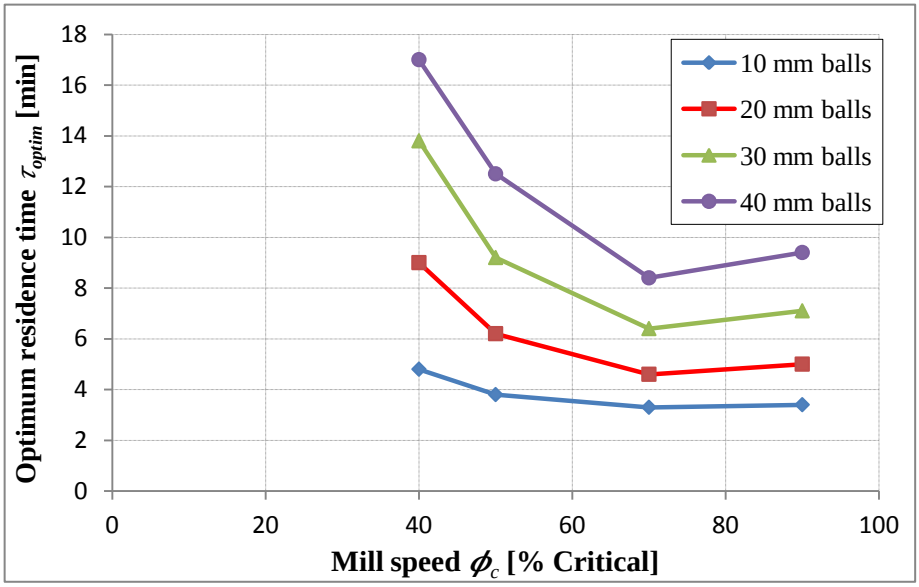


Figure 7.10 Optimum mean residence time τ_{optim} as a function of mill speed ϕ_c for J = 30 % under varying ball diameters.

The effect of ball size on optimum residence time on the extent of mill speed is summarised in Figure 7.10. This shows that the residence time is largely dependent on ball diameter, and that the residence time can be optimized by the correct adjustment of ball size.

The results presented in this chapter also underscore the importance of mill speed as an operating parameter that could play a major role in the optimisation of milling. Although these findings suggest that mill speed should be tuned to the target product m_2, it is interesting to note that mill speed is seldom adjusted in industrial practice at present, as this is normally optimized at the time when the plant is being installed.

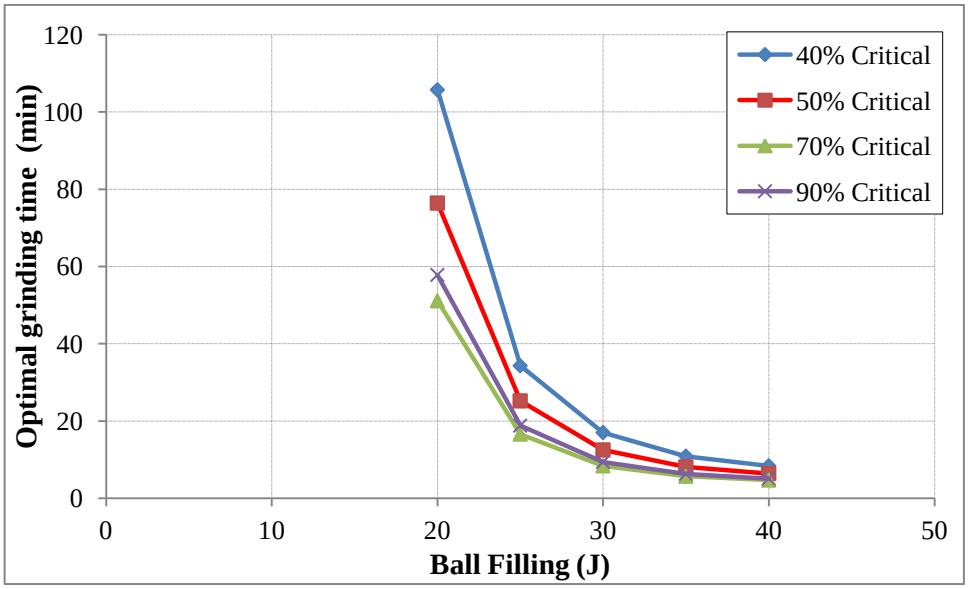


Figure 7.11 Optimal residence time versus ball filling at different speeds.

Based on what is shown in Figure 7.11, it can be affirmed that when the mill is run at low speed, the material is retained in the mill for longer. At a higher ball filling, the difference in residence time for different speeds is insignificant. The highest optimal residence time is that for 40 % of critical speed, which is 8.4 min, and the lowest is that for 70 % of critical speed, which is 4.7 min. This clearly suggests that operating at a higher ball filling and a low speed is a better choice if the mill is to be optimised, and also corroborates the results in Figure 7.7, which show that the combination of lower mill speed and higher ball filling generate the lowest energy consumption.

Chapter 8 Conclusions and recommendations

8.1 Introduction

This thesis explores by computer simulation ways to improve comminution circuits and in particular ball milling. For a target size range between 75 and 9 μm which optimally meets flotation requirements, it has been shown how mill filling, ball size and residence time can be controlled to maximize production of this size range. Presented in this chapter is the summary of the major results and observations arising from the studies undertaken as well as conclusions and suggestions for future work.

8.2 Characterisation of the PGM ore

One of the objectives of this research was to determine the milling parameters of the PGMs. Key breakage function and some selection function parameters were determined. The milling tests of the PGM ore done using the Wits laboratory mill. The remaining selection function parameters were successfully back-calculated within the PBM framework. The milling parameters obtained which provide information on the milling characteristics of the PGM ores are given in Table 8.1. These milling parameters of PGMs are normally not in the public domain as most platinum industries treat these as industrial secrets.

Table 8.1 The PGMs ore breakage characteristics

Breakage function parameters	β	6.2
	γ	0.8
	Φ	0.6
Selection function parameters	α	1.40
	Λ	4.74
	a_T	0.32
	μ_T	4.2

Further verification on additional batch experimental data showed that these parameters were good estimates for the ore.

8.3 Extension of the AR region method to continuous milling

Previous studies focused on applying AR to batch grinding. In this thesis, the AR has been extended to continuous milling. Mill profiles defining the throughput of the desired size class as a function of residence time were generated for continuous milling, in order to get some insight on how to target milling operations to maximize the yield of a desired size range. This could avail new possibilities for the optimisation of the residence time in continuous mills hence achieving the maximum throughput of the desired size class for the downstream process.

8.4 Summary of the major findings

The key outcome of control and operation of the grinding circuit is to produce an optimum size range for the downstream process such as flotation, since both adequate mineral liberation and avoidance of slimes are required for good recovery. The operational factors such as the slurry filling, ball filling, mill rotational speed, grinding media size and residence time must therefore be appropriately addressed to achieve desired mill product. These factors are complexly interactive and thus a graphical approach such as AR can help with visualization of the possible solutions more easily.

The ore that was used in this study is platinum group minerals ore. Throughout the study, the goal had been to optimize the production of the product of specific size range that enables maximum recovery during flotation. The population balance model and the analytical tool originally developed for analysis of chemical engineering systems called attainable region, were used in a complimentary fashion to accomplish the goal hence providing an alternative approach of how to arrive at a product size distribution that can be optimally controlled to maximise recovery during flotation. The product size distribution is

used to set the standard operating procedure of the mill. This work will contribute to the determination of milling parameters at both laboratory and industrial scale paramount to enabling better control of the product size distribution as well as establishing good ground for the development of AR in the minerals industry.

Our investigation began with the determination of the breakage and selection function parameters of a PGM ore. Our choice was driven by the existence of the processing challenges associated with the liberation of PGMs due to their fineness and gangue association. The unavailability of information concerning the ore due to competition was another important decision-making factor.

The research successfully demonstrated that even if all the milling parameters are not determined in the laboratory due to limited data, the remaining parameters can be determined indirectly by back-calculation from the available experimental data, thereby reducing the need for major amounts of experimental work. The trends of the variation of breakage function values with feed size for all media sizes led us to assume that breakage function values are normalizable. A good match was observed between the experimental and the product size distribution predicted using the determined parameters. Experiments done for additional grinding time further confirms the validity of the determined parameters.

The extension of the work from determining milling parameters of the laboratory batch data for a platinum ore to scaling it up using empirical models ascertained the viability of the parameters. This stage of the research project also provided the opportunity to test the AR tool on an industrial scale to see whether its capacity to predict changes and ascertain optimal mill operating conditions could be successfully applied to a preselected industrial mill to optimize the product size distribution for flotation purposes. The reason was that the results of AR analysis on the laboratory scale have often come into conflict with some of the traditionally-acceptable milling conditions for batch grinding under which most concentrators are operated.

Using AR analysis, the effect of varying the optimal operating conditions – ball filling (J), powder filling (U), mill speed (ϕ_c) and ball diameter d – on the amount

of the desired size class m_2 produced was determined. It was shown that a high media filling level (J = 40 %) yielded the largest amount of the desired size class m_2. Running the mill at low speeds was found to result in maximum production of the desired size class, which confirms suggestions made previously by Metzger *et al*. (2009). Bigger diameter balls (40 mm) have also proved to be a better choice if production of the desired size class has to be maximised, presumably because smaller balls quickly grind smaller particles owing to their increased surface area and produce more slimes. Powder filling of U = 1 was optimal to achieving the maximum amount of m_2 and that agrees with Katubilwa's (2012) findings. The influence of mill rotational speed on the amount of the desired size class was clearly noticeable, rendering it the first factor a circuit designer would need to consider when optimizing milling to achieve the maximum production of the desired size class. Low grinding speed (40% of critical speed) yield maximum amount of m_2. It is also interesting to note that all these factors produced a coarser product as shown by the PSD analysis.

Finally, application of the AR was extended to determining both the optimal residence time of a full-scale ball mill and the energy requirements of that mill. Three mill transportation models: the plug flow, the well-mixed and the tanks-in-series models, were used for the residence time investigation. The last of these models work well when applied to industrial data. The residence time investigations were performed on an industrial overflow mill under different operational conditions (that is, variations in the slurry filling, ball filling, mill rotational speed and grinding media size). The power draw of the mill, corresponding with the given milling conditions, was estimated using the model proposed by Morrell (1993) to determine the energy use as a function of mill throughput.

The trends observed in the results revealed that an increase in ball filling shortens the mean residence time necessary for the maximum production of the desired size class, which agrees with industrially-accepted practice. Smaller balls were also found to promote a faster production of fine particles, which confirmed a widely-accepted theory pertaining to the effects of ball size on milling. The

optimal residence time was shown to increase in linear relation to a rise in ball size. Notwithstanding the significant reduction in residence time achieved by using smaller balls, their use in industrial applications is believed to be limited by their higher cost. The investigations into the effects of mill speed on mill throughput reveals that an optimum mill speed ϕ_c between 70–80 % of critical offers the most rapid means of producing the size class of interest m_2, which explains the shorter residence time.

The enquiry into the energy consumption of mill provided a number of interesting insights. The slowest rotation rate (ϕ_c = 40 % of critical) produces the maximum yield of the desired size class while using the lowest amount of energy, this is in agreement with the findings of Metzger (2011) that operation at the slowest rotation is the best policy for making the fullest use of energy. This is believed to be the case because slowing down the mill promotes cascading motion and cause the tumbling charge to be in contact with the ore most of the time. For a large diameter mill that was simulated it should be expected that the tumbling charge achieves significant kinetic energy to cause breakage even when there is very little cataracting. For a much harder ore a higher speed would be expected to be the optimal. Furthermore, it was found that the lowest amount of energy was consumed when grinding was done with a higher ball filling. When the range of ball fillings was investigated, energy consumption was shown to increase inversely with the media filling. It was also found that operating at a higher ball filling and low speed is a better choice if the mill is to be optimized. A higher filling which also results in a greater fraction of the charge cascading also reinforces grinding rate. These results provide further confirmation that although mill speed is seldom adjusted in industrial operations, it is an important factor in the optimisation of milling and therefore, should be accurately determined at plant installation to guarantee maximum production of the desired size class.

The grinding simulation exercise using the PBM approach and use of the AR analytical technique has highlighted options that may be used to optimize product size distribution of an industrial mill.

8.5 Overall conclusion

The key objective of this research work was to use computational and experimental techniques to obtain an advanced understanding of all the design and operational factors that affect breakage in an industrial overflow mill. This allowed the performance of a milling circuit to be controlled and optimized to achieve the maximum amount of the desired particle size class for flotation. In fulfilling these objectives, the research focused on providing the technical tools needed to bring about an improvement in the milling of PGMs by providing the engineer with specific details of the operating conditions required to achieve a specific objective function. The research work also aimed to justify the further use of AR analysis in the minerals industry, since the AR analysis undertaken in this study has demonstratively produced the process target and the control policy to achieve the target by showing that, higher ball filling, lower mill rotation speed and higher ball sizes give the best mill performance.

8.6 Recommendations for future work

Mill speed has been identified as an operating parameter that plays a major role in the optimisation of milling. In the future, researchers should look at mill speed while taking into consideration the economics of milling. A comprehensive simulation model that integrates all the relevant aspects of a milling operation needs to be developed so as to generate useful data. One possible route would be to resort to simulators such as Modsim^{TM} to generate data that can be optimised by means of the AR technique, which shows great promise when used in the analysis and optimisation of industrial mineral processing circuits. The research work presented here is the first step towards that objective in that it has demonstrated that combining the PBM with the AR technique could provide an alternative analytical approach to improving mineral engineering processes.

Another field in which further research is necessary is the integration of more realistic RTDs with the analysis of continuous milling. This would make possible a more thorough investigation of the following milling parameters: the solids concentration in slurry, the feed flow-rate and the ball size distribution. It is

evident that this will require a validation of the underlying mathematical models used with industrial data. This can be achieved by testing all the conclusions drawn from the AR analysis on the pilot plant since most of the existing mills are not run by variable speed motors. Then, the study of milling circuit configurations would be integrated in order to consolidate the position of the AR technique as an alternative analysis tool.

List of references

Arbiter, N., Harris, C.C., 1982. Scale-up and dynamics of large grinding mills – a case study. Design and installation of comminution circuits, Mular. A.L. and Jergensen II.G.V. (eds) AIME, New York, Chap. 26, pp. 491 – 505.

Austin, L.G., Gardner, R.P., 1962. Prediction of size-weight distribution from selection and breakage data. Proceedings, 1st European Symposium Zerkleinern, H. Rumpf and D. Behrens, ed., Verlag Chemie, Weinheim, pp. 232 – 248.

Austin, L.G., 1971/72. A review introduction to the mathematical description of grinding as a rate process. Powder Technology, vol. 5, no. 1, pp. 1 – 7.

Austin, L.G., Shoji, K., Luckie, P.T., 1976. The effect of ball size on mill performance. Powder Technology, vol. 14, no. 1, pp. 71 – 79.

Austin, L.G., Trimarchi, T., Weymont, N.P., 1977. An analysis of some cases of non-first-order breakage rates, Powder Technology, vol. 17, no. 1, pp. 109 – 113.

Austin, L.G., Baggal, P., Celik, M., 1981. Breakage properties of some materials in laboratory ball mill. Powder Technology, vol. 28, no. 2, pp. 235 – 241.

Austin, L.G., Klimpel, R.R., Luckie, P.T., 1984. Process Engineering of Size Reduction: Ball Milling. Society of Mining Engineers of the AIME, New York.

Austin, L.G., Cho, H., 2002. An alternative method for programming mill models. Powder Technology, vol. 122, no. 2 – 3, pp. 96 – 100.

Austin, L.G., Julianelli, K., Sampaio de Souza, A., Schneider, C.L., 2007. Simulation wet ball milling of iron ore at Carajas, Brazil. International Journal of Mineral processing, vol. 84, pp. 157 – 171.

Bilgili, E., Hamey, R., Scarlett, B., 2005. Nano-milling of pigment agglomerates using a wet stirred media mill: Elucidation of the kinetics and breakage mechanisms. Chemical Engineering Science, vol. 61, no. 1, pp. 149 – 157.

Bilgili, E., Yepes, J., Scarlett, B., 2006. Formulation of a non-linear framework for population balance modeling of batch grinding: Beyond first-order kinetics. Chemical Engineering Science, vol. 61, no. 1, pp. 33 – 44.

Bilgili, E., 2007. On the consequences of non-first-order breakage kinetics in comminution processes: Absence of self-similar size spectra. Particle and Particle System Characterization, vol. 24, no. 1, pp. 12 – 17.

Boateng, A.A., Barr, P.V., 1996. Modelling of particle mixing and segregation in the transverse plane of a rotary kiln. Chemical Engineering Science, vol. 51, no. 17, pp. 4167 – 4181.

Bryson, M.A.W., 2004. Mineralogical control of minerals processing circuit design. Journal of Southern African Institute of Mining and Metallurgy, vol. 104, no. 6, pp. 301 – 310.

Capece, M. Bilgili, E., Dave, R., 2011. Identification of the breakage rate and distribution parameters in a non-linear population balance model for batch milling. Powder Technology, vol. 208, no. 1, pp. 195 – 204.

Chimwani, N., Glasser, D., Hildebrandt, D., Metzger, M.J., Mulenga, F.K., 2012. Determination of the milling parameters of a platinum group minerals ore to optimize product size distribution for flotation purposes. Minerals Engineering, vol. 43 – 44, pp. 67 – 78.

Cho, H., Austin, L.G., 2002. The equivalence between different residence time distribution models in ball milling. Powder Technology, vol. 124, no. 1 – 2, pp. 112 – 118.

Cho, H., Austin, L.G., 2004. A study of the exit classification effect in wet ball milling. Powder Technology, vol. 143 – 144, pp. 204 – 214.

Coleman, R., 1983. Metallurgical testing procedures (Chap. 9), Mineral processing plant design, AIME, 2nd Edition, pp. 144 – 182.

Cramer, L.A., 2001. The extractive metallurgy of South Africa's platinum ores. Journal of Mining, vol. 53, no. 10.

Danckwerts, P.V., (1953), Continuous flow systems: distribution of residence times, Chemical Engineering Science, vol. 2, no. 1, pp. 1 – 13.

Datta, A., Rajamani, K., 2002. A direct approach of batch grinding in ball mills using population balance principles and impact energy distribution. International Journal of Mineral processing, vol. 64, pp. 181 – 200.

V. Deniz., 2012. The effects of ball filling and ball diameter on kinetic breakage parameters of barite powder, Advanced Powder Technology, vol. 23, pp. 640 – 646.

Dong, H., Moys, M.H., 2002. Assessment of discrete element method for one ball bouncing in a grinding mill. International Journal of Mineral Processing, vol. 65, no. 3 – 4, pp. 213 – 226.

Fuerstenau, D.W., Kapur, P.C., Velamakanni, B., 1990. A multi-torque model for the effects of dispersants and slurry viscosity on ball milling. International Journal of Mineral Processing, vol. 28, no. 1 – 2, pp. 81 – 98.

Fortsch, D.S., Smidth, F.L., 2006. Ball charge loading – Impact of specific power consumption and capacity. Personal Communication, pp. 69 – 70.

Glasser, D., Hildebrandt, D., 1997. Reactor and process synthesis. Computers in Chemical Engineering, vol. 21, Suppl. 1, pp. S775 – S783.

Gupta, A., Yan, D.S., 2006. Mineral processing design and operation: An introduction. Elsevier, Perth.

Hay, P.M., Roy, R., 2010. A case study of optimizing UG2 flotation performance. Part: Bench, pilot and plant scale factors which influence Cr2O3 entrainment in UG2 flotation. Minerals Engineering, vol. 23, no. 11 – 13, pp. 855 – 867.

Herbst, J.A., Fuerstenau, D.W., 1980. Scale-up procedure for continuous grinding mill design using population balance models. International Journal of Mineral Processing, vol. 7, pp. 1 – 31.

Herbst, J. A., Siddique, M., Rajamani, K., Sanchez, E., 1981. Population balance approach to ball mill scale-up: Bench and pilot scale investigations. Trans. SME/AIME 272, 1945 – 1954.

Hlabangana, N., Vetter, D., Metzger, M.J., Glasser, D., Hildebrandt, D., 2012. Industrial application of the attainable region analysis to a joint milling and leaching process. Minerals Engineering, Proceedings of the VIII International Comminution Symposium – Comminution '12, Cape Town, South Africa.

Hogg, R., Fuerstenau, D.W., 1972. Power relationships for tumbling mills. SME – AIME Transactions, vol. 252, pp. 418 – 423.

Katubilwa, F.M., Moys, M.H., 2009. Effect of ball size distribution on milling rate. Minerals Engineering, vol. 22, no. 15, pp. 1283 – 1288.

Katubilwa, F.M., Moys, M.H., Glasser, D., Hilderbrandt, D., 2011. An attainable region analysis of the effect of ball size on milling. Powder Technology, vol. 210, no. 1, pp. 36 – 46.

Katubilwa, F.M., 2012. Effects of pool volume on wet milling efficiency. PhD Thesis, University of the Witwatersrand, Johannesburg.

Kelly, E.G., Spottiswood, D.J., 1990. The breakage function; What is it really?. Minerals Engineering, vol. 3, no. 5, pp. 405 – 414.

Kelsall, D.F., Reid, K.J., Restarick, C.J., 1968. Continuous grinding in a small wet ball mill – Part I. A study of the influence of ball diameter. Powder Technology, vol. 1, no. 5, pp. 291 – 300.

Kelsall, D.F., Reid, K.J., Restarick, C.J., 1969. Continuous grinding in a small wet ball mill – Part II. A study of the influence of hold-up weight. Powder Technology, vol. 2, no. 3, pp. 162 – 168.

Kelsall, D.F., Reid, K.J., Restarick, C.J., 1969/1970. Continuous grinding in a small wet ball mill – Part III. A study of distribution of residence time. Powder Technology, vol. 3, no. 1, pp. 170 – 178.

Kelsall, D.F., Stewart, P.S.B., Weller, K.R., 1973. Continuous grinding in a small wet ball mill – Part IV. A study of the influence of grinding media load and density. Powder Technology, vol. 7, no. 5, pp. 293 – 301.

Kelsall, D.F., Stewart, P.S.B., Weller, K.R., 1973. Continuous grinding in a small wet ball mill – Part V. A study of the influence of media shape. Powder Technology, vol. 8, no. 1 – 2, pp. 77 – 83.

Khumalo, N., 2007. The application of the attainable region analysis in comminution. PhD Thesis, University of the Witwatersrand, Johannesburg.

Khumalo, N., Glasser, D., Hildebrandt, D., Hausberger, B., Kauchali, S., 2006. The application of the attainable region analysis to comminution. Chemical Engineering Science, vol. 61, no. 18, pp. 5969 – 5980.

Khumalo, N., Glasser, D., Hildebrandt, D., Hausberger, B., 2007. An experimental validation of a specific energy-based approach for comminution. Chemical Engineering Science, vol. 62, no. 10, pp. 2765 – 2776.

Khumalo, N., 2007. The application of the attainable region analysis in comminution. PhD Thesis, University of the Witwatersrand, Johannesburg.

Khumalo, N., Glasser, D., Hildebrandt, D., Hausberger, B., 2008. Improving comminution efficiency using classification: An attainable region approach. Powder Technology, vol. 187, no. 3, pp. 252 – 259.

King, R.P., 2001. Modeling and simulation of mineral processing systems, Butterworth-Heinemann, ISBN: 0-7506-4884-8.

Koka, V.R., Trass, O., 1988. Estimation of breakage parameters in grinding operations using a direct search method. Mineral Processing, vol. 23, pp. 137 – 150.

Latchireddi, S., Morrell, S., 2003. Slurry flow in mills: grate-only discharge mechanism (Part 1). Minerals Engineering, vol. 16, no. 7, pp. 625 – 633.

Levenspiel, O., 1962. Chemical reaction engineering. Wiley, New York.

Makokha, A.B., Moys, M.H., 2006. Towards optimizing ball-milling capacity: Effect of the lifter design. Minerals Engineering, vol. 19, no. 14, pp. 1439 – 1445.

Makokha, A.B., 2011. Measuring, characterization and modelling of load dynamic behaviour in a wet overflow-discharge ball mill. PhD Thesis, University of the Witwatersrand, Johannesburg.

McIvor, R.E., Finch, J.A., 1990. A guide to interfacing of plant grinding and floatation operations. Minerals Engineering, vol. 4, no. 1, pp. 9 – 23.

Metzger, M.J., Glasser, D., Hausberger, B., Hildebrandt, D., Glasser, B.J., 2009. Use of the attainable region analysis to optimize particle breakage in a ball mill. Chemical Engineering Science, vol. 64, no. 17, pp. 3766 – 3777.

Metzger, M.J., 2011. Numerical and experimental analysis of breakage in a mill using the attainable region approach, PhD Thesis, Rutgers, The State University of New Jersey – New Brunswick.

Metzger, M. J., Desai, S. P., Glasser, D., Hildebrandt, D. and Glasser, B. J., 2012. Using the attainable region analysis to determine the effect of process parameters on breakage in a ball mill. American Institute of Chemical Engineers Journal, vol. 58, no. 9, pp. 2665 – 2673.

Morrell, S., 1993. The prediction of power drawn in wet tumbling mills. PhD thesis, University of Queensland, Australia.

Moys, M.H., 1990. A model for mill power as affected by mill speed, load volume and liner design. in Schonert, K. (Ed.), Preprints of the 7th European Symposium on Comminution, University of Yugoslavia, Ljubljana, pp. 595 – 607.

Moys, M.H.,Van Nierop M.A., Smit, I., 1996. Progress in measuring and modelling load behaviour in pilot and industrial mills. Minerals Engineering, vol. 9, no. 12, pp. 1201 – 1214.

Napier-Munn, T.J., Morrell, S., Morrison, R.D., Kojovic, T., 1996. Mineral comminution circuits – Their operation and optimization. JKMRC Monograph Series, University of Queensland.

Ozkan, A., M. Yekeler, and M. Calkaya, 2009. Kinetics of fine wet grinding of zeolite in a steel ball mill in comparison to dry grinding. International Journal of Mineral Processing, vol. 90, no. 1 – 4, pp. 67 – 73.

Rajamani, K., 1991. Acceleration and Deceleration of breakage rates in batch grinding. SME, Preprint number, pp. 91 – 160.

Reid, K.J., 1965. A solution to batch grinding equation. Chemical Engineering Science, vol. 20, no. 11, pp. 953 – 963.

Rule, C.M., Anyimadu, A.K., 2007. Flotation cell technology and circuit design – An Anglo Platinum perspective, SAIMM Conference, Flotation Cell Technology in the 21st Century, 20 June 2007.

Shoji, K., Lohrasb, S., Austin, L.G., 1980. The variation of breakage parameters with ball and powder loading in dry ball milling. Powder Technology, vol. 25, no. 1, pp. 109 – 114.

Shoji, K., Austin, L.G., Smaila, F., Brame, K., Luckie, P.T., 1982. Further studies of ball and powder filling effects in ball milling. Powder Technology, vol. 31, no. 1, pp. 121 – 126.

Tangsathitkulchai, C., 2002. Acceleration of particle breakage rates in wet batch ball milling. Powder Technology, vol. 124, no. 1 – 2, pp. 67 – 75.

Tangsathitkulchai, C., 2003. Effects of slurry concentration and powder filling on the net mill power of a laboratory ball mill. Powder Technology, vol. 137, no. 3, pp. 131 – 138.

Tangsathitkulchai, C., 2003. Effects of slurry concentration and powder filling on the net mill power of a laboratory ball mill. Powder Technology, vol. 137, no. 3, pp. 131 – 138.

Trahar, W.J., Warren, L.J., 1975. The floatability of very fine particles – A review. International Journal of Mineral Processing, vol. 3, no. 2, pp. 103 – 131.

Wills, B.A., Napier-Munn, T.J., 2005. Wills' mineral processing technology: An introduction to the practical aspects of ore treatment and mineral recovery. Seventh Edition, Elsevier, London, ISBN: 0750644508.

Yekeler, M., 2007. Breakage and morphological parameters determined by laboratory tests (Chapter 9). in Handbook of Powder Technology, vol. 12, pp. 437 – 486, ISSN 0167-3785.

Yildirim, K., Cho, H., Austin, L.G., 1999. The modeling of dry grinding of quartz in tumbling media mills, Powder Technology, vol. 105, no. 1 – 3, pp. 210 – 221.

Appendices

A.1 Batch grinding data

A mono-size (-850 +600 µm), (-600 +425 µm) and (-425 +300 µm) were milled in the Wits laboratory mill for different grinding times and the data collected was presented as fraction passing per grinding times in % as shown in the following tables.

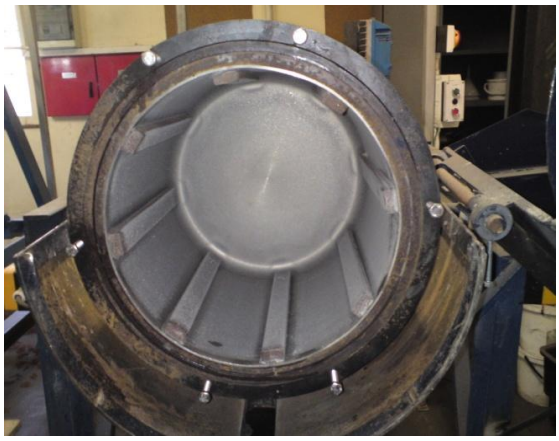


Figure A.1 The Wits laboratory ball mill used for experimentation

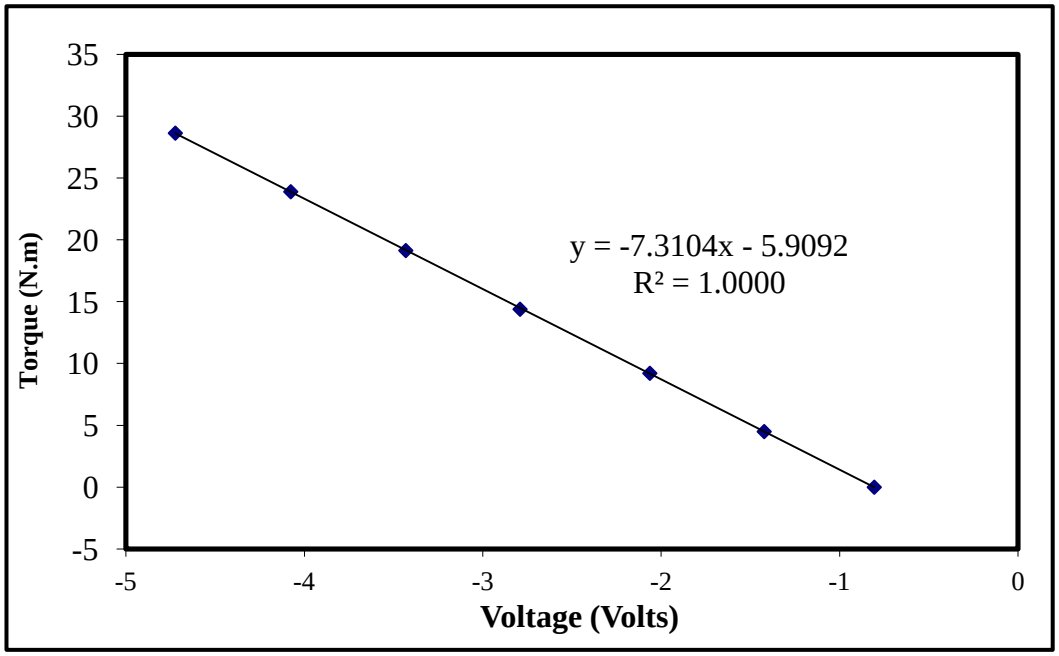


Figure A.2 Power calibration chart of the laboratory mill

Table A.1 Measured particle size distribution for ball size 10 mm, feed size (-850 +600 µm), U = 0.75, J = 20 %, ϕ_c = 75 of critical, f_c = 0.06

Size x_i [mm]	Fraction Passing per Grinding times in %						
	0.5 min	**1 min**	**2 min**	**4min**	**8 min**	**15 min**	**30 min**
850	100	100	100	100	100	100	100
600	22.6	33.7	46.3	60.8	77.9	88.6	95.7
425	9.5	16.9	26.3	39.2	57.1	74.3	91.3
300	4.8	9.6	15.0	24.1	39.0	57.1	88.4
212	2.4	6.0	8.8	16.5	27.3	42.9	75.4
150	1.2	3.6	5.0	10.1	18.2	30.0	60.9
106	0.0	2.4	3.8	6.3	11.7	20.0	46.4
75	0.0	1.2	2.5	3.8	7.8	14.3	37.7
53	0.0	1.2	1.3	1.3	3.9	8.6	27.5
45	0.0	1.2	1.3	1.3	3.9	7.1	24.6
25	0.0	1.2	1.3	1.3	2.6	2.9	17.4

Table A.2 Measured particle size distribution for ball size 10 mm, feed size (-600 +425 µm), U = 0.75, J = 20 %, ϕ_c = 75 of critical, f_c = 0.06

Size x_i [mm]	Fraction Passing per Grinding times in %						
	0.5 min	**1 min**	**2 min**	**4min**	**8 min**	**15 min**	**30 min**
600	100	100	100	100	100	100	100
425	27.3	38.6	49.4	65.3	79.5	91.7	98.6
300	9.1	16.9	22.8	38.7	53.4	72.2	91.4
212	5.7	10.8	12.7	22.7	34.2	50.0	75.7
150	3.4	6.0	7.6	16.0	24.7	36.1	61.4
106	2.3	3.6	3.8	12.0	16.4	25.0	45.7
75	1.1	2.4	2.5	9.3	12.3	18.1	34.3
53	0.0	1.2	1.3	6.7	8.2	12.5	24.3
45	0.0	1.2	1.3	5.3	6.8	11.1	21.4
25	0.0	1.2	1.3	4.0	5.5	6.9	15.7

Table A.3 Measured particle size distribution for ball size 10 mm, feed size (-425 +300 µm), U = 0.75, J = 20 %, ϕ_c = 75 of critical, f_c = 0.06

Size x_i [mm]	Fraction Passing per Grinding times in %						
	0.5 min	**1 min**	**2 min**	**4min**	**8 min**	**15 min**	**30 min**
425	100	100	100	100	100	100	100
300	25.3	32.5	45.6	58.2	75.3	90.7	98.6
212	8.0	10.8	20.3	29.1	43.8	65.3	90.3
150	4.6	6.0	12.7	19.0	28.8	48.0	76.4
106	3.4	3.6	8.9	12.7	17.8	32.0	58.3
75	2.3	2.4	6.3	8.9	12.3	22.7	44.4
53	1.1	1.2	3.8	6.3	8.2	14.7	30.6
45	1.1	1.2	2.5	5.1	6.8	12.0	26.4
25	1.1	1.2	2.5	3.8	4.1	8.0	19.4

Table A.4 Measured particle size distribution for ball size 20 mm, feed size (-850 +600 µm), U = 0.75, J = 20 %, ϕ_c = 75 of critical, f_c = 0.06

Size x_i [mm]	Fraction Passing per Grinding times in %						
	0.5 min	**1 min**	**2 min**	**4min**	**8 min**	**15 min**	**30 min**
850	100	100	100	100	100	100	100
600	18.0	28.2	44.8	67.9	87.9	95.9	98.9
425	9.4	16.1	30.2	45.0	66.7	82.5	92.0
300	6.3	10.5	22.4	35.8	53.5	68.0	83.0
212	3.9	7.3	17.2	28.4	42.4	55.7	69.3
150	2.3	4.8	12.9	22.0	33.3	45.4	56.8
106	1.6	3.2	9.5	16.5	25.3	36.1	45.5
75	0.8	2.4	6.9	12.8	19.2	28.9	38.6
53	0.0	1.6	4.3	10.1	14.1	22.7	31.8
45	0.0	0.8	2.6	7.3	10.1	18.6	26.1
25	0.0	0.8	1.7	5.5	7.1	12.4	17.0

Table A.5 Measured particle size distribution for ball size 20 mm, feed size (-600 +425 µm), U = 0.75, J = 20 %, ϕ_c = 75 of critical, f_c = 0.06

Size x_i [mm]	Fraction Passing per Grinding times in %						
	0.5 min	**1 min**	**2 min**	**4min**	**8 min**	**15 min**	**30 min**
600	100	100	100	100	100	100	100
425	27.9	35.5	47.9	63.1	78.4	90.2	97.8
300	8.5	12.9	22.2	35.1	51.0	67.6	84.9
212	4.7	7.3	13.7	23.4	35.3	50.0	66.7
150	3.1	4.0	8.5	15.3	23.5	35.3	49.5
106	1.6	1.6	5.1	9.9	15.7	24.5	35.5
75	0.8	0.8	3.4	7.2	11.8	18.6	26.9
53	0.0	0.0	1.7	4.5	8.8	14.7	21.5
45	0.0	0.0	0.9	3.6	6.9	12.7	18.3
25	0.0	0.0	0.9	2.7	4.9	8.8	11.8

Table A.6 Measured particle size distribution for ball size 20 mm, feed size (-425 +300 µm), U = 0.75, J = 20 %, ϕ_c = 75 of critical, f_c = 0.06

Size x_i [mm]	Fraction Passing per Grinding times in %						
	0.5 min	**1 min**	**2 min**	**4min**	**8 min**	**15 min**	**30 min**
425	100	100	100	100	100	100	100
300	39.1	43.9	50.8	59.5	70.5	81.3	93.6
212	15.6	18.7	24.6	32.4	43.8	56.3	75.5
150	9.4	10.6	14.4	19.8	28.6	38.5	57.4
106	5.5	6.5	8.5	11.7	18.1	26.0	41.5
75	3.9	4.9	5.9	8.1	13.3	19.8	31.9
53	3.1	4.1	5.1	6.3	10.5	15.6	25.5
45	2.3	3.3	4.2	5.4	8.6	13.5	23.4
25	1.6	2.4	3.4	4.5	5.7	8.3	18.1

Table A.7 Measured particle size distribution for ball size 30 mm, feed size (-850 +600 µm), U = 0.75, J = 20 %, ϕ_c = 75 of critical, f_c = 0.06

Size x_i [mm]	Fraction Passing per Grinding times in %						
	0.5 min	**1 min**	**2 min**	**4min**	**8 min**	**15 min**	**30 min**
850	100	100	100	100	100	100	100
600	19.7	29.4	42.9	71.8	89.5	97.1	99.2
425	7.9	15.1	24.1	48.2	68.6	84.3	96.0
300	4.7	9.2	15.2	32.7	50.5	65.7	84.8
212	3.1	5.9	9.8	23.6	38.1	51.0	69.6
150	1.6	3.4	6.3	16.4	27.6	38.2	55.2
106	0.8	1.7	3.6	11.8	20.0	28.4	42.4
75	0.0	0.8	2.7	9.1	15.2	21.6	33.6
53	0.0	0.0	1.8	7.3	12.4	16.7	27.2
45	0.0	0.0	0.9	5.5	9.5	13.7	24.8
25	0.0	0.0	0.0	3.6	5.7	9.8	16.8

Table A.8 Measured particle size distribution for ball size 30 mm, feed size (-600 +425 µm), U = 0.75, J = 20 %, ϕ_c = 75 of critical, f_c = 0.06

Size x_i [mm]	Fraction Passing per Grinding times in %						
	0.5 min	**1 min**	**2 min**	**4min**	**8 min**	**15 min**	**30 min**
600	100	100	100	100	100	100	100
425	14.6	26.0	39.2	55.8	76.9	92.1	98.4
300	6.9	11.4	20.0	33.6	51.9	67.3	87.5
212	4.6	7.3	13.3	23.9	38.5	51.5	71.9
150	3.1	4.9	8.3	16.8	27.9	38.6	54.7
106	2.3	3.3	5.0	11.5	20.2	27.7	34.4
75	1.8	2.4	3.3	8.8	15.4	20.8	26.6
53	1.4	1.6	2.5	4.4	9.6	13.9	12.5
45	1.2	1.4	1.7	3.5	8.7	11.9	10.9
25	0.8	0.8	0.8	2.7	4.8	7.9	6.3

Table A.9 Measured particle size distribution for ball size 30 mm, feed size (-425 +300 µm), U = 0.75, J = 20 %, ϕ_c = 75 of critical, f_c = 0.06

Size x_i [mm]	Fraction Passing per Grinding times in %						
	0.5 min	**1 min**	**2 min**	**4min**	**8 min**	**15 min**	**30 min**
425	100	100	100	100	100	100	100
300	11.2	17.5	26.7	41.6	59.0	76.5	91.9
212	3.4	8.3	15.5	25.7	41.0	57.1	77.2
150	1.9	5.0	10.3	16.8	28.6	42.9	61.0
106	1.2	2.5	6.0	10.6	20.0	30.6	46.3
75	0.9	1.7	4.3	8.0	14.3	23.5	37.4
53	0.8	0.8	2.6	5.3	9.5	17.3	29.3
45	0.8	0.8	2.6	4.4	7.6	15.3	26.8
25	0.8	0.8	1.7	3.5	4.8	10.2	20.3

Table A.10 Breakage function values calculated using the BII-method from laboratory data and later used to determine breakage function parameters

(850 - 600 µm)	**Breakage function values**		
	10 mm	**20 mm**	**30 mm**
1	1	1	1
0.705882	0.490667	0.513677	0.445968
0.5	0.267386	0.329891	0.26447
0.352941	0.163559	0.214185	0.168258
0.249412	0.095405	0.134643	0.0973
0.176471	0.063577	0.08919	0.062
0.124706	0.037207	0.056723	0.041

(600 - 425 µm)	**Breakage function values**		
	10 mm	**20 mm**	**30 mm**
1	1	1	1
0.708333	0.352849	0.352025	0.451688
0.5	0.206075	0.202808	0.293503
0.353333	0.117519	0.123567	0.191151
0.25	0.068223	0.067617	0.127644
0.176667	0.041217	0.042694	0.095432
0.125	0.031	0.029	0.062273

(425 - 300 µm)	Breakage function values		
	10 mm	20 mm	30 mm
1	1	1	1
0.705882	0.33642	0.383113	0.459816
0.498824	0.19577	0.213915	0.2797
0.352941	0.130378	0.123131	0.161495
0.249412	0.08	0.075	0.115588
0.176471	0.053	0.043	0.07374
0.125	0.03	0.028	0.05

A.2 Determination of the milling properties of the ore

Breakage function and some of the selection function parameters were determined from the laboratory data presented above, then the remaining selection function parameters were back-calculated within the population balance model framework. Presented below are the Matlab® codes used for parameter search and simulation.

A.2.1 Search engine for population balance model parameters

Note: The %% or % lines in the code are comments and do not affect the execution of the code.

A.2.1.1 The driver used for the parameter search based on batch grinding data available

```
% Matlab script for data acquisition
% The code reads batch test results from an Excel spreadsheet and
% sorts it so as to compare them to predicted ones using
LabDataSearch.m
%
%% Initial treatment
% Extract data from Batch test results.xls
data = xlsread('Batch test results');
% Sort data as particle size distributions and size classes
Screens = data(:, 1);
MeasuredPsd = data(:, 2:length(data(1, :)));
%
%% Parameter search
% Initial guesses of PBM parameters
% Parameters are given in the following order:
% x0 = [A, alpha, lamdba, mu, beta, gamma, phi]
x0 = [1.58, 1.23, 6.2, 1.32, 0.59];
% Our search domain is defined as follows:
% 0.1 < A < 3.0; 0.5 < alpha < 3.0; 1.3 < lambda < 8.0; 0 < mu < 5;
```

```
% 5 < beta < 15; 0 < gamma < 2; 0 < phi < 1
lb = [0.1, 1.4, 6.2, 0, 0.60];
ub = [10.0, 1.4, 6.2, 5, 0.60];
% Note that lambda > alpha
[x, fval, exitflag] = fmincon(@LabDataSearch, x0, [], [], [], [], lb,
ub);

%% Printing output and convergence criteria
fprintf('\nValue of the Objective Function at termination = %g\n',
fval);
if exitflag
    fprintf('\nSuccess: The search converged to a solution\n');
    fprintf('\n A = %4.2f; alpha = %4.2f\n', x(1:2));
    fprintf('\n beta = %4.2f; gamma = %4.2f; phi = %4.2f\n', x(3:5));
else
    fprintf('Error: Maximum number of iterations reached\n')
end
%
```

A.2.1.2 The function file for the generation of product side distribution once PBM parameters are inputted.

This function is named ‘LabDataSearch.m’

```
%% Matlab function that computes particle size distributions with
the following parameters:
% - Selection function parameters A and alpha
% - Breakage function parameteres beta, gamma, and phi
% Refer to 'Austin, L.G., Klimpel, R.R., Luckie, P.T., 1984.
Process Engineering
% of Size Reduction: Ball Milling. Society of Mining Engineers of
the AIME, New York'
% for more on the Population Balance Model used here
%
%% Definition of the LabDataSearch function
function y = LabDataSearch(x)
% Extraction of selection function variables
A = x(1); alpha = x(2); beta = x(3); gamma = x(4); phi = x(5);
%
%% Initial data
% Screen sizes used in the lab and extras for simulation purposes
x = [evalin('base', 'Screens'); 19];
x = x/1000; % Sizes are converted to mm
% Input feed size distribution
f = [100 zeros(1, length(x))];
f = f/100; % Mass fractions passing size class
% Input grinding times considered throughout the batch milling
test in min
t = [0 0.5 1 2 4 8 15 30];
%
%% Various calculations
% Number of size classes considered
n = length(x) - 1;
% ---------------------------------------------------------------
% Selection function values for the different particle sizes
S = A*(x(1:n).^alpha);
% ---------------------------------------------------------------
```

```
% Cumulative breakage function matrix B(i, j)
B = [diag(diag(ones(n))); zeros(1, n)];
for i = 2:n
    for j = 1:n-1
        if (i <= n) && (i > j)
            B(i, j) = phi*(x(i)/x(j+1))^gamma + (1-
phi)*(x(i)/x(j+1))^beta;
        end
    end
end
% ---------------------------------------------------------------------
% Primary breakage function matrix b(i, j)
b = tril(B(1:n, :) - B(2:n+1, :));
% ---------------------------------------------------------------------
% Matrix a(i, j)
% Populate matrix a(i, j) with zeros
a = zeros(n);
% Case (i == j) && (j ==1)
a(1, 1) = f(1);
% Other cases
for i = 1:n
    for j = 1:n
        if (i < j)
            a(i, j) = 0;
        elseif (i == j) && (i ~= 1)
            a(i, j) = f(i) - sum(a(i, 1:j-1));
        elseif (i > j)
            a(i, j) = 1/(S(i) - S(j))*sum(S(j:i-1).*(b(i, j:i-
1))'.*a(j:i-1, j));
        end
    end
end
% ---------------------------------------------------------------------
% Mass fraction in each size interval for different grinding times
% Retained mass fractions
m = zeros(length(S), length(t));
for k = 1:length(t)
    m(:, k) = a*exp(-S*t(k));
end
%
% Correction of the retained mass in the sink fraction
m(n, :) = m(n, :) + (1 - sum(m));
% ---------------------------------------------------------------------
% Percent passing particle size
Predicted = 100*flipud(cumsum(flipud(m)));
% ---------------------------------------------------------------------
%% Definition of the objective function
% Capture of 'MeasuredPsd' from the Matlab base workspace
Measured = evalin('base', 'MeasuredPsd');
% Sum of Squared Errors
y = sum(sum((Measured - Predicted).^2));
%
%% Presentation of results
% Plot of the predicted product size distributions
% semilogx(x(1:n), p(:, 2:k), 'o-')
% xlabel('Particle size in mm')
% ylabel('Passing fraction')
% ---------------------------------------------------------------------
```

A2.1.3 The plotting facility of the product size distribution based on back-calculated parameters.

The file is named 'PlotResults.m'

```
% Matlab function that plots particle size distributions with the
% following parameters:
% - Selection function parameters A and alpha
% - Breakage function parameteres beta, gamma, and phi
% The above parameters are those optimised using the Matlab
function file 'LabDataSearch.m'
% following the Back-calculation method proposed by 'Austin, L.G.,
Klimpel, R.R.,
% Luckie, P.T., 1984. Process Engineering of Size Reduction: Ball
Milling. Society of Mining
% Engineers of the AIME, New York'
%
%% Definition of the PlotResult function
function PlotResults(x)
% Extraction of variables
A = x(1); alpha = x(2); beta = x(3); gamma = x(4); phi = x(5);
%
%% Initial data
% Screen sizes used in the lab and extras for simulation purposes
x = [evalin('base', 'Screens'); 19];
x = x/1000; % Sizes are converted to mm
% Input feed size distribution
f = [100 zeros(1, length(x))];
f = f/100; % Mass fractions passing size class
% Input grinding times considered throughout the batch milling
test in min
t = [0 0.5 1 2 4 8 15 30];
%
%% Various calculations
% Number of size classes considered
n = length(x) - 1;
% ---------------------------------------------------------------
% Selection function values for the different particle sizes
S = A*(x(1:n).^alpha);
% ---------------------------------------------------------------
% Cumulative breakage function matrix B(i, j)
B = [diag(diag(ones(n))); zeros(1, n)];
for i = 2:n
    for j = 1:n-1
        if (i <= n) && (i > j)
            B(i, j) = phi*(x(i)/x(j+1))^gamma + (1 -
phi)*(x(i)/x(j+1))^beta;
        end
    end
end
% ---------------------------------------------------------------
% Primary breakage function matrix b(i, j)
b = tril(B(1:n, :) - B(2:n+1, :));
% ---------------------------------------------------------------
% Matrix a(i, j)
% Populate matrix a(i, j) with zeros
a = zeros(n);
% Case (i == j) && (j == 1)
```

```
a(1, 1) = f(1);
% Other cases
for i = 1:n
    for j = 1:n
        if (i < j)
            a(i, j) = 0;
        elseif (i == j) && (i ~= 1)
            a(i, j) = f(i) - sum(a(i, 1:j-1));
        elseif (i > j)
            a(i, j) = 1/(S(i) - S(j))*sum(S(j:i-1).*(b(i, j:i-
1))'.*a(j:i-1, j));
        end
    end
end
% ------------------------------------------------------------------
% Mass fraction in each size interval for different grinding times
% Retained mass fractions
m = zeros(length(S), length(t));
for k = 1:length(t)
    m(:, k) = a*exp(-S*t(k));
end
%
% Correction of the retained mass in the sink fraction
m(n, :) = m(n, :) + (1 - sum(m));
% ------------------------------------------------------------------
% Percent passing particle size
Predicted = 100*flipud(cumsum(flipud(m)));
% ------------------------------------------------------------------
%% Capture of 'MeasuredPsd' from the Matlab base workspace
Measured = evalin('base', 'MeasuredPsd');
% ------------------------------------------------------------------
%% Presentation of results in semilog scale
% First figure
figure(1)
% Plot of the predicted product size distributions
semilogx(x(1:n), Predicted(:, 2:k))
hold on
% Plot of the measured product size distributions
semilogx(x(1:n), Measured(:, 2:k), 'o')
xlabel('Particle size in mm')
ylabel('Mass fraction passing in %')
hold off
% ------------------------------------------------------------------
%% Presentation of results in semilog scale
% Second figure
figure(2)
% Plot of the predicted product size distributions
loglog(x(1:n), Predicted(:, 2:k))
hold on
% Plot of the measured product size distributions
loglog(x(1:n), Measured(:, 2:k), 'o')
xlabel('Particle size in mm')
ylabel('Mass fraction passing in %')
hold off
% ------------------------------------------------------------------


% Matlab script for data acquisition
% The code reads batch test results from an Excel spreadsheet
```

```
% and sorts it so as to compare them to predicted ones using
% PbmSearch.m
%
%% Initial treatment
% Extract data from Batch test results.xls
data = xlsread('Batch test results');
% Sort data as particle size distribtuions and size classes
Screens = data(:, 1);
MeasuredPsd = data(:, 2:length(data(1, :)));
%
%% Parameter search
% Initial guesses of PBM parameters
% Parameters are given in the following order:
% x0 = [A, alpha, lamdba, mu, beta, gamma, phi]
x0 = [1.58, 1.23, 6.2, 1.32, 0.59];
% Our search domain is defined as follows:
% 0.1 < A < 3.0; 0.5 < alpha < 3.0; 1.3 < lambda < 8.0;
% 0 < mu < 5;
% 5 < beta < 15; 0 < gamma < 2; 0 < phi < 1
lb = [0.1, 1.4, 6.2, 0, 0.60];
ub = [10.0, 1.4, 6.2, 5, 0.60];
% Note that lambda > alpha
[x, fval, exitflag] = fmincon(@PbmSearch, x0,[],[],[],[], lb, ub);
%
%% Printing output and convergence criteria
fprintf('\nObjective Function at termination = %g\n', fval);
if exitflag
    fprintf('\nSuccess: The search converged to a solution\n');
    fprintf('\n A = %4.2f; alpha = %4.2f\n', x(1:2));
    fprintf('\n beta=%4.2f; gamma=%4.2f; phi=%4.2f\n', x(3:5));
else
    fprintf('Error: Maximum number of iterations reached\n')
end
%
```

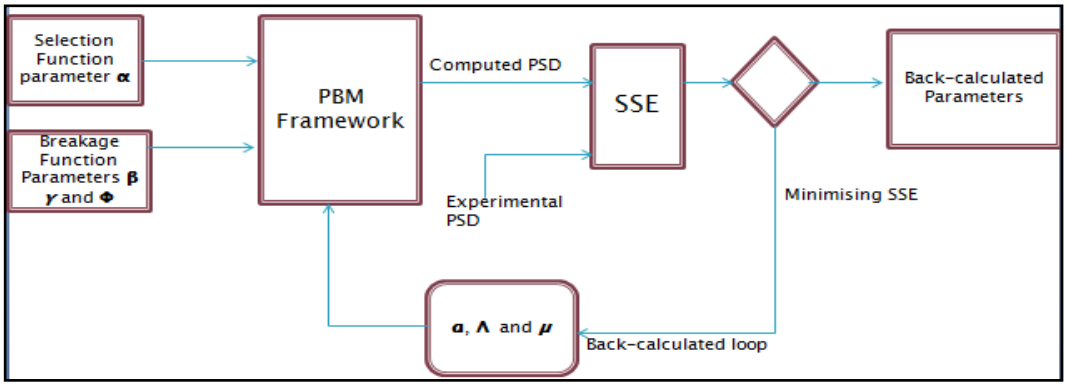
A.2.2 Simulator for the milling kinetics of the size class of interest

```
% Matlab function that plots particle size distributions with the
% following parameters:
% - Selection function parameters A and alpha
% - Breakage function parameters beta, gamma, and phi
% The above parameters are those optimised using the Matlab
% function file 'BatchDataParam.m' following the back-calculation
% method proposed by 'Austin, L.G., Klimpel, R.R., Luckie, P.T.,
% 1984. Process Engineering of Size Reduction: Ball Milling.
% Society of Mining Engineers of the AIME, New York'
%
%% Definition of the PbmSearch function
% Input manually the selection function variables
A = 0.32; alpha = 1.23; mu = 4.2; lambda = 3.0;
% Input manually the selection function variables
beta = 6.8; gamma = 1.27; phi = 0.60;
%
%% Initial data
% Screen sizes used in the lab and extras for simulation purposes
```

```
x = [600; 425; 300; 212; 150; 106; 75; 53; 45; 25; 19];
x = x/1000; % Sizes are converted to mm
% Input feed size distribution
f = [100 zeros(1, length(x))];
f = f/100; % Mass fractions passing size class
% Input grinding times considered throughout the batch milling
test in min
t = [0 0.5 1 2 4 8 15 30];
%
%% Various calculations
% Number of size classes considered
n = length(x) - 1;
% ------------------------------------------------------------------
% Selection function values for the different particle sizes
S = A*(x(1:n).^alpha)./(1 + (x(1:n)/mu).^lambda);
% ------------------------------------------------------------------
% Cumulative breakage function matrix B(i, j)
B = [diag(diag(ones(n))); zeros(1, n)];
for i = 2:n
    for j = 1:n-1
        if (i <= n) && (i > j)
            B(i, j) = phi*(x(i)/x(j+1))^gamma ...
                            + (1 - phi)*(x(i)/x(j+1))^beta;
        end
    end
end
% ------------------------------------------------------------------
% Primary breakage function matrix b(i, j)
b = tril(B(1:n, :) - B(2:n+1, :));
% ------------------------------------------------------------------
% Matrix a(i, j)
% Populate matrix a(i, j) with zeros
a = zeros(n);
% Case (i == j) && (j == 1)
a(1, 1) = f(1);
% Other cases
for i = 1:n
    for j = 1:n
        if (i < j)
            a(i, j) = 0;
        elseif (i == j) && (i ~= 1)
            a(i, j) = f(i) - sum(a(i, 1:j-1));
        elseif (i > j)
            a(i, j)=1/(S(i)-S(j))...
                        *sum(S(j:i-1).*(b(i,j:i-1))'.*a(j:i-1,j));
        end
    end
end
% ------------------------------------------------------------------
% Mass fraction in each size interval for different grinding times
% Retained mass fractions
m = zeros(length(S), length(t));
for k = 1:length(t)
    m(:, k) = a*exp(-S*t(k));
end
%
% Correction of the retained mass in the sink fraction
m(n, :) = m(n, :) + (1-sum(m));
% ------------------------------------------------------------------
```

```
% Percent passing particle size
Predicted = 100*flipud(cumsum(flipud(m)));
% ------------------------------------------------------------------
%% Variables to be saved in a spreadsheet
% m are mass fractions in each size class.
% These mass fractions are to be multiplied by 100.
% x are particle size defining the size classes
% S are the selection function values for each size class
% t are the grinding times used in the batch tests
% ------------------------------------------------------------------
```

A.2.3 Flowchart for the parameter search algorithm



A.3 Scale-up procedure for laboratory-based PBM parameters

The parameters determined in Chapter 5 were scaled-up using empirical models and the following Matlab code was used.

```
%% Description of the Mode
% This Matlab script scales up laboratory batch grinding results
% to industrial scale following the procedure presented in
% Austin, L.G., Klimpel, R.R., Luckie, P.T., 1984. Process
% engineering of size reduction: Ball milling. SME of AIME,
% New York
%
%% Measured selection function parameters
a_test = 0.32;
alpha = 1.37;
mu = 4.2;
lambda = 4.74;
%
%% Batch grinding conditions
Dt = 0.3; % Mill diameter in metres
Jt = 0.2; % Ball filling
Ut = 0.75; % Slurry filling
SpeedT = 0.75; % Mill speed in fraction of critical speed
dt = 0.02; % Diameter of grinding balls in metres
%
%% Industrial conditions
D = 7.312; % Diameter of industrial mill in metres
J = 0.6; % Ball volumetric filling of industrial mill
U = 1.65; % Slurry filling of industrial mill
Speed = 0.40; % Fractional speed of industrial mill
d = 0.1; % Larger ball size used in industrial mill in metres
%
%% Computation of scale-up parameters
% ------------------------------------------------------------------
% Definition of exponent factor matrix
% These values need to be fine-tuned to suit industry
% N(1) represents the effect of ball size on milling kinetics
% N(2) represents the effect of industrial mill design
% N(3) represents the effect of mill diameter due to scale-up
N = [1 0.5 0.2];
% ------------------------------------------------------------------
% Dry versus wet milling
% This parameter allows for the presence of water in the mill
c = 1.32; % Wet milling c = 1.32 and Dry milling c = 1.20
% The next parameter allows for the ball wear rate
% delta = 0 models a surface area-based wear law
% delta = 1 models a mass-based wear law
% and delta = 2 models ball wear rate in wet milling
delta = 2;
% Preallocation of scale-up matrix
C = zeros(1, 6);
%
C(1) = (D/Dt)^N(3) * (d/dt)^2;
%
C(2) = (Dt/d)^N(1);
%
if D <= 3.81
```

```
    C(3) = (D/Dt)^N(2);
else
    C(3) = (3.81/Dt)^N(2) * (D/3.81)^(N(2) - delta);
end
%
C(4) = (1 + 6.6*(Jt^2.3))/(1 + 6.6*(J^2.3)) * exp(-c*(U - Ut));
%
C(5) = ((Speed - 0.1)/(SpeedT - 0.1))*...
      ((1 + exp(15.7*(SpeedT - 0.94)))/(1 + exp(15.7...
      *(Speed - 0.94))));
%
%% Industrial Selection function values
% Particle sizes in microns
x = [850 600 425 300 212 150 106 75 53 38 25 19 12 9 6];
x = x/1000; % Conversion of particle sizes to mm
% Populating the Selection function matrix with industrial values
S = a_test*(x.^alpha)./(1./(1+(x./(C(1)*mu)).^lambda)) ...
      *C(2)*C(3)*C(4)*C(5);
% -------------------------------------------------------------------
%% Initial data
% Input feed size distribution
f = [1; zeros(length(x)-1, 1)];
% Input grinding times considered throughout the batch milling
% test in min
t = [0.5, 1, 2, 4, 8, 15, 30];
% Input breakage function parameters [0.51; 3.2; 0.53]
phi = 0.60; beta = 6.2; gamma = 0.79;
%
%% Various calculations
% Calculate the number of size classes considered
n = length(x) - 1;
% -------------------------------------------------------------------
% Define selection function values for different particle sizes
S = S(1:n)';
% -------------------------------------------------------------------
% Calculate the cumulative breakage function matrix B(i, j)
B = [diag(diag(ones(n))); zeros(1, n)];
for i = 2:n
    for j = 1:n-1
        if (i <= n) && (i > j)
            B(i, j) = phi*(x(i)/x(j+1))^gamma ...
                + (1 - phi)*(x(i)/x(j+1))^beta;
        end
    end
end
% -------------------------------------------------------------------
% Calculate the primary breakage function matrix b(i, j)
b = tril(B(1:n, :) - B(2:n+1, :));
% -------------------------------------------------------------------
% Calculate matrix a(i, j)
% Populate matrix a(i, j) with zeros
a = zeros(n);
% Case (i == j) && (j == 1)
a(1, 1) = f(1);
% Other cases
for i = 1:n
    for j = 1:n
        if (i < j)
            a(i, j) = 0;
```

```
        elseif (i == j) && (i ~= 1)
            a(i, j) = f(i) - sum(a(i, 1:j-1));
        elseif (i > j)
            a(i, j) = 1/(S(i) - S(j)) ...
                *sum(S(j:i-1).*(b(i, j:i-1))'.*a(j:i-1, j));
        end
    end
end
% ---------------------------------------------------------------------
% Calculate mass in size intervals for different grinding times
% Retained masses
m = zeros(length(S), length(t));
for k = 1:length(t)
    m(:, k) = a*exp(-S*t(k));
end
%
% Correction of the retained mass in the sink fraction
m(n, :) = m(n, :) + (1 - sum(m));
% ---------------------------------------------------------------------
% Fraction passing particle size
p = flipud(cumsum(flipud(m)));
% ---------------------------------------------------------------------
%% Presentation of results
% Plot of the predicted product size distributions
loglog(x(1:n), p(:, 2:k), 'o-')
xlabel('Particle size in mm')
ylabel('Passing fraction')
%
%% Exporting plotted results to Excel spreadsheet
% Matrix 'data ' of particle size and Cumulative percent passing
data = [x(1:14)' p*100];
% Exporting 'data' to Excel
% The spreadsheet is named 'ScaledUpPsd.xls' and will be
% automatically created by Matlab in the Current Directory
xlswrite('ScaledUpPsd.xls', data, 'Sheet1')
% The first simulation will be saved in spreadsheet 'Sheet1'
% Please update the next simulation so as to save it into 'Sheet2'
% and so on
%
% ---------------------------------------------------------------------
%% Restituting scale-up selection function parameters
% Value of A
if D <= 3.8
    A = a_test*((D/Dt)^0.5)*((1 + 6.6*Jt^2.3)/(1 + 6.6*J^2.3)) ...
        *exp(1 - 1.32*(U - Ut));
else
    A = a_test*((3.8/Dt)^0.5)*((D/Dt)^0.3) ...
            *((1 + 6.6*Jt^2.3)/(1 + 6.6*J^2.3))* ...
            exp(1 - 1.32*(U - Ut));

end
% Value of mu
MU = mu*(d/dt)^1.2;
%
```

The scaled up parameters presented in Table A.11 below were used to generate the simulated PSDs using the above Matlab code. Table A.12 presents PSD measured for the actual industrial mill and the predicted PSDs simulated from the scaled up parameters.

Table A.11 Breakage parameters as scaled-up to industrial mill

Based on the following Parameters		
Selection function parameters	a	3.74
	alpha	1.40
	Lambda	4.74
	mu	9.65
Breakage function parameters	Phi	0.6
	beta	6.2
	gamma	0.8

Table A.12 Measured versus scaled-up particle size distributions

	Flowrate slurry tph							
	343.8		333.0		348.3		314.3	
Sizes	**Expt**	**Model**	**Expt**	**Model**	**Expt**	**Model**	**Expt**	**Model**
1.7	100	100	100	100	100	100	100	100
1.18	100	100	100	99.9997	100	99.9997	100	99.9998
0.85	99.9957	99.9967	99.992	99.991	99.9893	99.9906	99.9899	99.9929
0.425	99.7611	99.8004	99.818	99.7062	99.7978	99.6728	99.8012	99.7435
0.3	99.1007	98.8919	99.2507	98.5757	99.2247	98.3952	99.3089	98.6174
0.212	96.9666	96.2063	97.249	95.4533	97.2725	94.7722	97.3753	95.2289
0.15	91.2129	90.0658	91.8114	88.4943	91.6904	86.9832	92.6313	87.5441
0.106	78.1235	79.2538	78.8489	76.3762	78.2911	73.7469	80.9904	74.2337
0.075	63.8013	66.8797	64.58	62.6728	63.397	59.425	67.2376	59.8654
0.053	50.636	54.2457	50.7291	49.8768	49.1176	46.585	53.162	46.8298
0.038	41.6501	43.6881	41.4992	39.7717	40.0243	36.7602	43.5674	37.2024

A.4 Optimisation of the residence time

The following Matlab code was written to generate data for the optimisation of the residence time

```
%% Definition of initial data
% ---------------------------------------------------------------------
% Clearing the workspace and command window
clear, clc
% Particle sizes in microns
x = [850 600 425 300 212 150 106 75 53 38 25 19 12 9 0];
x = x/1000; % Conversion of particle sizes to mm
% Input feed size distribution
f = [1; zeros(length(x) - 2, 1)];
% ---------------------------------------------------------------------
% MEAN RESIDENCE TIME OF THE MILL
```

```
tau = 3:.1:90; % in MINUTES; STARTING POINT IS 3 MIN FOR A REAL
MILL
% Calculate TauL, TauS, and TauD
% Residence time of large fully mixed reactor
TauL = 0.841*tau - 2.531;
% Residence time of small fully mixed reactor
TauS = 0.057*tau + 1.377;
% Residence time of delay zone or dead time
TauD = 0.046*tau - 0.222;
% ---------------------------------------------------------------
% Breakage function parameters [0.51; 3.2; 0.53]
beta = 6.2; % Default = 3.2
gamma = 0.79; % Default = 0.53
phi = 0.6; % Default = 0.51
%
%% Initial data for the scale-up procedure
% ---------------------------------------------------------------
% Measured selection function parameters
a_test = 0.32;
alpha = 1.40;
mu = 4.2;
lambda = 4.74;
% ---------------------------------------------------------------
% Batch grinding conditions
Dt = 0.3; % Mill diameter in metres
Jt = 0.2; % Ball filling
Ut = 0.75; % Slurry filling
SpeedT = 0.75; % Mill speed in fraction of critical speed
dt = 0.02; % Diameter of grinding balls in metres
% ---------------------------------------------------------------
% Full-scale milling conditions
D = 7.312; % Diameter of industrial mill in metres
J = 0.20; % Ball volumetric filling of industrial mill
U = 2.78; % Slurry filling of industrial mill
Speed = 0.50; % Fractional speed of industrial mill
d = 0.04; % Larger ball size used in industrial mill in metres
%
%% Computation of scale-up parameters
% ---------------------------------------------------------------
% Definition of exponent factor matrix
% These values need to be fine-tuned to suit industry
% N(1) represents the effect of ball size on milling kinetics
% N(2) represents the effect of industrial mill design
% N(3) represents the effect of mill diameter due to scale-up
N = [1 0.5 0.2];
% ---------------------------------------------------------------
% Dry versus wet milling
% This parameter allows for the presence of water in the mill
c = 1.32; % Wet milling c = 1.32 and Dry milling c = 1.20
% The next parameter allows for the ball wear rate
% delta = 0 models a surface area-based wear law
% delta = 1 models a mass-based wear law
% and delta = 2 models ball wear rate in wet milling
delta = 2;
% ---------------------------------------------------------------
% Preallocation of scale-up matrix
C = zeros(1, 6);
%
C(1) = (D/Dt)^N(3) * (d/dt)^2;
```

```
%
C(2) = (dt/d)^N(1);
%
if D <= 3.81
      C(3) = (D/Dt)^N(2);
else
      C(3) = (3.81/Dt)^N(2) * (D/3.81)^(N(2) - delta);
end
%
C(4) = (1 + 6.6*(Jt^2.3))/(1 + 6.6*(J^2.3)) * exp(-c*(U - Ut));
%
C(5) = ((Speed - 0.1)/(SpeedT - 0.1))*...
((1 + exp(15.7*(SpeedT - 0.94)))/(1 + exp(15.7*(Speed - 0.94))));
%
%% Industrial Selection function and breakage function
% ---------------------------------------------------------------
% Populating the Selection function matrix with industrial values
S = a_test*(x.^alpha)./(1./(1+(x./(C(1)*mu)).^lambda)) ...
      *C(2)*C(3)*C(4)*C(5);
% Calculate the number of size classes considered
n = length(x) - 1;
% ---------------------------------------------------------------
% Define selection function values for different particle sizes
S(n) = []; % Accommodating the sink class for which S = 0
S = S';
% ---------------------------------------------------------------
% Calculate the cumulative breakage function matrix B(i, j)
B = [diag(diag(ones(n))); zeros(1, n)];
for i = 2:n
      for j = 1:n - 1
            if (i <= n) && (i > j)
                  B(i, j) = phi * (x(i)/x(j+1))^gamma ...
                              + (1 - phi) * (x(i)/x(j+1))^beta;
            end
      end
end
% ---------------------------------------------------------------
% Calculate the primary breakage function matrix b(i, j)
b = tril(B(1:n, :) - B(2:n + 1, :));
%
%% Model of residence time distribution
% Choice of type of flow along the mill
rtd = menu('CHOOSE RTD PROFILE', 'Plug flow mill', ...
      'Fully mixed mill', 'Real mill');
% Preallocate matrix relative to RTD profile e(i, j)
e = zeros(length(S), length(tau));
% Calculate matrix e(i, j)
if rtd == 1
   for j = 1:length(tau)
      for i = 1:length(S)
            e(i, j) = exp(-S(i)*tau(j));
      end
   end
elseif rtd == 2
  for j = 1:length(tau)
      for i = 1:length(S)
            e(i, j) = 1./(1 + S(i)*tau(j));
      end
  end
```

```
elseif rtd == 3
    for j = 1:length(tau)
        for i = 1:length(S)
            e(i, j) = exp(-S(i)*TauD(j))./((1+S(i)*TauS(j))^2 ...
                *(1+S(i)*TauL(j)));
        end
    end
end
%
%% Product size distribution of the mill
% Calculate matrix c(i, j)
c = diag(diag(ones(n)));
for j = 1:n
   for i = 1:n
      if i > j
         c(i, j) = 1/(S(i) - S(j))...
                  * sum(S(j:i-1).*b(i, j:i-1)'.*c(j:i-1, j));
      elseif i < j
         c(i, j) = - sum(c(i, i:j-1).*c(j, i:j-1));
      end
   end
end
% ---------------------------------------------------------------------
% Calculate the transfer function 3D-matrix d(i, j, k)
d = zeros(n, n, n);
for k = 1:length(tau)
  for i = 1:n
    for j = 1:n
      if i == j
        d(i, j, k) = e(j, k);
      elseif i > j
        d(i, j, k) = sum(c(i,j:i-1).*c(j, j:i-1).*(e(j:i-1, k) ...
                        - e(i, k))');
      end
    end
  end
end
% ---------------------------------------------------------------------
% Calculate the retained product size distributions p(i)
p = zeros(n, length(tau));
for k = 1:length(tau)
  for i = 1:n
      p(i, k) = d(i, 1:i, k) * f(1:i) * 100; % in percents
  end
end
% Calculate cumulative particle size distributions P(i)
P = flipud(cumsum(flipud(p))); % in percents
%
%% Milling kinetics: Attainable Region analysis
% Choice of cut-off sizes
cutoff = inputdlg({'CHOOSE CUT-OFF SIZES FROM SIEVES BELOW:', ...
'Enter upper cut-off size from the list of sieves above:', ...
'Enter lower cut-off size from the list of sieves above:'}, ...
'SIZE CLASS OF INTEREST', ...
1, {num2str(x*1000,'%5.0f'), '75', '9'});
% Extraction of user-defined cut-off sizes
sieve = str2double(cutoff)/1000;
% Mass percent fraction in the size class of interest
mass = P(x == sieve(2), :) - P(x == sieve(3), :);
```

```
plot(tau, mass)
ylabel('Mass fraction in size class of interest in %')
xlabel('Mean residence time {\it\tau} in minutes')
%
% ------------------------------------------------------------------
%% Particle size distribution output
% To retrieve this information, type the following
% in the command window
% [1000*x(1:n)', P]
% Note that particle size will be in microns
% whereas fraction passing will be in percents
%
```

A.5 Matlab version of the Morrell power model

```
%% Description of the code
% The Matlab code calculates the effects of slurry pool on
% net power as described by Morrell, S., 1993. The prediction of
% net power draw in wet tumbling ball mills. PhD Thesis
% University of Queensland, Australia
%
%% Clearing workspace and command window
clear, clc
%
%% Input initial data
% Diameter D inside liners in metres
D = 7.312;
% Belly length L inside liners in metres
L = 9.6;
% Fraction of critical speed
Phi = 0.9;
% Revolutions per minute of the mill
N = 42.3*Phi/sqrt(D);
% Specific density of ore
RhoO = 3.47;
% Specific density of balls
RhoB = 7.8;
% Percent solids by mass Cw in discharge slurry
Cw = 0.65;
% Percent solids by volume S in discharge slurry
S = Cw/(RhoO - Cw*(RhoO - 1));
% Ball fractional filling J of the mill
J = 0.30;
%
%% Charge density
% Morrell's assumptions
U = 1;
e = 0.40;
% Mill charge density
RhoC = (J*RhoO*(1-e+e*U*S) + J*(RhoB-RhoO)*(1-e) + J*e*U*(1-S))/J;
%
%% Load behaviour
% Slurry toe angle
ThetaTO = 3.395;
% ---------------------------------------------------------------
% Toe angle
if Phi > 0.35*(3.364 - J)
    PhiC = Phi;
else
    PhiC = 0.35*(3.364 - J);
end
%
A = 2.5307*(1.2796 - J);
B = 19.42;
%
ThetaT = A.*(1 - exp(-B*(PhiC - Phi))) + pi/2;
% ---------------------------------------------------------------
% Shoulder angle
E = 0.3386 + 0.1041*Phi;
F = 1.54 - 2.5673*Phi;
%
```

```
ThetaS = pi/2 - (ThetaT - pi/2).*(E + F*J);
%
%% Charge inner surface radius
% Initial inputs
rm = D/2;  % Radius of the mill
Nm = N/60; % Revolutions per second of the mill
% Times inside the mill charge
Nbar = Nm/2;
tc = (2*pi - ThetaT + ThetaS)/(2*pi*Nbar);
%
rbar = rm/2*(1 + (1 - 2*pi*J/sqrt(2*pi + ThetaS - ThetaT)));
g = 9.81;
tf = sqrt((2*rbar*(sin(ThetaS) - sin(ThetaT)))/g);
%
beta = tc/(tc + tf);
% Inner radius
ri = rm * sqrt(1 - (2*pi*beta*J)/(2*pi + ThetaS - ThetaT));
%
%% Calculate z parameter
z = (1 - J)^(0.4532);
%
%% Theoretical power
% Specific density of slurry
RhoS = RhoO/(RhoO - Cw*(RhoO - 1));
% Net power Pnet
Pnet = pi*g*L*Nm*rm/(3*(rm - z*ri))*(2*(rm^3) - 3*z*(rm^2)*ri ...
    + (ri^3)*(3*z - 2))*(RhoC*(sin(ThetaS) - sin(ThetaT)) ...
    + RhoS*(sin(ThetaT) - sin(ThetaTO))) ...
    + L*RhoC*((Nm*rm*pi/(rm - z*ri))^3)*(((rm - z*ri)^4) ...
    - (ri^4)*(z - 1)^4);
% No-load power Pno
Pno = 1.68*((D^2.5)*L*Phi)^0.82;
% Total power Ptot
Ptot = 1.215*Pnet + Pno;
% Print total power in kW
fprintf('\n Total Power in kiloWatts = %4.3f\n', Ptot/1000);
%
```

A.6 Matlab code to calculate energy

```
%% Definition of initial data
% ---------------------------------------------------------------------
% Clearing the workspace and command window
clear, clc
% Particle sizes in microns
x = [850 600 425 300 212 150 106 75 53 38 25 19 12 9 0];
x = x/1000; % Conversion of particle sizes to mm
% Input feed size distribution
f = [1; zeros(length(x) - 2, 1)];
% ---------------------------------------------------------------------
% MEAN RESIDENCE TIME OF THE MILL
tau = 3:.1:90; % in MINUTES
% STARTING POINT IS 3 MIN FOR A REAL MILL
% Calculate TauL, TauS, and TauD
% Residence time of large fully mixed reactor
TauL = 0.841*tau - 2.531;
% Residence time of small fully mixed reactor
TauS = 0.057*tau + 1.377;
% Residence time of delay zone or dead time
TauD = 0.046*tau - 0.222;
% ---------------------------------------------------------------------
% Breakage function parameters [0.51; 3.2; 0.53]
beta = 6.2; % Default = 3.2
gamma = 0.79; % Default = 0.53
phi = 0.6; % Default = 0.51
%
%% Initial data for the scale-up procedure
% ---------------------------------------------------------------------
% Measured selection function parameters
a_test = 0.32;
alpha = 1.40;
mu = 4.2;
lambda = 4.74;
% ---------------------------------------------------------------------
% Batch grinding conditions
Dt = 0.3; % Mill diameter in metres
Jt = 0.2; % Ball filling
Ut = 0.75; % Slurry filling
SpeedT = 0.75; % Mill speed in fraction of critical speed
dt = 0.02; % Diameter of grinding balls in metres
% ---------------------------------------------------------------------
% Full-scale milling conditions
D = 7.312; % Diameter of industrial mill in metres
L = 9.6; % Belly length inside liners of industrial mill in metres
J = 0.3; % Ball volumetric filling of industrial mill
U = 1.35; % Slurry filling of industrial mill
Speed = 0.5; % Fractional speed of industrial mill
d = 0.04; % Larger ball size used in industrial mill in metres
%
%% Computation of scale-up parameters
% ---------------------------------------------------------------------
% Definition of exponent factor matrix
% These values need to be fine-tuned to suit industry
% N(1) represents the effect of ball size on milling kinetics
% N(2) represents the effect of industrial mill design
% N(3) represents the effect of mill diameter due to scale-up
```

```
N = [1 0.5 0.2];
% ------------------------------------------------------------------
% Dry versus wet milling
% This parameter allows for the presence of water in the mill
c = 1.32; % Wet milling c = 1.32 and Dry milling c = 1.20
% The next parameter allows for the ball wear rate
% delta = 0 models a surface area-based wear law
% delta = 1 models a mass-based wear law
% and delta = 2 models ball wear rate in wet milling
delta = 2;
% ------------------------------------------------------------------
% Preallocation of scale-up matrix
C = zeros(1, 6);
%
C(1) = (D/Dt)^N(3) * (d/dt)^2;
%
C(2) = (dt/d)^N(1);
%
if D <= 3.81
C(3) = (D/Dt)^N(2);
else
C(3) = (3.81/Dt)^N(2) * (D/3.81)^(N(2) - delta);
end
%
C(4) = (1 + 6.6*(Jt^2.3))/(1 + 6.6*(J^2.3)) * exp(-c*(U - Ut));
%
C(5) = ((Speed - 0.1)/(SpeedT - 0.1))*...
((1 + exp(15.7*(SpeedT - 0.94)))/(1 + exp(15.7*(Speed - 0.94))));
%
%% Industrial Selection function and breakage function
% ------------------------------------------------------------------
% Populating the Selection function matrix with industrial values
S = a_test*(x.^alpha)./(1./(1+(x./(C(1)*mu)).^lambda)) ...
      *C(2)*C(3)*C(4)*C(5);
% Calculate the number of size classes considered
n = length(x) - 1;
% ------------------------------------------------------------------
% Define the selection function values for the different particle
sizes
S(n) = []; % Accommodating the sink class for which S = 0
S = S';
% ------------------------------------------------------------------
% Calculate the cumulative breakage function matrix B(i, j)
B = [diag(diag(ones(n))); zeros(1, n)];
for i = 2:n
   for j = 1:n - 1
     if (i <= n) && (i > j)
        B(i, j) = phi * (x(i)/x(j+1))^gamma ...
                  + (1 - phi) * (x(i)/x(j+1))^beta;
     end
   end
end
% ------------------------------------------------------------------
% Calculate the primary breakage function matrix b(i, j)
b = tril(B(1:n, :) - B(2:n + 1, :));
%
%% Model of residence time distribution
% Choice of type of flow along the mill
rtd = menu('CHOOSE RTD PROFILE', 'Plug flow mill', ...
```

```
'Fully mixed mill', 'Real mill');
% Preallocate matrix relative to RTD profile e(i, j)
e = zeros(length(S), length(tau));
% Calculate matrix e(i, j)
if rtd == 1
   for j = 1:length(tau)
      for i = 1:length(S)
          e(i, j) = exp(-S(i)*tau(j));
      end
   end
elseif rtd == 2
   for j = 1:length(tau)
      for i = 1:length(S)
          e(i, j) = 1./(1 + S(i)*tau(j));
      end
   end
elseif rtd == 3
    for j = 1:length(tau)
        for i = 1:length(S)
            e(i, j) = exp(-S(i)*TauD(j))./((1+S(i)*TauS(j))^2 ...
                *(1+S(i)*TauL(j)));
        end
    end
end
%
%% Product size distribution of the mill
% Calculate matrix c(i, j)
c = diag(diag(ones(n)));
for j = 1:n
   for i = 1:n
      if i > j
          c(i, j) = 1/(S(i) - S(j))...
                    * sum(S(j:i-1).*b(i, j:i-1)'.*c(j:i-1, j));
      elseif i < j
          c(i, j) = - sum(c(i, i:j-1).*c(j, i:j-1));
      end
   end
end
% ---------------------------------------------------------------------
% Calculate the transfer function 3D-matrix d(i, j, k)
d = zeros(n, n, n);
for k = 1:length(tau)
   for i = 1:n
      for j = 1:n
         if i == j
            d(i, j, k) = e(j, k);
         elseif i > j
            d(i, j, k) = sum(c(i, j:i-1).*c(j, j:i-1).* ...
                          (e(j:i-1, k) - e(i, k))');
         end
      end
   end
end
% ---------------------------------------------------------------------
% Calculate the retained product size distributions p(i)
p = zeros(n, length(tau));
for k = 1:length(tau)
   for i = 1:n
       p(i, k) = d(i, 1:i, k) * f(1:i) * 100; % in percents
```

```
   end
end
% Calculate cumulative particle size distributions P(i)
P = flipud(cumsum(flipud(p))); % in percents
%
% ========================================================================
%% Morrell's power model
Nrpm = 42.3*Speed/sqrt(D); % Revolutions per minute of the mill
% Specific density of ore
RhoO = 3.47;
% Specific density of balls
RhoB = 7.8;
% Percent solids by mass Cw in discharge slurry
Cw = 0.65;
% Percent solids by volume S in discharge slurry
S = Cw/(RhoO - Cw*(RhoO - 1));
%
%% Charge density
% Morrell's assumptions
e = 0.40;
% Mill charge density
RhoC = (J*RhoO*(1-e+e*U*S) + J*(RhoB-RhoO)*(1-e) + J*e*U*(1-S))/J;
%
%% Load behaviour
% Slurry toe angle
ThetaTO = 3.395;
% ------------------------------------------------------------------------
% Toe angle
if Speed > 0.35*(3.364 - J)
    SpeedC = Speed;
else
    SpeedC = 0.35*(3.364 - J);
end
%
A = 2.5307*(1.2796 - J);
B = 19.42;
%
ThetaT = A.*(1 - exp(-B*(SpeedC - Speed))) + pi/2;
% ------------------------------------------------------------------------
% Shoulder angle
E = 0.3386 + 0.1041*Speed;
F = 1.54 - 2.5673*Speed;
%
ThetaS = pi/2 - (ThetaT - pi/2).*(E + F*J);
%
%% Charge inner surface radius
% Initial inputs
rm = D/2;  % Radius of the mill
Nm = Nrpm/60; % Revolutions per second of the mill
% Times inside the mill charge
Nbar = Nm/2;
tc = (2*pi - ThetaT + ThetaS)/(2*pi*Nbar);
%
rbar = rm/2*(1 + (1 - 2*pi*J/sqrt(2*pi + ThetaS - ThetaT)));
g = 9.81;
tf = sqrt((2*rbar*(sin(ThetaS) - sin(ThetaT)))/g);
%
beta = tc/(tc + tf);
% Inner radius
```

```
ri = rm * sqrt(1 - (2*pi*beta*J)/(2*pi + ThetaS - ThetaT));
%
%% Calculate z parameter
z = (1 - J)^(0.4532);
%
%% Theoretical power
% Specific density of slurry
RhoS = RhoO/(RhoO - Cw*(RhoO - 1));
% Net power Pnet
Pnet = pi*g*L*Nm*rm/(3*(rm - z*ri))*(2*(rm^3) - 3*z*(rm^2)*ri ...
    + (ri^3)*(3*z - 2))*(RhoC*(sin(ThetaS) - sin(ThetaT)) ...
    + RhoS*(sin(ThetaT) - sin(ThetaTO))) ...
    + L*RhoC*((Nm*rm*pi/(rm - z*ri))^3)*(((rm - z*ri)^4) ...
    - (ri^4)*(z - 1)^4);
% No-load power Pno
Pno = 1.68*((D^2.5)*L*Speed)^0.82;
% Total power Ptot
Ptot = 1.215*Pnet + Pno;
%
%% Milling kinetics: Attainable Region analysis
% Choice of cut-off sizes
cutoff = inputdlg({'CHOOSE CUT-OFF SIZES FROM SIEVES BELOW:', ...
'Enter upper cut-off size from the list of sieves above:', ...
'Enter lower cut-off size from the list of sieves above:'}, ...
'SIZE CLASS OF INTEREST', ...
1, {num2str(x*1000,'%5.0f'), '75', '9'});
% Extraction of user-defined cut-off sizes
sieve = str2double(cutoff)/1000;
% Mass percent fraction in the size class of interest
mass = P(x == sieve(2), :) - P(x == sieve(3), :);
plot(60*tau*Ptot, mass)
ylabel('Mass fraction in size class of interest in %')
xlabel('Energy consumed in Joules')
%
```